Title	Identification of IRS4 and TOP2A as novel CDC7 kinase interacting proteins
Author(s)	Wu, Kevin Zhi Loong
Publication Date	2016-02-08
Item record	http://hdl.handle.net/10379/5539

Identification of IRS4 and TOP2A as novel CDC7 kinase interacting proteins

A thesis submitted to the National University of Ireland, Galway in fulfillment of the requirement for the degree of

Doctor of Philosophy

By

Kevin Zhi Loong Wu

Centre for Chromosome Biology,
Discipline of Biochemistry, School of Natural Sciences,
National University of Ireland, Galway

Supervisor: Prof. Corrado Santocanale

February 2016

Table of Contents

List of Figures

6

List of Tables

Abbreviations

ACA	Anti-centromere antibody
ADP	Adenosine diphosphate
APC/C	Anaphase promoting complex/cyclosome
APS	Ammonium persulfate
ATM	Ataxia telangiectasia mutated
ATP	Adenosine triphosphate
ATR	ATM- and RAD3-related
ATRIP	ATR-interacting protein
b.p.	base pair(s)
BCA	Bicinchoninic acid
BRCT domain	BRCA1 N-terminal domain
BrdU	5-bromo-2'-deoxyuridine
BSA	Bovine serum albumin
CDC	Cell division cycle protein
CDK	Cyclin-dependent kinase
ChIP	Chromatin immunoprecipitation
CHK1	Checkpoint kinase 1
CMG	CDC45-MCM2-7-GINS
CRM1	Chromosome region maintenance 1 / Exportin 1
C-terminus	Carboxyl-terminus
Da	Dalton
DAPI	4',6-diamidino-2-phenylindole
DDR	DNA damage response
DMEM	Dulbecco's Modified Eagle Medium
DMSO	Dimethlysulfoxide
DNA	Deoxyribonucleic acid
DNA-PK	DNA-dependent protein kinase
dNTP	deoxyribonucleotide triphosphate

DRT	Differential Retention of Topoisomerase
DSB	Double-strand break
dsDNA	Double-stranded DNA
DTT	Dithiothreitol
EDTA	Ethylenediaminetetraacetic acid
EdU	5-ethynyl-2'-deoxyuridine
EGFP	Enhanced GFP
EGS	Ethylene glycol bis(succinimidyl succinate)
EGTA	Ethylene glycol tetraacetic acid
FBS	Fetal bovine serum
FL	Full-length
g	Gravitational constant
GDP	Guanosine diphosphate
GFP	Green fluorescent protein
GINS	Go-Ichi-Ni-San complex
GTP	Guanosine triphosphate
h	hour(s)
HEPES	4-(2-hydroxyethyl)-1-piperazineethanesulfonic acid
HFF	Human foreskin fibroblasts
hTERT	Human telomerase reverse transcriptase
HU	Hydroxyurea
IF	Immunofluorescence
IP	Immunoprecipitation
IPTG	Isopropyl-β-D-thiogalactoside
IRS	Insulin Receptor Substrate
KD	Kinase-dead
MCM	Mini-chromosome maintenance
min	Minute(s)
MNase	Micrococcal nuclease
N-terminus	Amino-terminus
ORC	Origin recognition complex

PBS	Phosphate buffered saline
PBS-T	PBS-Tween 20
PBS-TX	PBS-Triton X-100
PCNT	Pericentrin
PCR	Polymerase chain reaction
PFA	Paraformaldehyde
PH	Plekstrin homology
PI	Propidium iodide
PI3K	Phosphoinositide 3-kinase
PLL	Poly-L-lysine
Pre-IC	Pre-initiation complex
Pre-RC	Pre-replication complex
PTB	Phosphotyrosine binding
qPCR	Quantitative PCR / Real-time PCR
RNA	Ribonucleic acid
RPA	Replication protein A
RTK	Receptor tyrosine kinase
s	Second(s)
SDS	Sodium dodecyl sulfate
SDS-PAGE	SDS polyacrylamide gel electrophoresis
SH2	Src homology 2
SILAC	Stable isotope labelling of amino acids in cell culture
siRNA	Silencing RNA
ssDNA	Single-stranded DNA
TCA	Trichloroacetic acid
TEMED	Tetramethylethylenediamine
TGF	Transforming growth factor
TLS	Translesion synthesis
TOP2	Topoisomerase 2
UFB	Ultrafine anaphase bridge
WT	Wild type

Author's Declaration

I certify that I am the sole author of this thesis and that I have not obtained a degree in this University or elsewhere on the basis of any of this work.

The experiments and data analysis presented in Figure 5.1 A-C, and Figure 5.2 B were performed by Gemma O'Brien, Edel Mullen, and Sandra Healy, and are included as contextual background for this work. Individual contributions are clearly stated at the beginning of the appropriate section(s).

Acknowledgements

I would like to thank my supervisor, Prof. Corrado Santocanale. Your guidance, advice, and sailing trips throughout the last four years have been invaluable (What is the question?). I greatly appreciate your reading (and re-reading) of this thesis.

To the other members of the lab, past and present, I am extremely grateful for the support, advice, food, laughter, and trips to Tesco that have kept me going when the science just wasn't. I cannot thank each of you enough.

I would also like to thank my friends in the CCB, ARC, REMEDI, and the original NCBES 1st floor crew for advice and reagents, and for simply, but importantly, distracting me from the science.

To the board games group, you have kept me relatively sane, and my write up time would have been infinitely more depressing if it wasn't for you!

To my sakais, thank you for always being there for me, no matter where in the world we may be. Our inane conversations constantly remind me how lucky I am to always have something to go back to.

Finally, I would like to thank my parents, without whom none of this would have been possible. You taught me to love science, and have always supported and encouraged me, and for that I am truly grateful.

Abstract

CDC7 is an essential serine/threonine kinase required for the initiation of DNA replication in eukaryotic cells, through phosphorylating the MCM helicase complex. Formation of an active kinase requires the binding to either of its regulatory subunits, DBF4 or DBF4B. The main aim of this project was to identify novel roles of CDC7 kinase through the identification of its interacting proteins. To aid their purification, we have generated human cell lines that conditionally express epitope-tagged CDC7, DBF4, and DBF4B, and we first describe the characterisation of these cell lines. We found that expression of DBF4 or DBF4B was able to increase MCM2 phosphorylation, but did not impair DNA replication or cell proliferation. Epitope-tagging also allowed us to determine the localisation of CDC7 kinase by immunofluorescence, and we present evidence of novel DBF4B localisation to centrosomes and microtubules in interphase cells.

Using a quantitative proteomics approach, we identified Insulin Receptor Substrate 4 (IRS4) as a novel CDC7-DBF4B interacting protein, and we confirmed this interaction through immunoprecipitation experiments. IRS4 associates with receptor tyrosine kinases, where it mediates the activation of key signalling pathways, including the PI3K/AKT pathway. The CDC7 kinase inhibitor, XL413, attenuated the PI3K-dependent phosphorylation of AKT S473 in untransformed fibroblasts, but this was not reproduced by siRNA depletion of CDC7, suggesting that the effect was independent of CDC7 kinase activity. We then investigated a potential role for IRS4 in mediating the activation of CDC7 kinase, but IRS4 depletion did not affect CDC7-dependent MCM2 phosphorylation or DNA replication either.

Topoisomerase 2-α (TOP2A) was identified through mass spectrometry analysis of proteins co-immunoprecipitated with DBF4. TOP2A mediates the decatenation of double stranded DNA molecules, and is therefore required for maintenance of proper chromatin structure, chromosome condensation, and accurate segregation of DNA into daughter cells. We showed that the DBF4-TOP2A interaction occurs early in S-phase, and that it is abolished by treatment with XL413, suggesting that it is dependent on CDC7 kinase activity. We have found that both DBF4 and TOP2A localise to centromeres in S-phase, and that depletion or chemical inhibition of CDC7-DBF4 affects the timing of centromeric TOP2A recruitment. We hypothesise that timely TOP2A recruitment may contribute to centromeric cohesion or replication, and this will be the subject for future investigation.

15

Chapter 1: **General Introduction**

1.1   The cell cycle

Omnis cellula e cellula; all cells arise from the division of pre-existing cells. Even though there is still some debate over who first proposed this key tenet of cell theory over 150 years ago, there is no doubt as to its contribution to the development of the field of cell biology [1]. To generate two daughter cells, a cell must pass through the cell cycle: a coordinated sequence of events that has to be completed in a precise and ordered manner. The cell cycle can be divided into four main stages, or phases, Gap 1 (G1), Synthesis (S), Gap 2 (G2), and M-phase (M; comprising mitosis and cytokinesis). Under certain conditions, cells may also enter a non-proliferative state, termed the Gap 0 or Resting (G0) phase (Fig. 1.1). Each of these phases will be discussed in the following paragraphs. Central to the control of these cell cycle events are two classes of proteins: cyclins, and their interacting partners, the cyclin-dependent kinases (CDKs). As their name suggests, cyclin levels oscillate throughout the cell cycle through their synthesis and degradation. Cyclins associate with, and activate CDKs activity, and it is these waves of cyclin-CDKs activity that drive transition between the phases (reviewed in [2,3]).

1.1.1 G1-phase

Typically the longest stage in somatic cells, G1-phase is dedicated to the synthesis of the proteins required for cell division, accompanied by an increase in cell size. In this phase, a cell must decide if conditions are conducive for cell division. For mammalian cells in culture, this involves the incorporation of various signals from growth factors, cell density, and attachment to substrate [4]. If conditions are unfavourable, for instance if growth factors are absent, cells can exit the proliferative state and enter G0-phase. Once cells have passed the restriction (R) point, they are no longer dependent on the aforementioned factors and must complete a full round of genome duplication and cell division [5]. Confusingly, there is evidence that two such independent points exist, both of which have been referred

16

to as R points [6]. The first, occurring relatively early in G1, is growth factor-dependent (hereon termed R), and the second, closer to the start of S-phase, which monitors cell nutritional status ("cell growth" checkpoint) [6]. At the molecular level, increasing levels of the G1 cyclin cyclin D-CDK4/6 promotes the expression of cyclin E, and transition through R. Nutritional status permitting, cyclin E-CDK2 induces the expression of many genes, including cyclin E itself in a positive feedback loop, which are required for entry into S-phase [6].
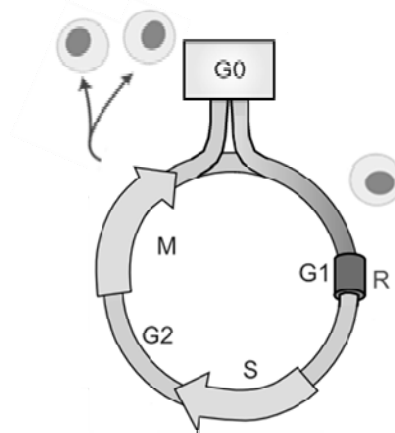
Figure 1.1 Phases of the eukaryotic cell cycle. *The cell cycle consists of four main stages. In preparation for mitotic cell division in M-phase, cells undergo two phases of growth, G1 and G2, and genome duplication in S-phase. Cells can also exit the cell cycle and enter a period of temporary quiescence (G0) or senescence under certain conditions. Adapted from [2].*

1.1.2 S-phase

The process of genome duplication begins at specific sites distributed throughout the genome, termed replication origins [7]. Replicative helicases unwind double-stranded DNA (dsDNA) in a bidirectional manner beginning at replication origins. This enables recruitment of a host of factors to single-stranded DNA (ssDNA) which ultimately results in the production of two identical dsDNA molecules (discussed further in Section 1.3). The passage of replication forks moving away from each other creates an expanding 'bubble' of replicated DNA,

between them, which eventually merges with another bubble originating from a neighbouring origin, finally resulting in complete replication of the genome [8]. The initiation and progression through S-phase is promoted by rising levels of cyclin A-CDK2. In addition to initiating DNA synthesis, cyclin A-CDK2 also prevents the assembly of further replication complexes, thus limiting the firing of each origin to once per cell cycle [9].

1.1.3 G2-phase

In G2, cells continue to grow and synthesise proteins required for M-phase. This temporal gap between S- and M-phases allows cells to ensure that genome duplication is complete before chromosomes are segregated [10]. It is also an opportunity for cells to check the fidelity of replicated DNA, and if required, prevent entry into M-phase until damaged DNA is repaired [10].

1.1.4 M-phase

The cell cycle culminates in the final, and perhaps the most visually impressive process of nuclear and cellular division. Chromosome segregation in mitosis can be subdivided into four phases: prophase, metaphase, anaphase, and telophase, which are subsequently followed by separation of the mother cell into two distinct daughter cells by cytokinesis [11]. Here, both cyclin A-CDK1 and cyclin B-CDK1 act to trigger the initial steps of mitosis [11].

In prophase, chromosomes are condensed, and the nuclear envelope breaks down. Kinetochores, large multi-protein complexes, are assembled on centromeres, one on each sister chromatid [12]. Microtubules originating from the centrosomes attach to kinetochores, such that each kinetochore of a sister chromatid pair is attached to opposing poles of the cell. This bi-oriented attachment is essential for equal chromosome segregation, and is monitored by the spindle assembly checkpoint (SAC; reviewed in [13]). SAC signalling is dependent on two factors, microtubule-kinetochore attachments, and inter-kinetochore tension. The bi-directional pulling from each pole aligns chromosomes along the cell equator in

metaphase. Once chromosomes are properly attached and aligned, SAC signalling ceases, and the anaphase promoting complex/cyclosome (APC/C) is activated. The APC/C is an ubiquitin ligase that marks proteins for degradation, and acts on proteins which inhibit anaphase progression [14]. Sister chromatids are held together by cohesin rings in metaphase, cleavage of which is carried out by separase. In metaphase, separase is inhibited by its interaction with securin. APC/C-directed degradation of securin in anaphase results in cohesin cleavage, allowing sister chromatid separation and segregation [15]. In telophase, the nuclear membrane reforms around each set of separated chromosomes, and chromosomes decondense. Finally, cytokinesis occurs through the formation of a contractile ring between the nuclei, progressively constricting the cell membrane until the two daughter cells are completely separated [16]. The APC/C is also responsible for the degradation of the mitotic cyclins A and B before re-entry into G1 [14].

1.1.5 Cell cycle exit: G0-phase and senescence

As alluded to earlier, cells are able to exit the proliferative cell cycle either temporarily (quiescence, G0-phase) or irreversibly (senescence) [17,18]. Cellular senescence can be triggered by various sources including, but not limited to, shortened telomeres, severe DNA damage, or oncogenic stress [18]. This is thought to be a pro-survival mechanism, as proliferation of aged or abnormal cells, which are more likely to be genetically unstable, increase the likelihood of tumorigenesis [19]. Quiescence, on the other hand, is a means for restraining proliferation until conditions are more favourable, or in the organismal context, when tissue growth or repair is required [17]. In the latter case, this is sensed or communicated through the secretion of growth factors and cytokines. Growth factors can bind to a specialised class of cell-surface receptors with intrinsic tyrosine kinase activity (receptor tyrosine kinases), which initiate a intracellular signalling cascade to trigger re-entry into the cell cycle [20].

1.2 Signalling by receptor tyrosine kinases

Receptor tyrosine kinases (RTKs) are a large family of cell-surface receptors composed of 58 known transmembrane receptors, divided into 20 subfamilies [20,21]. RTKs mediate multicellular communication in metazoans by sensing extracellular signals and transmitting them into the interior of the cell to initiate the desired response. They are involved in the regulation of a wide range of critical cellular processes, including cell cycle control, proliferation and differentiation, survival, metabolism, and migration [20]. As such, RTK signalling is usually subject to tight control, and their untimely activation is frequently linked to oncogenic transformation [21].

1.2.1 Mechanisms of RTK activation and signalling

All RTKs have conserved molecular features, consisting of ligand-binding extracellular domains, a membrane-spanning helix, and a cytoplasmic region containing a protein tyrosine kinase (TK) domain as well as additional C-terminal and juxtamembrane regulatory domains [20]. The exact molecular events that govern RTK activation are remarkably varied, but share a common theme. Under basal conditions, RTKs adopt an autoinhibitory structure (for instance with obstructed ATP or substrate binding pockets). Ligand binding induces receptor dimerization (or in some cases oligomerization), which then allows *trans*-phosphorylation between partners, which relieves the autoinhibition and adoption of an active kinase configuration. It is thought that even when autoinhibited, TK domains maintain a sufficient basal level of activity to phosphorylate its partner when stabilised in a dimer/oligomer (reviewed in [20]). Once activated, RTKs rapidly undergo several phases of autophosphorylation, serving to further increase TK activity, and create phosphotyrosine-based binding sites for recruitment of downstream signalling molecules containing phosphotyrosine-binding (PTB) and Src homology 2 (SH2) domains (Fig. 1.2) [22].
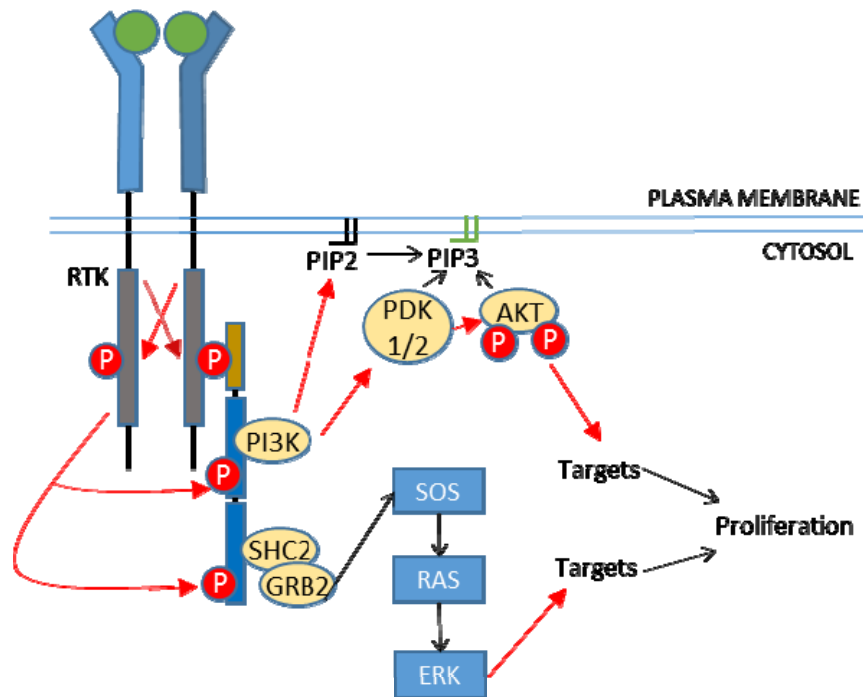
Figure 1.2 Ligand binding to RTK results in activation of intracellular signalling pathways. *The activated RTK phosphorylates multiple tyrosine residues on itself and scaffolding proteins (red arrows), such as Insulin Receptor Substrates (see Section 1.2.3), which form binding sites for downstream signalling molecules containing PTB and SH2 domains. This results in the parallel activation of the PI3K/AKT and ERK pathways (discussed in Section 1.2.2). Figure adapted from [20].*

1.2.2 Signalling pathways downstream of RTK activation

Recruitment of a host of signalling molecules either by direct binding or through scaffold proteins nucleates the formation of multi-protein signalling complexes at the activated receptor. While there are several different pathways that can be activated depending on the ligand and RTK involved, we will be focusing on two major pathways involved in the proliferative response.

1.2.2.1   Phosphoinositide 3-kinase – AKT pathway

Activation of the phosphoinositide 3-kinase – AKT (PI3K–AKT) signalling pathway is probably the most vital and best characterised process regulated by RTK activation. PI3K is a heterodimer consisting of a p85 regulatory subunit and a p110 catalytic subunit with lipid kinase activity [23]. The tandem SH2 domains of the p85 subunit promote the translocation of PI3K to the activated receptor by binding to phosphotyrosine-containing motifs. At the membrane, it phosphorylates the 3'OH group of the inositol membrane lipid phosphatidylinositol-4,5-bisphosphate (PIP_2) to produce the second messenger phosphatidylinositol-4,5,6-trisphosphate (PIP_3) [24]. Accumulation of PIP_3 at the membrane recruits other signalling proteins through direct binding with their pleckstrin homology (PH) domains, including AKT, a protein serine/threonine (S/T) kinase, which is the major effector of PI3K [25,26]. AKT localisation to the membrane stimulates its phosphorylation on two key residues essential for full activation of its kinase activity: Ser308 and Ser473, by phosphoinositide-dependent kinase 1 (PDK1), and PDK2 (now identified to be the mTORC2 complex) respectively [27,28]. In turn, AKT acts on a wide range of substrates to promote cell proliferation and survival, including inhibitory phosphorylation of the CDK inhibitor p21, increasing transcription and translation of cyclin D, inhibition of pro-apoptotic caspases, and upregulation of insulin signalling (reviewed in [29]).

1.2.2.2   Mitogen-activated protein kinase pathway

The mitogen activated protein kinase (MAPK) pathway is also known as the Ras–Raf–MEK–ERK pathway (where MEK and ERK are Mitogen-activated ERK Kinase and Extracellular-signal-Regulated Kinases respectively). This pathway is activated in an analogous manner to the PI3K–AKT pathway. Through a complex consisting of SHC2–GRB2–SOS proteins, Ras is recruited to the activated receptor [30]. Ras is a GTP-binding protein which is inactive in its GDP-bound form, and SOS is a guanine nucleotide exchange factor that converts Ras from its GDP-bound form into its GTP-bound form [31]. Activated Ras directly binds Raf Ser/Thr

kinases (B-Raf and C-Raf) and recruits them to the membrane. At the membrane, Rafs are activated through a complex series of events involving multiple factors, including phosphorylation/dephosphorylation and dissociation from inhibitory proteins [32]. Rafs then phosphorylate and activate MEK, whose predominant downstream target is ERK. ERKs are also S/T kinases, but in contrast to MEK, ERK has multiple targets, such as the transcription factors MYC, CREB, and c-JUN, which can upregulate genes involved in proliferation and the cell cycle [32,33].

1.2.2.3   Signalling pathway integration

As mentioned earlier, there are 58 identified transmembrane RTKs, each stimulating different cellular responses, yet these effects are mediated by a surprisingly small number of signalling pathways [20]. To complicate matters further, the same pathways are also often used in cytokine receptor signalling [34]. How the activation of the same pathway by different receptors, or even by the same receptor in different contexts, can result in differential biological effects is a matter of great interest. Although they have been portrayed here as independent linear pathways for simplicity, this is not an accurate reflection of signalling *in vivo*. The existence of positive and negative feedback loops, both within and between pathways, form an elaborate network, which allows integration of signals from multiple receptor inputs. In addition, differences in the number, extent, and kinetics of receptor activation, and also cell lineage, all play a role in determining the exact cellular outcome [20]. A detailed molecular and quantitative understanding of these processes is a long standing goal within the field, as these pathways are frequently dysregulated in cancer, and targeting of these pathways may have significant therapeutic potential [35,36].

1.2.3 Insulin Receptor Substrate proteins

The Insulin Receptor Substrates (IRS) are a family of proteins associated with RTK signalling. Currently, there are 5 known members in humans, IRS1, 2, 4, 5, and 6 (IRS3 is only present in mice) [37]. IRS1 was the first identified member,

and was initially detected as a protein that was tyrosine phosphorylated upon insulin stimulation [38]. IRSs interact directly with a number of different RTKs, including the insulin receptor and insulin-like growth factor 1 (IGF-1) receptor [39-42]. IRSs are extensively phosphorylated by activated receptors, and while they do not have catalytic activity, they contain binding sites for the recruitment and activation of downstream signalling molecules, including PI3K and GRB2 [37]. They therefore function as protein scaffolds that mediate the recruitment of other proteins to membranes and RTKs. The specific recruitment domains that are present varies between IRS proteins [37]. All IRSs contain a PH and PTB domain on their N-terminus, which allow recruitment to the membrane through interaction with phosphatidylinositol lipids and phosphorylated receptors, respectively. IRS1, 2, and 4 additionally have PI3K and GRB2 docking sites, whereas the distantly related proteins IRS5 and 6 are truncated at their C-termini and their role in signalling is unclear (Fig. 1.3) [43].
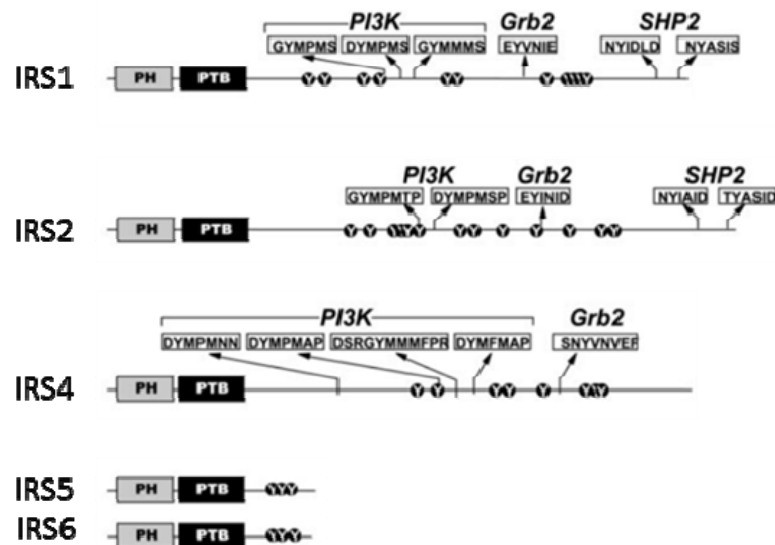
Figure 1.3 IRS proteins in humans. All five members of the IRS family contain a pleckstrin homology (PH) and a phosphotyrosine binding (PTB) domain on their N-termini. Potential phosphotyrosine sites are marked (Y), and known binding motifs are indicated in boxes below the interacting partners. Figure adapted from [44].

Despite similarities in structure and functions (such as PI3K activation), IRSs have non-interchangeable roles in RTK signalling. IRS1 and IRS2 are the primary effectors of insulin-stimulated mitogenesis and glucose metabolism in most cell types, but are differentially expressed [44]. In addition, IRS1- and IRS2-deficient mice do not have identical phenotypes. Due to reduced sensitivity to IGF-1, IGF-2, and insulin, IRS1-deficient mice exhibit growth retardation and are less sensitive to the blood glucose-lowering effects of insulin compared to normal mice, but do not develop diabetes (i.e. have normal glucose tolerance) [45]. On the other hand, IRS2-deficient mice have mildly reduced growth compared to normal mice, but profound insulin resistance, and impaired pancreatic β-cell function [46]. These phenotypic differences are not likely due to tissue-specific expression alone, as it has been demonstrated that IRS1 and IRS2 mediate differential signalling events in the same cells [47].

In contrast, disruption of IRS4 in mice, expression of which is limited to a comparatively smaller number of tissues, resulted in only mild defects in growth, reproduction, and glucose tolerance, arguing against a major physiological role for IRS4 in mammals [48,49]. However, IRS4 is highly expressed in some cell lines and tissue types, including the liver. In rats, it is dramatically upregulated after partial hepatectomy, suggesting a role in liver regeneration [50]. In addition, IRS4 was found to be upregulated in primary hepatocellular carcinoma [51], and IRS4 depletion in the human hepatoblastoma cell line HepG2 impairs IGF-1-dependent proliferative signalling, and sensitises HepG2 cells to Actinomycin D- and TNF-α-mediated cell death [39,52]. Consistent with this, IRS proteins have been implicated in tumour proliferation, motility, and invasion (reviewed in [53]).

In summary, cells receive extracellular signals, in the form of growth factors, which bind to their respective RTKs at the cell surface. RTK activation results in the recruitment and activation of multiple signalling molecules, a process which is mediated by scaffold proteins such as the IRSs. Extracellular signals from different receptors converge on a common set of signalling pathways, and this allows the cell to integrate signals from multiple inputs to determine if conditions are conducive to

cell cycle re-entry. If proliferation is the desired response, cells prepare to enter S-phase and replicate their DNA.

1.3   DNA replication

According to the latest genome assembly, each diploid human cell contains over 6.4 billion nucleotides spread over 46 chromosomes (GRCh38.p4, June 2015, http://www.ncbi.nlm.nih.gov/assembly/GCF_000001405.30/) [54]. To ensure timely completion of human genome duplication, replication is initiated from an estimated 30,000 – 50,000 origins in every S-phase [55]. This process requires precise coordination, as it is crucial that the entire genome of a eukaryotic cell is fully replicated exactly once and only once per cell cycle. Failure to do so can have catastrophic effects, particularly as cells attempt to segregate their chromosomes. Under- or overreplication can lead to cell inviability or genomic instability, which is a major contributing factor to cancer [56]. DNA replication can be divided into three distinct stages, initiation, elongation, and termination. Important events are summarised in Figure 1.4 and are discussed in the following sections.

Much of what we now know of the cell cycle stems from studies first performed in the budding yeast *Saccharomyces cerevisiae*, and other model organisms [57,58]. Due to its experimental and genetic tractability, and the fact that its replication origins are well defined, *S. cerevisiae* has contributed immensely to the study of the processes involved in DNA replication in particular [59,60]. Many of these processes have since been found to be conserved in humans. As such, the following discussion (and corresponding references) will refer to the human homologues as far as has been determined. Where protein function has been determined in other model organisms, this will be distinguished by the prefix Sc or Xl for budding yeast or *Xenopus laevis*, respectively.

1.3.1 DNA replication initiation

1.3.1.1   Origin licensing

The first step of replication initiation, origin licensing, actually occurs in late mitosis to early G1-phase, and involves the assembly of pre-replicative complexes (pre-RC) at recognised origins. This is achieved by the binding of the hexameric Origin Recognition Complex (ORC), comprising subunits ORC1-6, to origin DNA in an ATP-dependent manner [61]. The ORC physically marks replication origins and forms the platform for subsequent assembly of the pre-RC. CDT1 and CDC6 then become independently associated with ORC-bound chromatin, and this allows recruitment of the replicative helicase MCM2-7 [62,63]. At this stage, MCM2-7 is only loosely associated with origins, and is loaded onto DNA in a series of events requiring ATPase activity of ORC1 and CDC6, finally resulting in the sequential loading of two MCM2-7 hexamers in a head-to-head conformation [64-66]. In cells progressing to S-phase from quiescence (G0), Cyclin E-CDK2 cooperates with CDC6 to promote pre-RC formation. It is believed that MCM2-7 loading is the essential goal of pre-RC formation, as XlORC and XlCDC6 are dispensable for replication initiation after this stage [67,68].

1.3.1.2   Origin firing

Transition from G1 to S-phase is marked by rising levels of cyclin A-CDK2 and CDC7 kinase [69,70]. The mechanisms leading to origin firing by the action of these kinases are rapidly being elucidated, and have recently been recapitulated *in vitro* with the minimal complement of purified *S. cerevisiae* proteins [71]. Replication competent origins were formed in three steps: pre-RC formation dependent on ORC binding, followed by the CDC7- and CDK-dependent recruitment of additional proteins to form the pre-initiation complex (pre-IC) in two independent steps [71]. These processes appear to have been mostly conserved in humans, although the specific phosphorylation events involved may differ. Phosphorylation of Treslin/TICRR by cyclin A-CDK2 facilitates its binding to BRCT domains on TOPBP1, and the resulting complex of TICRR/TOPBP1/MTBP

27

is essential for the recruitment of GINS, MCM10, and DNA polymerase ε (Pol ε) to the pre-RC [72,73]. CDC7 kinase, on the other hand, associates with CDT1 and is required for the recruitment of CDC45 [63]. This assortment of factors is termed the pre-IC [74]. Tight association of the CDC45-MCM2-7-GINS (CMG) complex is established, followed by the dissociation of TICRR, TOPBP1, and MTBP from the origin, leaving behind the components required for replication fork progression [8]. The CMG complex contains the key helicase machinery, and phosphorylation of MCM2-7 by CDC7 kinase triggers the unwinding of dsDNA and entry into S-phase [69].
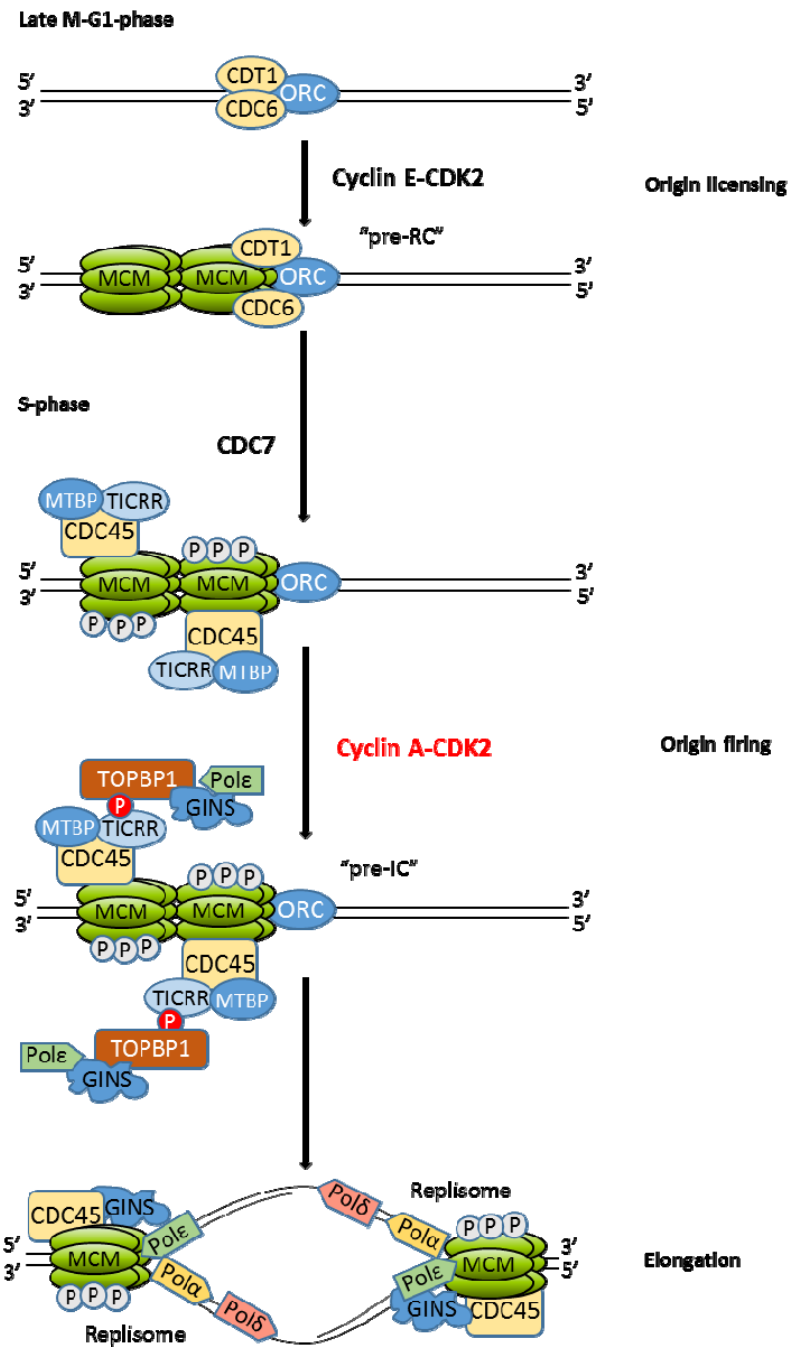
Figure 1.4 Major steps in the initiation and elongation steps of DNA replication. *Origin licensing occurs in G1-phase through the recruitment of CDC6, CDT1, and MCMs to ORC-bound origins. Assembly of replication competent origins requires the action of both CDC7 kinase and CDKs for the recruitment of critical replication proteins. Note that a number of important proteins were omitted in this scheme for the sake of simplicity. See text for more details. Grey and red Ps indicate important phosphorylation events mediated by CDC7 and Cyclin A-CDK2 respectively. Figure adapted from [64].*

1.3.1.3   Regulation of DNA replication initiation

1.3.2 Elongation and DNA synthesis

The activation of MCM2-7 helicase activity results in the unwinding of parental DNA to expose two ssDNA strands which are used as templates for replication. The single-stranded DNA binding protein Replication Protein A (RPA) binds to the exposed strands to prevent them from re-annealing or forming secondary structures [75]. Three different DNA polymerases, Pol α, δ, and ε, are recruited to replication forks for unperturbed replication, all of which are only able to synthesise DNA in the 5' to 3' direction, therefore necessitating a different system for synthesis of each antiparallel strand of the fork [76]. Synthesis of the leading strand occurs in a continuous manner, as the template is read in the 3' to 5' direction, and this is carried out by the processive DNA polymerase Pol ε, whose association with origins was established during formation of the pre-IC. The lagging strand is synthesised discontinuously through the alternating action of Pol α and Pol δ which produce 100-200 nucleotide (nt) Okazaki fragments which are then joined to form a single uninterrupted strand [77]. The actions of Pol ε and Pol δ on either strand are dependent on the Pol α-primase complex. DNA synthesis is initiated by the primase activity of the Pol α-primase complex with a ~10 nt RNA primer, which is elongated by its DNA polymerase activity for another ~20 nt. At this point, polymerase switching occurs, and strand elongation is resumed by Pol ε and Pol δ on the leading and lagging strands respectively [76]. Additional factors also contribute to uninterrupted progression of the replication fork. The sliding clamp Proliferating Cell Nuclear Antigen (PCNA) is a ring shaped protein which is loaded around each template DNA strand by the Replication Factor C (RFC) complex. PCNA binding to Pol ε and Pol δ facilitates polymerase switching from Pol α, and increases their processivity [78]. Described here is the now generally accepted model that Pol ε and Pol δ contribute to leading and lagging strand replication respectively, as concluded from genetic analysis of ScPol mutants [79,80]. It is important to note, however, that

recent data proposes an alternative interpretation where Pol δ is responsible for the bulk of DNA synthesis on both strands [81].

1.3.3 DNA replication termination

Replication termination occurs when replication forks from neighbouring origins converge. This mechanisms underlying this process are poorly understood, particularly in metazoans, since the stochastic nature of origin firing leads to asynchronous and non-sequence-specific termination events [55]. Some insights have been gained from studies of the simian virus 40 (SV40) *in vitro* replication system, where it was found that converging replication forks stall during termination [82]. The replicative helicase (large T antigen) was also found to dissociate from the replisome, leaving gaps of about 60 nt on the daughter strands that are filled in at a later stage [83]. Recently, an elegant study by the Walter group described a system for the synchronous and site-specific generation of termination events in *Xenopus* egg extracts [84]. By introducing tandem *lac* operators (LacO) into a plasmid, they were able to generate a physical barrier to replication through the binding of *lac* repressors (LacR), and that could be removed by the addition of IPTG. In contrast to SV40 replication, they found that replication proceeds linearly to completion upon removal of the barrier, with no evidence of replication fork stalling. They were also able to map the 3' end of the leading strand to within a few nucleotides of the 5' end of the lagging strand along the same parental strand, indicating that gaps on the daughter strand are rapidly filled in. Finally, it was demonstrated that CMG helicase complexes on converging forks travel pass each other by maintaining their association with the leading strands. Thus, replication termination occurs when a replisome travelling with a leading strand encounters a lagging strand from a neighbouring fork, allowing rapid completion of DNA synthesis [84].

1.4 The DNA replication checkpoint

Each cell experiences tens of thousands of DNA lesions per day [85]. Some of these arise *via* physiological processes, such as base-pairing mismatches during replication, or spontaneous DNA deamination and oxidation [86]. Lesions can also be caused by environmental factors, such as ultraviolet light and ionising radiation from sunlight, radioactivity, as well as carcinogenic compounds found in cigarette smoke [85,86]. These lesions can interfere with normal replication or transcription, and if left unrepaired, can lead to the transmission and accumulation of mutations that are detrimental to cell or organismal viability.

To maintain the fidelity of the genome, cells have a collection of surveillance mechanisms to detect and respond to DNA damage and replication stress, in the form of checkpoints. Although activated in response to different events, DNA damage checkpoints and the replication checkpoint involve partially overlapping signalling pathways and can elicit similar responses (reviewed in [87,88]). The following sections will address checkpoint signalling and responses solely in the context of the replication checkpoint. Establishment of the checkpoint response is dependent on the actions of three classes of checkpoint proteins, namely the sensors, transducers, and effectors [89]. Central to the detection of DNA damage and replication stress, and the subsequent initiation of signalling are the sensor proteins, Ataxia telangiectasia mutated (ATM), ATM- and RAD3-related (ATR), and DNA-dependent protein kinase (DNA-PK) [90]. ATM, ATR, and DNA-PK all have well characterised roles in double-strand break (DSB) repair, but ATR also plays the primary role in the response to replication stress [88].

1.4.1 Initiation of checkpoint signalling

The replication checkpoint is activated in response to stalled replication forks. Replication fork stalling can occur either through impeding the progression of the DNA polymerases, or the helicase [91]. Every base pair in the genome has to be unwound and replicated, thus any DNA-bound proteins or DNA structures have the potential to act as replication fork barriers. DNA polymerase stalling is typically

caused by alkylated DNA bases, dNTP depletion (such as through inhibition of ribonucleotide reductase by hydroxyurea), or pharmacological inhibition of the polymerase, while helicase stalling can occur through encounter with bulky DNA adducts, as well as protein-DNA or DNA-DNA inter-strand crosslinks [91]. Polymerase stalling leads to its uncoupling from the helicase, which continues to unwind dsDNA, and this results in extended stretches of ssDNA [92]. RPA binds to the exposed ssDNA strands, and these long RPA-ssDNA tracts recruit ATR and its functional partner ATRIP to the stalled fork. In addition, ATR-ATRIP activation is also dependent on the recruitment of the RAD17-RFC complex, the RAD9-RAD1-HUS1 (9-1-1) complex, and TOPBP1 [93]. The RAD17-RFC complex independently recognises the ssDNA/dsDNA junctions at stalled forks and loads the 9-1-1 complex onto dsDNA. Localisation of all the required components at the stalled fork leads to full activation of ATR kinase activity ([93] and references therein).
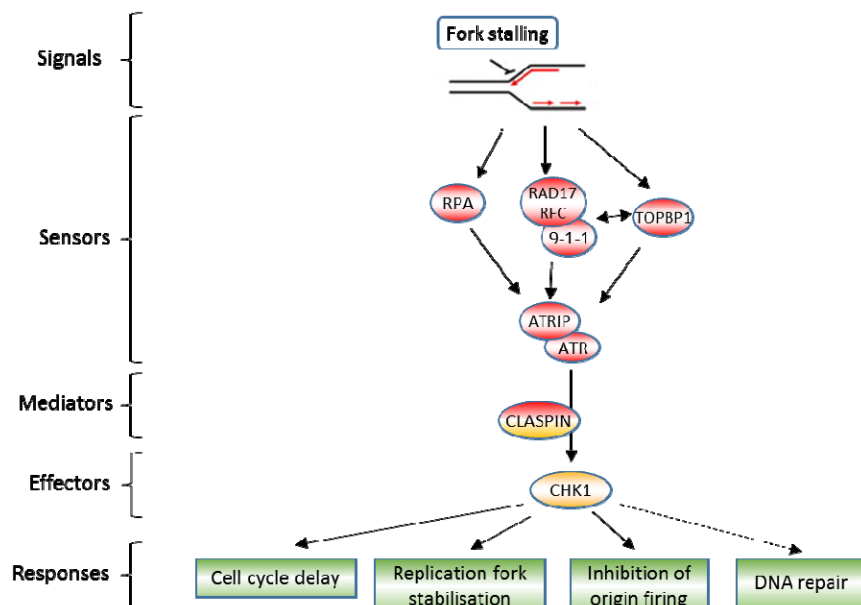
Figure 1.5 DNA replication checkpoint signalling through the ATR-CHK1 axis. Sensor proteins detect replication fork stalling and recruit ATR to initiate checkpoint signalling. ATR phosphorylates and activates the key effector kinase CHK1 in a CLASPIN-dependent manner. CHK1 substrates mediate a range of responses to maintain cell viability during replication stress. Figure adapted from [94].

33

Once activated, ATR phosphorylates a number of different proteins at the fork, including the key effector kinase CHK1 [95]. Phosphorylation of CHK1 by ATR activates its kinase activity, and this is dependent on the mediator protein CLASPIN [95]. CLASPIN interacts directly with several components of the replisome including the MCM helicase and Pol ε, and is thought to couple their activity in unperturbed replication [96]. This makes it ideally positioned to act as a sensor of ongoing replication [97]. As the effector kinase, CHK1 mediates the downstream phosphorylation of a broad range of cytoplasmic and nuclear substrates, with three important outcomes: cell cycle delay, inhibition of origin firing, and fork stabilisation [98].

1.4.2 Response to checkpoint activation

Checkpoint activation imposes a S-M phase cell cycle delay through CHK1 phosphorylation of the cell cycle regulators CDC25C and WEE1 [99]. CDC25C activates cyclin B-CDK1 through its phosphatase function, while WEE1 inhibits CDK1 through phosphorylation. CHK1 phosphorylation inhibits CDC25C, and activates WEE1, thus downregulating CDK activity and preventing mitotic entry until replication is complete [100].

Not all replication origins are fired simultaneously at the beginning of S-phase, in fact, firing occurs throughout S-phase in a characteristic temporal order known as the replication timing program [101]. In addition, dormant origins are licensed but never fired in an unperturbed cell cycle (Section 1.3.1.3). Since origins cannot be relicensed in S-phase, there are a limited number of available origins for activation, and these late-firing and dormant origins may become essential for the completion of genome duplication in the event that early replication forks stall and irrecoverably collapse [102]. Thus, it is key that the firing of these origins be suppressed until the replication stress is resolved. Inhibition of pre-IC formation and firing of these late and dormant origins is achieved by downregulation of CDK activity (*via* CDC25 inactivation) and regulation of CDC7 kinase activity (*via* direct ATM/ATR phosphorylation of its regulatory subunit DBF4 [103]).

However, it has been suggested that the essential function of the checkpoint is the stabilisation of stalled replication forks. When cells experiencing hydroxyurea-induced replication stress (caused by dNTP depletion) are treated with an ATR inhibitor, they lose the ability to complete replication within 45 min of exposure, and are unable to recover even when the source of replication stress and ATR inhibition are removed [104]. Failure to prevent fork collapse results in the loss of replisome components, such as the MCM helicase, that cannot be reloaded [105]. It is less clear how ATR mediates fork stabilisation, but is thought to depend mainly on its direct regulation of factors required for fork remodelling or DNA repair [106]. In summary, checkpoint signalling through the ATR/CHK1 axis, through several parallel mechanisms, provides the opportunity for cells to repair defects before DNA replication or cell division is resumed.

1.5   Topoisomerase 2-α (TOP2A)

Over 6 billion base pairs of DNA have to be contained within the nucleus of each diploid human cell [54]. To achieve this, DNA is wound around nucleosomes composed of histone proteins in the characteristic "beads-on-a-string" structure, which is then further compacted through the formation of higher-order structures [107]. These structures do not remain static, and are continuously being unpackaged and repackaged, since cellular processes such as replication, transcription, and repair, require DNA to be accessible to various protein factors. Additionally, the entire genetic material is duplicated every cell cycle, and sister chromatids have to be completely untangled to allow proper chromosome segregation. These processes generate major topological challenges to the cell in the form of DNA supercoiling and entanglements that are resolved by specialised enzymes called topoisomerases [108]. Type I topoisomerases catalyse the transient nicking and re-ligation of one strand of a dsDNA duplex. In contrast, type II topoisomerases (TOP2) introduce transient DSBs in one duplex of dsDNA, allowing passage of a second duplex through the break, followed by religation of the first strand. Both of these reactions

can allow relaxation of topological stress, but only the latter allows the untangling, or decatenation, of DNA strands [109].
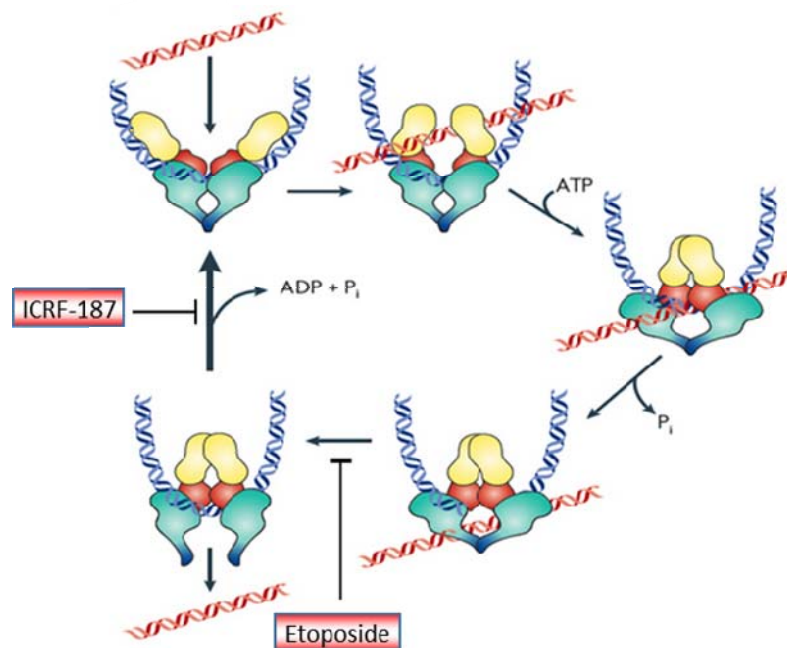
Figure 1.6 Catalytic cycle of TOP2A. *TOP2A is a homodimer that catalyses the transient breakage and reunion of one dsDNA strand (blue) while allowing passage of a second strand (red). The topoisomerase poison etoposide, and catalytic inhibitor ICRF-187 inhibit TOP2A activity at different stages of the cycle (Section 1.5.4). Figure adapted from [129].*

Two isoforms of TOP2 exist in mammals, TOP2A and TOP2B. Both enzymes catalyse similar enzymatic reactions *in vitro*, but have different cellular roles. TOP2A is essential for all proliferating cells, and is the predominant enzyme involved in chromosome condensation and segregation [110]. TOP2B is essential for normal development, but is dispensable in some cell types and is thought to be mainly involved in transcription-related processes [110,111]. The catalytic domains of TOP2A and TOP2B are located on the N-terminal three-quarters of the proteins and share significant sequence homology [112]. Differences in their function and regulation appears to be conferred through their divergent C-terminal domains, which are dispensable for catalytic activity *in vitro* but are vital for cell viability

36

[113]. Consistent with this idea, TOP2 enzymes are subject to differential post-translational modifications on their C-terminal domains in a cell cycle-dependent manner [114,115].

1.5.1 TOP2A in DNA replication

About 30,000 – 50,000 origins are activated within each S-phase in humans [55], producing twice as many replication forks. The unwinding of the DNA double helix structure results in the progressive build-up of positive supercoiling ahead of, and negative supercoiling behind each replication fork. If left unresolved, the accumulation of torsional tension would eventually impede fork progression and even fork reversal – leading to the activation of the replication checkpoint (discussed in Section 1.4) [116]. Depletion of TOP2 in *S. cerevisiae* and human cells, however, led to the timely completion of replication, suggesting that this is not the essential function of the enzyme [110,117]. Type I topoisomerases can also promote relaxation of supercoiling and likely play a redundant role here. While it is not required for DNA synthesis, studies in the *Xenopus* system have also shown that TOP2A is involved in the dissociation of ORC1/2 from origins upon completion of S-phase, and also regulates MCM2-7 helicase loading at the origin licensing step [118,119].

1.5.2 Decatenation checkpoint

During the process of replication of a chromosome, the resulting sister chromatids become intertwined due to the helical structure of DNA [120]. Removal of these entanglements is carried out by TOP2A, and completion of this process is monitored by the decatenation checkpoint [121]. Cells do not sense the catenation status of chromosomes directly, but the checkpoint is instead activated in response to abortive TOP2A activity or catalytic inhibition of TOP2A [122,123]. Catalytically inactivated TOP2A recruits the checkpoint mediator protein MDC1 to chromatin to initiate checkpoint signalling [122]. Phosphorylation of TOP2A at S1524 is essential for MDC1 recruitment, but the kinase responsible for this *in vivo* has yet to be

determined [122]. The G2-M-phase transition is prevented through activation of the ATR/CHK1 pathway to inhibit CDC25 phosphatase (see Section 1.4.2) and PLK1, a kinase which triggers mitotic entry [124].

1.5.3 TOP2A in mitosis

Although DNA replication appears to progress normally in TOP2A depleted cells, mitotic entry is accompanied by an increase in the number of amorphous and severely entangled chromosomes, suggesting defects in chromosome condensation and failure to separate sister chromatids [110]. Indeed, TOP2A was one of only six minimal purified factors that were reported to be necessary to reconstitute *Xenopus* mitotic chromatid condensation *in vitro* [125].

While the decatenation checkpoint ensures that sister chromatids are fully separated prior to entry into mitosis, decatenation of centromeric DNA is restrained until cohesin cleavage at the metaphase-anaphase transition [126] (see Section 1.1.4). As such, centromere decatenation is not always completed before chromosome segregation, and ultrafine anaphase bridges (UFB), which are not stainable by conventional DNA dyes, are often formed during mitosis even in unperturbed cells [127]. TOP2A is recruited to UFBs by TOPBP1 to resolve these structures before cytokinesis can occur [128].

1.5.4 Chemical inhibition of TOP2A

Topoisomerases are essential for cell division and are already a major target for many anti-tumour drugs (reviewed in [129,130]. TOP2 inhibitors can be divided into two broad groups depending on their mechanism of action: poisons, and catalytic inhibitors. TOP2 poisons include the chemotherapeutic drugs etoposide and mitoxantrone, and are so named because they produce DNA damage or lesions, in the form of breaks and covalent protein-DNA linkages [131,132]. TOP2 poisons trap TOP2 at a stage of its catalytic cycle post strand-breakage, where it is covalently linked to DNA. The accumulation of TOP2-DNA covalent complexes rapidly causes protein-linked DNA strand breaks to be formed, which contributes to cellular

toxicity [133]. On the other hand, TOP2 catalytic inhibitors block TOP2 at a later stage of its catalytic cycle after strand passage, but before release of the strands. Inhibited TOP2 remains as a closed clamp around both DNA strands involved [134,135]. Unlike poisons, short term exposure to catalytic inhibitors does not generate a DNA damage response [136]. In fact, a class of catalytic inhibitors, bisdioxopiperazines, are mainly used in the clinic to reduce the cardiotoxicity of some TOP2 poisons [137].

1.6 CDC7 kinase

CDC7 is the catalytic subunit of a serine/threonine kinase which was first identified in *S. cerevisiae* as a gene essential for the initiation of DNA replication [138]. An independent screen of growth-arrested yeast mutants later lead to the discovery of its regulatory subunit DBF4, which, in complex with CDC7, forms an active kinase [25,139]. In higher eukaryotes, a second regulatory subunit, DBF4B, has been identified. Both DBF4 and DBF4B are capable of activating CDC7 kinase, and form mutually exclusive complexes with CDC7 [140,141]. Levels of the CDC7 subunit remain relatively constant throughout the cell cycle, but kinase activity is dependent on DBF4 and DBF4B, the levels of which gradually increase from late G1 to M-phase. Regulation of DBF4 at the transcriptional level has been reported [142,143]. ScDBF4 is also degraded in an APC/C dependent manner [144,145], although post-translational regulation of human CDC7 kinase in an unperturbed cell cycle has yet to be demonstrated.

1.6.1 Regulatory subunits of CDC7

DBF4 and DBF4B have very limited overall sequence similarity, but share three short conserved regions (40-45 amino acids each) within their N-terminal halves, termed the N, M, and C motifs based on the order in which they are located, from the N- to the C-termini [140,146]. The M and C motifs form a bipartite interaction with CDC7 which stabilises the kinase subunit in an active conformation [147]. Through determination of its crystal structure, it was shown that the DBF4 M and C motifs pack against the C and N lobe of CDC7 respectively, and stabilise

CDC7 through a reduction in overall exposed hydrophobic surface area [147]. Although the DBF4 M and C motifs (and the intervening sequence) are minimally sufficient for activation of human CDC7 kinase *in vitro* and increase MCM2 phosphorylation *in vivo* [148], expression of a DBF4 protein lacking motif N is unable to support the proliferation of mouse embryonic stem cells, probably due to loss of protein-protein interactions mediated by this motif [149]. The C-terminal half of the protein (or "tail" region), which was not included in the determination of the crystal structure of CDC7 kinase, contains no recognisable motifs [147].
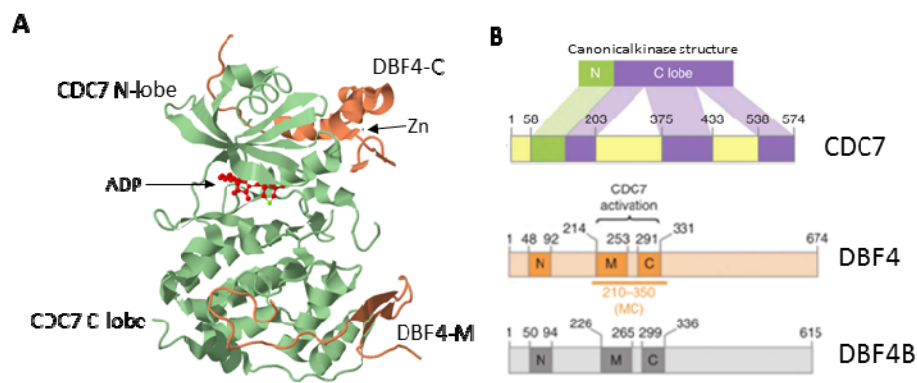
Figure 1.7 Activation of CDC7 kinase by binding to its regulatory subunits. (*A*) *Crystal structure of CDC7 (green) bound to DBF4-MC (orange). ADP is shown in red. DBF4-M and C motifs stabilise an active conformation of CDC7. Obtained from RCSB Protein Data Bank (http://www.rcsb.org/pdb/explore/explore.do?structureId=4F9A), as reported by [147]. (B) Locations of the conserved portions of CDC7, DBF4, and DBF4B. DBF4 and DBF4B share three short conserved motifs within their N-terminal halves. MC motifs are sufficient for CDC7 activation, while motif N is thought to mediate protein-protein interactions. Adapted from [147].*

DBF4 is the only CDC7 activating subunit present in *S. cerevisiae*, and is also more abundant than DBF4B in most human cell types [140,150]. Depletion of DBF4 in human fibroblasts and mouse embryonic stem cells (*via* antibody microinjection and conditional knockout, respectively) causes cessation of DNA replication and cell growth [146,149], while siRNA depletion of DBF4B has comparatively milder effects on S-phase progression in HeLa cells [141]. In the

Xenopus system, CDC7-DBF4B complexes play the major role in replication initiation at early stages of embryonic development, but DBF4B levels fall during the later stages and are replaced by DBF4 [151]. Currently, it is not known if CDC7-DBF4 and CDC7-DBF4B complexes are functionally distinct.

1.6.2 CDC7 kinase is required for initiation of DNA replication

Perhaps the best characterised role of CDC7 is its function in the initiation of DNA replication. Microinjection of anti-CDC7 antibodies inhibits DNA replication in HeLa cells [152]. CDC7 kinase activity is required for the recruitment of several pre-IC proteins to individual origins, including CDC45 [63]. CDC7 also promotes the stable association between CDC45 and MCM2-7, two components of the CMG complex [153,154]. Several subunits of the MCM2-7 helicase have been shown to be substrates for CDC7 kinase *in vitro* and *in vivo* [152,155,156], and it appears that this is its essential function in replication. CDC7 kinase phosphorylates a number of residues on the MCM2 N-terminal, and it was demonstrated, using unphosphorylatable and phosphomimetic mutants, that this phosphorylation was essential for MCM helicase loading [155,157]. Furthermore, a single point mutation of ScMCM5 (P83L) was found to bypass the requirement for ScCDC7 activity for replication initiation, likely through effecting a conformational change of the helicase, mimicking its phosphorylation by ScCDC7 [158,159]. Similarly, a deletion of the N-terminal domain of ScMCM4 allows replication to occur in the absence of ScCDC7 [160]. However, growth is impaired as cells exhibit defects in the efficiency of origin firing and S-phase progression, and are unable to activate the replication checkpoint, indicating important roles for CDC7 in other aspects of the cell cycle [159,160].

1.6.3 CDC7 in the replication stress response

In addition to its roles in unperturbed DNA replication, it is also emerging that CDC7 kinase plays additional roles in the response to replication stress. It was demonstrated that CDC7 remains active and maintains cell viability under such

conditions where further origin firing is unnecessary, or otherwise detrimental to cell survival [161]. CDC7 contributes to this through several mechanisms. Firstly, DBF4 is directly phosphorylated by ATM and ATR in response to DNA damage and replication stress [103]. ATM/ATR phosphorylation of DBF4 stabilises chromatin-bound CDC7-DBF4, and inhibits its origin firing function, while maintaining CDC7-DBF4 kinase activity for the stabilisation of stalled replication forks (Section 1.4.2) [103,162]. CDC7 phosphorylation of the mediator protein CLASPIN has also been shown to be important for the recruitment of CHK1 to stalled forks to allow its phosphorylation and activation by ATR [163,164]. CDC7 also contributes to pro-survival signalling through the phosphorylation and stabilisation of the anti-apoptotic protein TOB1 during DNA damage to allow the opportunity for DNA repair [165]. As discussed in Section 1.4.1, DNA polymerase stalling can occur upon encounter with DNA lesions. To maintain fork progression on damaged templates, trans-lesion synthesis (TLS) is performed by a specialised group of low fidelity "error-prone" DNA polymerases to allow completion of S-phase and post-replication repair of the lesions [166]. In this process, CDC7 mediates the chromatin binding of RAD18, and promotes its association with the TLS Pol η to direct their efficient recruitment to stalled forks [162,167].

1.6.4 Additional roles for CDC7

Studies on CDC7 kinase in human cells have understandably been focused mainly on its role in the initiation step of DNA replication, where it interacts with, and phosphorylates, multiple subunits of the MCM2-7 helicase complex [153,155,160,168]. However, work carried out in other model organisms is strongly supportive of potential roles for CDC7 kinase outside of S-phase. In *S. cerevisiae*, CDC7 has been shown to be involved in the regulation of the mitotic exit network, as well as several aspects of meiosis including meiotic-specific transcription, replication, recombination, and homologous chromosome segregation (for a list of substrates/interactors and references see Table 1.1). In *Xenopus* egg extracts, CDC7 is involved in establishing chromosome cohesion [169], while in a mouse cell line it

was reported to mediate TGF-β-induced smooth muscle cell differentiation and maturation [170,171].

Despite its essential nature and the variety of roles ascribed to CDC7 across different model organisms (Table 1.1), the number of proteins currently reported to interact with, or are phosphorylated by, human CDC7 kinase are surprisingly few (see Table 1.2). This is likely due to intrinsic limitations of working with human cells, particularly in the study of meiosis and development. Most of these were identified as substrates for human CDC7 using targeted approaches through predictions based on their functions in similar pathways (e.g. DNA replication or the S-phase checkpoint) [63,164,167,168], and in some cases, CDC7 itself was identified as a result of a screen [165,172-174].

Table 1.1   Functions of CDC7 outside of DNA replication

Protein(s)	CDC7 kinase function	Species
SCC2-SCC4	Promotes chromatin association of SCC2-SCC4 and cohesin loading to establish sister chromatid cohesion [169]	*X. laevis*
SMAD3	Promotes SMAD3-dependent gene expression in TGF-β-induced smooth muscle differentiation [170,171]	*M. musculus*
CDC5	Inhibits CDC5 to regulate the mitotic exit network [175,176]	*S. cerevisiae*
MER2, TOF1, CSM3	Regulates SPO11 recruitment for meiotic DSB formation [177-179]	*S. cerevisiae*
SUM1	Promotes NDT80 transcription and meiotic entry [63,180,181]	*S. cerevisiae*
LRS4	Regulates monopolin localization for homologous chromosome segregation (meiosis I) [173,182]	*S. cerevisiae*
REC8	Promotes cohesin cleavage (meiosis I) [183]	*S. cerevisiae*

Table 1.2   **Known human CDC7-interacting proteins and substrates**

Protein	Function of protein	Function of CDC7 interaction	Method of identification
DBF4	Kinase-activating subunit	Forms active CDC7 kinase complex [152]	Homology to *S. cerevisiae* DBF4
DBF4B	Kinase-activating subunit	Forms active CDC7 kinase complex [140]	Homology to DBF4
MCM2-7	Replicative DNA helicase	Promotes replication origin firing [153,155,160,168]	Conserved from *S. cerevisiae*
CDT1	Replication origin licensing	Promotes CDC45 recruitment to origins [63]	Targeted (related functions in replication)
CINP	Component of active Cyclin E and Cyclin A complexes	Undefined [173]	Yeast 2 hybrid
CLASPIN	S-phase checkpoint mediator	Required for full CHK1 activation [163,164]	Targeted (Functional interaction in S-phase checkpoint)
CAF1	Chromatin assembly	Promotes CAF1-PCNA binding [172]	Yeast 2 hybrid
RAD18	Recruitment of Pol η for Translesion synthesis (TLS)	Promotes RAD18-Pol η interaction at stalled forks [167]	Targeted (Genetic interaction with TLS pathway)
TOB1	Prevents DNA damage-induced apoptosis	Stabilises TOB1 during mild DNA damage [165]	Mass spectrometry-based screen

1.6.5 CDC7 overexpression in cancer

CDC7 is highly expressed in ~50% of the NCI-60 human tumour cell line panel, with DBF4 frequently co-expressed in the same cell lines [184]. In the same study, elevated levels of CDC7 were detected in primary breast, colon, and lung tumours. Intriguingly, the level of CDC7-DBF4 expression did not correlate with the proliferation rate of the cells. Thus, if CDC7 does not contribute directly to cell cycle progression, it stands to reason that high CDC7 levels must confer some other selective advantage(s). One of the hallmarks of cancer cells is the loss, or evasion, of growth suppressive signals, such as the 'guardian of the genome' TP53 (reviewed in [185-187]). The absence of such genome surveillance mechanisms increases the likelihood of developing further oncogenic mutations (an 'enabling characteristic'), but at the expense of enhanced replication stress and genomic instability [188]. As discussed earlier (Section 1.6.3), CDC7 plays important roles in the response to replication stress, for instance through its involvement in the ATR-CHK1 pathway, as well as in DNA lesion bypass [162,164]. Cancer cells would therefore become more dependent on DNA damage response factors, including CDC7, for their survival. In fact, TP53 inactivation highly correlated with CDC7-DBF4 overexpression in the NCI-60 cell lines [184]. Furthermore, depletion of CDC7 resulted in enhanced cell death in cancer cell lines, but in normal fibroblasts, an abortive cell cycle is prevented through activation of a TP53-dependent checkpoint [189]. Similarly, untransformed breast epithelial cells depleted of CDC7 resulted in a reversible G1-phase arrest, while TP53 deficient breast cancer cells undergo apoptotic cell death [190]. Comparative proteomics of CDC7-depleted normal fibroblasts showed that the maintenance of cell cycle arrest in this "poised quiescence" state involves changes across a broad range of processes and cellular compartments [191,192]. The sensitivity of cancer cells to CDC7 loss has led to the development of CDC7 inhibitors for cancer therapy [174,193-196].

1.7 Project aims

The general aim of this project was to elucidate the function of CDC7 kinase and its regulatory subunits by:

(a) Expressing and purifying CDC7, DBF4, and DBF4B

(b) Identifying novel interacting proteins

(c) Characterising the functions of selected interactors and their relationship with CDC7 kinase

Chapter 2: Materials and methods

2.1   Materials

2.1.1 Reagents and buffers

General laboratory and analytical grade reagents were purchased from Sigma-Aldrich (Arklow, Ireland) and Thermo Fisher Scientific (Leicestershire, UK). EdU (5-ethynyl-2'-deoxyuridine) and 6-carboxyfluorescein TEG-azide were purchased from Berry & Associates (Dexter, MI, USA). Details of specific reagents used are provided as they appear in the text. Buffers used in this study are presented in Table 2.1.

Table 2.1 Composition of buffers used in this study.

Buffer	Composition	Application
Buffer A-H	10 mM HEPES pH 7.9, 1.5 mM $MgCl_2$, 10 mM KCl, 0.5 mM DTT	Hypotonic swelling buffer for nuclear isolation
Buffer A-L	10 mM HEPES pH 7.9, 1.5 mM $MgCl_2$, 10 mM KCl, 1% Nonidet P-40, 0.5 mM DTT	Cell lysis buffer for nuclear isolation
ChIP buffer A	100 mM Tris pH 8, 10 mM DTT	Hypotonic swelling buffer for nuclear isolation
ChIP buffer B	10 mM HEPES pH 7.5, 0.25% Triton X-100	Cell lysis buffer for nuclear isolation
ChIP buffer C	10 mM HEPES pH 7.5, 200 mM NaCl	Nuclei wash buffer
ChIP Elution buffer	0.1 M $NaHCO_3$, 1% SDS	Reversal of antibody binding
ChIP IP buffer	20mM Tris pH 8, 150mM NaCl, 2.5mM $MgCl_2$, 0.5% Triton X-100, 0.1% Nonidet P-40	ChIP antibody binding and wash buffer

ChIP LiCl wash buffer	10 mM Tris pH 8, 1 mM EDTA, 250 mM LiCl$_2$, 1% Nonidet P-40, 1% sodium deoxycholate	ChIP wash buffer
Click reaction solution	10 μM 6-carboxyfluorescein TEG-azide or azide-fluor 545, 10 mM sodium-L-ascorbate, 2 mM CuSO$_4$	EdU labelling of nascent DNA
HPEM extraction buffer	30 mM HEPES, 65 mM PIPES, 10 mM EGTA, 2 mM MgCl$_2$, 0.5% Triton X-100, 100-350 mM NaCl	Extraction of soluble proteins for IF
Laemmli sample buffer (5X)	300 mM Tris-Cl pH 6.8, 20% (v/v) glycerol, 10% (w/v) SDS, 20% (v/v) β-mercaptoethanol, 0.1% (w/v) bromophenol blue	Sample preparation for SDS-PAGE
MNase buffer	50 mM Tris pH 8, 5 mM CaCl$_2$	Micrococcal nuclease digestion
Nonidet P-40 lysis buffer	50 mM Tris pH 7.5, 300 mM NaCl, 10 mM MgCl$_2$, 0.1% Nonidet P-40, 1 mM DTT	IP buffer
NP-T lysis buffer	50 mM NaH$_2$PO$_4$ pH 8, 300 mM NaCl, 0.05% Tween-20	IP buffer
PBS	10 mM phosphate buffer, 137 mM NaCl, 2.7 mM KCl	Wash buffer for cell pellet preparation
Ponceau S stain	0.1% (w/v) Ponceau S, 5% (v/v) acetic acid	Reversible staining of nitrocellulose membrane
PTEM extraction buffer	50 mM PIPES pH 7.2, 10 mM EGTA, 1 mM MgCl$_2$, 0.2% Triton X-100	Extraction of soluble proteins for IF
SDS-PAGE running buffer	25 mM Tris, 0.1% SDS, 190 mM glycine	Gel running buffer
SDS-PAGE transfer buffer	25 mM Tris, 190 mM glycine, 20% methanol	Protein transfer onto nitrocellulose membrane
TAE buffer (1X)	40 mM Tris-acetate pH 8, 1mM EDTA	Agarose gel electrophoresis
TE buffer	10 mM Tris pH 8, 1 mM EDTA	ChIP wash buffer and nucleic acid storage

Tris lysis buffer	50 mM Tris pH 7.6, 150 mM NaCl, 2 mM MgCl$_2$, 1 mM EDTA, 1% Triton X-100	Nuclear lysis/IP buffer

2.1.2 Antibodies

Details of primary antibodies used, including dilutions and amounts used for immunofluorescence (IF), immunoblotting (IB), and chromatin immunoprecipitation (ChIP) are shown in Table 2.2. Secondary antibodies used for IF and IB are shown in 2.3. All Alexa Fluor-conjugated secondary antibodies for IF were purchased from Thermo Fisher Scientific (Leceistershire, UK), and secondary antibodies for IB were from LI-COR Biosciences (Lincoln, NE, USA).

Table 2.3 Secondary antibodies used in this study.

Application	Catalogue number	Antibody	Dilution
Immunofluorescence	A11003	α-Mouse IgG 546	1:300
	A11001	α-Mouse IgG 488	1:300
	A11010	α-Rabbit IgG 546	1:300
	A11008	α-Rabbit IgG 488	1:300
	A21445	α-Human IgG 647	1:300
Immunoblotting	926-68020	IRDye 680LT Goat Anti-Mouse IgG	1:20,000
	926-68021	IRDye 680LT Goat Anti-Rabbit IgG	1:20,000
	926-32214	IRDye 800CW Donkey (pAb) anti-goat IgG	1:10,000
	926-32210	IRDye 800CW Goat Anti-Mouse IgG	1:10,000
	926-32211	IRDye 800CW Goat Anti-Rabbit IgG	1:10,000

Table 2.2 Primary antibodies used in this study.

Catalogue number	Source	Protein/Antigen	Immuno-fluorescence	Western blot	ChIP (μg)	Notes
4058	Cell Signalling	AKT pS473		1:2000		Gift from PCI, NUIG
DCS-342	MBL	CDC7		1:1000		
-	[161]	CDC7 (Clone 12A10)	1:100		5	
15-234-0001	Antibodies Incorporated	Centromere proteins (ACA)	1:200			
-	-	DBF4 (Clone 6F46)			5	
-	[140]	DRF1/DBF4B (Clone 5G4)	1:250			
F4049	Sigma	FLAG M2	1:100	1:1000		
2118L	Cell Signalling	GAPDH		1:5000		
ab10158	Abcam	Histone H4		1:2000		
sc-8189	Santa Cruz	IRS-4	1:100	1:1000		
50-172-131	Upstate	IRS-4	1:200	1:1000		
MCA1859	AbD Serotec	MCM2		1:2000		
-	[155]	MCM2 pS40/41		1:5000		
A00626	GenScript	NWSHPQFEK (Strep-tag)	1:500	1:5000	3	
IHC-00264	Bethyl Laboratories	PCNT	1:300			
sc-899	Santa Cruz	RPB1			3	Gift from Adrian Bracken, TCD
ab26212	Abcam	SSRP1		1:500		
MAB4197	Milipore	TOP2A	1:150	1:1000		
GTX100689	GeneTex	TOP2A		1:2000		
A1978	Sigma	β-actin		1:10000		
sc-9104	Santa Cruz	β-tubulin		1:5000		

2.1.3 Plasmids

The following plasmids used (Table 2.4) were generated in the Santocanale laboratory.

Table 2.4 Plasmids used in this study.

Plasmid name	Protein expressed	Epitope tag (s)
pAB1-CDC7	CDC7	FLAG-Strep (C-term)
pAB1-DBF4	DBF4	FLAG-Strep (C-term)
pAB1-DBF4B (tagged)	DBF4B	FLAG-Strep (C-term)
pAB1-DBF4B (untagged)	DBF4B	None
pIC111-DBF4B	DBF4B	GFP (C-term)

2.2   Methods

2.2.1 Cell culture

2.2.1.1   Maintenance

HEK293T were obtained from American Type Culture Collection (ATCC), U2OS osteosarcoma cells from the Centre for Chromosome Biology, NUI Galway, human foreskin fibroblasts immortalised by hTERT expression were as described in [197], and host Flp-In T-REx 293 cells were from Invitrogen. All cell lines were validated by short tandem repeat (STR) analysis. Cell lines were maintained in high glucose DMEM supplemented with 10% (v/v) heat-inactivated fetal bovine serum (FBS) and 1% (v/v) Penicillin-Streptomycin solution (Sigma-Aldrich, Arklow, Ireland). Sterile cell culture plastics were obtained from Sarstedt AG (Nümbrecht, Germany). The cells were cultured in a Steri-Cycle CO_2, HEPA Class 100 incubator (Thermo Scientific, Rockford, USA) at 37˚C and 5% CO_2.

2.2.1.2   Cell number determination

Cell density was determined using a Countess Automated Cell Counter (Thermo Fisher Scientific, Leceistershire, UK) according to the manufacturer's

instructions. Briefly, 10 μl of a trypsinised single cell suspension was mixed with 10 μl of Trypan blue solution, and 10 μl of this mixture was loaded onto a Countess Chamber Slide. Cell number and viability was assessed by Trypan blue exclusion. Samples were diluted to fall within the linear range of the instrument ($<4.0 \times 10^6$ cells/ml).

2.2.1.3 Cryopreservation and resuscitation

Cells were counted and resuspended in freezing medium (DMEM, 10% (v/v) FBS, and 10% (v/v) DMSO) at a density of between 1-2 $\times 10^6$ cells/ml. Cells were frozen in 1 ml aliquots in cryogenic vials. Tubes were stored in a -80˚C freezer overnight and transferred to a liquid nitrogen storage system for long term storage.

Cells were resuscitated by rapid thawing of the cell suspension in a 37˚C waterbath. Once fully thawed, the cell suspension was added to 6 ml of pre-warmed medium and centrifuged at 600 xg at room temperature for 5 min. 6 ml of supernatant was aspirated, and cells were gently resuspended in the remaining 1 ml of medium and transferred into a T25 flask.

2.2.1.4 Plasmid transfection

Transfections were carried out with jetPEI (Polyplus Transfection, llkirch-Graffenstaden, France) according to manufacturer's recommendations. DNA and jetPEI reagent were added to two separate tubes containing 150 mM NaCl solution, vortexed, and centrifuged briefly. NaCl solution containing the jetPEI reagent was added to the DNA solution, vortexed, and centrifuged. DNA/jetPEI mixture was left at room temperature for 15 min before being added to the cells. Volumes and DNA amounts used are as shown in Table 2.5.

Table 2.5   Optimised conditions for DNA transfection with jetPEI reagent.

Plate format	Surface area (cm^2)	Amount of DNA (µg)	Volume of jetPEI reagent (µl)	Total NaCl volume (µl)
4-well plate	2	0.25	0.5	50
6-well plate	10	1	2	200
15 cm plate	150	20	40	1000

2.2.1.5   siRNA transfection

siRNA transfections were carried out with jetPRIME (Polyplus Transfection, llkirch-Graffenstaden, France) according to manufacturer's protocol. Cells were plated in a total of 2 ml media in a 6-well plate. In a sterile tube, the required amount of siRNA (50-100 nM final concentration) was added to 200 µl of jetPRIME buffer, vortexed, and centrifuged briefly. 4 µl of jetPRIME reagent was added, vortexed, and centrifuged again. Solution was left for 10 min at room temperature, and added to the cells. Media was replaced 6 h after transfection and cells were left to grow for 24 to 48 h depending on depletion efficiency and the assay requirements. A list of siRNAs used in this study is shown in Table 2.6.

Table 2.6 siRNAs used in this study.

siRNA	Sequence	Reference/Source
siCTRL	AGU ACU GCU UAC GAU ACG G	Ambion
siIRS4-A	GGU CGU GUU UGU GAG GCU GAA	[52]
siIRS4-B	Beginning at position 354 (sequence not provided)	Predesigned, Sigma Aldrich
siCDC7-pool	-	SMARTpool, Dharmacon
siDBF4-pool	-	SMARTpool, Dharmacon

2.2.1.6   Stable isotope labelling of amino acids in cell culture (SILAC)

All SILAC reagents were obtained from Dundee Cell Products (Dundee, UK). Flp-In T-REx 293 Empty vector, DBF4B, and CDC7 WT cells were maintained in DMEM media containing unlabelled arginine and lysine (R0K0; light); ^{13}C labelled arginine and ^{2}H labelled lysine (R6K4; medium); and ^{13}C and ^{15}N labelled arginine and ^{13}C and ^{15}N labelled lysine (R10K8; heavy) respectively. All culture media was supplemented with 10% (v/v) dialysed FBS and 1% (v/v) Penicillin-Streptomycin solution. Cells were maintained in SILAC media for at least six passages over a two week period.

2.2.1.7   Cell synchronisation

2.2.1.7.1   Mimosine and nocodazole block

24 h after plating, cells were treated with 1 mM mimosine or 1 µM nocodazole (Sigma-Aldrich, Arklow, Ireland) for 19 h to arrest cells in G1/early S-phase or mitosis, respectively.

2.2.1.7.2   Mimosine block and release

24 h after plating, cells were treated with 1 mM mimosine. After 15 h, media was aspirated. Cells were washed once with prewarmed media. Fresh prewarmed media was carefully added onto the cells to minimise cell detachment from the culture plates.

2.2.2   Nucleic acid methods

2.2.2.1   Agarose gel electrophoresis

Depending on DNA fragment size to be analysed, agarose gels of between 1.0% to 2.0% (w/v) were prepared using electrophoresis grade agarose in 1X TAE buffer. Electrophoresis was carried out in 1X TAE buffer at 60-110V in the Mini

Horizontal Gel Units (Medical Supply Co. Ltd., Dublin, Ireland) until desired separation is achieved. Gels were stained by incubation with SYBR Safe (diluted 1:50,000 in 1X TAE buffer) for 30 min. Imaging was carried out on a Molecular Imager PharosFX Plus System (Bio-Rad).

2.2.2.2   Bacterial transformation using heat shock

Competent *E. coli* DH5α cells were thawed on ice. 50 ng of plasmid was added to 50 µl of competent cells. Cells were placed on ice for 20 min, heat shocked for 45 s at 42ºC, and placed back on ice for 2 min. 1 ml of prewarmed Luria-Bertani (LB; Sigma-Aldrich) media was added to the cells, and incubated in a shaking incubator at 37ºC for 1 h. Cell suspension was centrifuged (21000 x*g*, 1 min, 25ºC). 900 µl of supernatant was disposed of. Cells were resuspended in the remaining volume of media, and spread onto LB agar (Sigma-Aldrich) plates containing the appropriate antibiotics for selection. Plates were placed in a bacterial incubator at 37ºC for 16 h.

2.2.2.3   Plasmid amplification and purification

Using a sterile pipette tip, single colonies from the bacterial transformation were picked and expanded in 7 ml LB media in a shaking incubator at 37ºC for 16 h. Plasmids were purified from 5 ml of this culture using the GenElute Plasmid Miniprep Kit (Sigma-Aldrich) according to manufacturer's instructions. For maxipreps, 150 µl of the initial 7 ml culture was added to 150 ml LB media, and incubated at 37ºC for 16 h. Plasmid purifications were then performed using the GenElute HP Plasmid Maxiprep Kit (Sigma-Aldrich) according to manufacturer's instructions.

2.2.2.4   DNA sequencing

DNA sequencing was performed by Eurofins Genomics with the appropriate sequencing primers. Sequences were confirmed with at least 2 different reads.

2.2.3 Protein methods

2.2.3.1 Protein extract preparation for Sodium dodecyl sulphate – polyacrylamide gel electrophoresis

2.2.3.1.1 Total cell extract

Cell pellet was resuspended in 1x Laemmli sample buffer or lysis buffer. Cell suspension was sonicated in a Bioruptor(R) waterbath (Diagenode) on high setting for at least 10 cycles (30 s on, 15 s off). Waterbath was refilled with ice-cold water every 5 cycles.

2.2.3.1.2 Soluble and insoluble extract

Cell pellet was resuspended in lysis buffer and incubated on ice for 10 min. Samples were then centrifuged at 21,000 xg for 10 min at 4ºC, and the supernatant was used as soluble extract. Insoluble pellets were washed twice with lysis buffer and sonicated.

2.2.3.1.3 Trichloroacetic acid extraction

Culture medium was aspirated and the plates were placed on ice. Cells were detached with a cell scraper and 20% (v/v) trichloroacetic acid (TCA) in Milli-Q water was added directly to the plates. The suspension was transferred to tubes and the plates were washed once with 20% TCA. 2 volumes of 5% TCA was added to each tube, vortexed briefly, and centrifuged at 21,000 xg for 10 min. The supernatant was aspirated carefully and disposed of, and the pellet was resuspended in Laemmli sample buffer with 5-10 μl of 1 M Tris base to neutralise residual acid. Where required, samples were sonicated briefly to assist solubilisation of the protein pellet.

2.2.3.2 Determination of protein concentration

2.2.3.2.1 Bradford protein assay

The concentration of all protein samples that were prepared in compatible buffers were determined using the Bradford assay. A standard solution of bovine serum albumin (BSA) dissolved in the appropriate lysis buffer was used to prepare a standard curve from 1 to 5 μg/μl protein. 1 μl of sample was pipetted into one well of a 96-well plate and 180 μl of Bradford reagent was added. All standards and samples were prepared in triplicate. The plate was incubated at room temperature for 5 min. The absorbance at 590 nm (A_{590}) was measured using the Wallac 1420 VICTOR[3] multilabel plate reader (Perkin Elmer, Massachusetts, USA). A graph of A_{590} against concentration was plot in Microsoft Excel and used to calculate the protein concentration of each unknown sample.

2.2.3.2.2 Bicinchoninic acid protein assay

For protein samples incompatible with the Bradford assay, the Bicinchoninic acid (BCA) Protein kit (Thermo Scientific, Rockford, USA) was used instead. Assay was carried out according to manufacturer's instructions. A series of BSA protein dilutions were used to create a standard curve. The appropriate lysis buffer was used as a blank. An aliquot of 10 μl of each sample and standard were diluted in 200 μl of BCA working reagent (50:1 solution A: solution B). The plate was incubated at 37ºC for 30 minutes. After cooling down to room temperature, the absorbance at 562 nm was measured and sample concentrations were calculated as described for the Bradford assay.

2.2.3.3 Sodium dodecyl sulphate-polyacrylamide gel electrophoresis

Protein lysates were separated by sodium dodecyl sulphate - polyacrylamide gel electrophoresis (SDS-PAGE) using the Mini-Protean® 3 Cell System (Bio-Rad). SDS-PAGE gels of the desired acrylamide-bisacrylamide content (concentrations

between 6-15% were used) were prepared according to Table 2.7. 10-30 μg of protein was mixed with the required volumes of water and 5X Laemmli sample buffer. Prior to loading, samples were heated to 95°C for 3 min in a heat block and centrifuged briefly. PageRuler Plus Prestained Protein Ladder (Thermo Scientific, Rockford, USA) was loaded in adjacent wells. Gel running tank was filled with SDS-PAGE running buffer and electrophoresis was carried out at 60-100V until the desired separation was reached.

Table 2.7 *SDS-PAGE gel recipes. Resolving gels were prepared with Tris-HCl pH 8.8, and stacking gels with pH 6.8. All volumes are in ml.*

	Resolving gel					Stacking gel
Acrylamide content	**6%**	**7.5%**	**10%**	**12.5%**	**15%**	**4%**
Water	4.10	3.60	2.76	1.93	1.10	3.61
30% Acrylamide/Bis-acrylamide, 37.5:	2.00	2.50	3.33	4.17	5.00	0.67
1M Tris-HCl pH 8.8 / 6.8	3.75	3.75	3.75	3.75	3.75	0.625
10% SDS	0.100	0.100	0.100	0.100	0.100	0.050
10% APS	0.050	0.050	0.050	0.050	0.050	0.025
TEMED	0.005	0.005	0.005	0.005	0.005	0.005
Total volume	10 ml					5 ml

2.2.3.4   Protein transfer

SDS-PAGE gels were soaked in transfer buffer for 5 minutes. Protran nitrocellulose membrane, with 0.2 μm pore size (GE Healthcare, Amersham, UK) was used. Sponge pads and filter paper were also soaked briefly in cold SDS-PAGE transfer buffer. The transfer cassettes were assembled with the nitrocellulose membrane on the cathode side and the SDS-PAGE gel on the anode side. Two sheets of filter paper were placed on either side of the membrane and gel, and the entire assembly was sandwiched between two foam pads in a gel holder cassette. The Mini Trans-Blot Cell System (Bio-Rad) transfer apparatus was assembled, an ice-pack was placed in the tank and the apparatus was filled with cold transfer buffer. Transfer was carried out at 250 mA for 2-3 h depending on protein size and gel acrylamide content. Transfer efficiency was checked by Ponceau S staining. Ponceau stain was removed from the membrane with several washes with PBS.

2.2.3.5 Phos-tag SDS-PAGE

5% SDS-PAGE gels supplemented with 5 μM Phos-tag acrylamide (Wako Pure Chemical Industries, Osaka, Japan) and 10 μM $MnCl_2$ were prepared. Samples were prepared as described for standard SDS-PAGE. Protein ladders were not used as they contain EDTA, which chelates Mn^{2+} and interferes with separation. Mock samples (with lysis buffer and Laemmli sample buffer) were loaded in empty lanes adjacent to samples, and in lanes between samples with different buffer compositions. Electrophoresis was carried out at 15 mA until the dye just runs off the bottom. Gels were soaked in transfer buffer supplemented with 10 mM EDTA for 30 min at room temperature to chelate Mn^{2+}, and washed three times with transfer buffer without EDTA for 10 min each. Protein was transferred onto nitrocellulose membrane at 150 mA for 18 h at 4ºC, and immunoblotting was carried out with the appropriate antibodies.

2.2.3.6 Immunoblotting

Free protein-binding sites were blocked by incubation with 3% (w/v) Marvel non-fat powdered milk (Premier Foods, UK) in PBS for 1 h at room temperature on a platform shaker. For Western blotting with primary antibodies against phosphoproteins or low abundance proteins, blocking solution with 1% to 5% (w/v) BSA was used instead.

Membranes were incubated with primary antibodies (see Table 2.2 for dilutions) in blocking solution (supplemented with 0.05% Tween 20) for 1 h at room temperature or overnight at 4˚C. Membranes were washed three times with PBS-T (PBS containing 0.05% Tween 20) for 5 min each to remove unbound antibody. Membranes were then incubated with the appropriate fluorescently-conjugated IRDye secondary antibodies (see Table 2.3) for 1 h at room temperature. Unbound antibody was removed by two washes with PBS-T and one wash with PBS, for 5 min each. Immunoreactive bands were visualised and quantified using an Odyssey Infrared Imaging System and Image Studio software (LI-COR Biosciences, NE, USA). Where required, normalisation was performed against a suitable loading control such as β-actin or GAPDH.

2.2.4 Protein purification

2.2.4.1 Nuclear protein isolation

Cells were detached by scraping and collected by centrifugation (1000 xg, 10 min, 4ºC). Cells were washed with PBS to remove residual media, followed by two washes with hypotonic Buffer A-H. Cells (~30x10^6 HEK293 from a 15 cm tissue culture dish at 80% confluency) were resuspended in 500 µl Buffer A-H and left to swell on ice for 20 min. One volume of lysis Buffer A-L was added, and the solution was vortexed briefly. Cells were returned to ice while the extent of cell lysis was checked by light microscopy of a small volume on a glass slide. Nuclei was collected by centrifugation (800 xg, 5 min, 4ºC) and washed with Buffer A-H. Supernatant (cytoplasmic fraction) was collected as required.

2.2.4.2 Benzonase extraction of chromatin-bound proteins

Nuclei were resuspended in 600 µl Tris lysis buffer containing Benzonase nuclease (0.25 U/µl; Sigma-Aldrich, Arklow, Ireland), and incubated at 4ºC with end-over-end rotation for 30 min. Extract was clarified by centrifugation (21,000 xg, 10 min, 4ºC).

2.2.4.3 Total soluble cell extract preparation

Cell pellets were resuspended in IP buffer containing protease and phosphatase inhibitor cocktails (Thermo Scientific, Rockford, USA), incubated on ice for 10 min, and clarified by centrifugation (21,000 xg, 15 min, 4ºC). Concentration of protein in the extract was determined by Bradford or BCA assay depending on compatibility of the IP buffer (see Section 2.2.3.2).

2.2.4.4 Strep-Tactin purification

2.2.4.4.1 Batch purification

Clarified extract was applied to Strep-Tactin Sepharose resin (IBA, Göttingen, Germany) pre-washed with IP buffer, and incubated with end-over-end

rotation for 2 h at 4ºC. Elutions were performed with IP buffer containing 10 mM biotin, or with 2x Laemmli sample buffer (3 min, 95ºC).

2.2.4.4.2 Column purification

Before use, Gravity flow Strep-Tactin Sepharose columns (0.2 ml bed volume; IBA) were equilibrated with 2 ml immunoprecipitation (IP) buffer. Protein extracts (prepared according to Section 2.2.4.3) were applied to the columns and allowed to pass through completely. At least 10 mg of protein at a concentration of 10 mg/ml was used for each purification. Columns were washed four times with 1 ml IP buffer. Protein was eluted by the application of IP buffer with 10 mM biotin and collected in six 100 µl fractions. Elution fractions were monitored for the presence of Strep-tagged proteins by Western blotting.

2.2.4.5 Immunoprecipitation

Typically 1 mg of protein extract was used per IP. Extracts were pre-cleared by incubation with 25 µl packed volume of Protein A or Protein G Resin (GeneSpin, Lombardy, Italy) for 1 h at 4ºC. 1-2 µg of antibody was bound to 25 µl of resin in a separate tube (1 h, 4ºC). Unbound antibody was removed by two washes with IP buffer. Pre-cleared extract was applied to antibody-bound resin and incubated with end-over-end rotation for 2 h at 4ºC. Beads were collected by centrifugation (450 x*g*, 2 min, 4 ºC), and washed five times with 500 µl IP buffer. Protein was eluted with 2x Laemmli sample buffer (3 min, 95ºC).

2.2.5 Immunofluorescence

2.2.5.1 Poly-L-lysine coating of coverslips

0.1 mg/ml poly-L-lysine (PLL) solution was prepared in sterile distilled water. Solution was pipetted onto sterile glass coverslips and incubated at 37ºC for at least 1 h. PLL solution was aspirated, and coverslips were rinsed with sterile water and allowed to air dry before cells were plated.

2.2.5.2　　　Pre-extraction and formaldehyde fixation of cells

Culture media was aspirated and cells were fixed by the addition of freshly prepared 4% (w/v) PFA (paraformaldehyde) in PBS for 10 min at room temperature. Where required, soluble proteins were pre-extracted on ice for 5 min with ice-cold PTEM or HPEM buffers prior to fixation.

2.2.5.3　　　Indirect immunofluorescence staining

All steps were performed at room temperature unless otherwise stated. Cells that had not been pre-extracted were permeabilised with PBS with 0.5% Triton X-100 (PBS-TX) for 5 min. Blocking was typically performed with 3% (w/v) BSA in PBS-TX (0.1%) for 30 min. Primary antibodies were diluted in blocking buffer and incubated with cells for 1 h in a humidified chamber (for dilutions see Table 2.2). Cells were washed 3 times with PBS-TX (0.1%) for 5 min each, and then incubated with secondary antibodies for a further 1 h in the dark (Table 2.3). Cells were washed 3 times with PBS-TX (0.1%), once with PBS, and rinsed with distilled water. Coverslips were left to air dry, mounted onto glass slides with Slowfade Gold (Thermo Fisher Scientific, Leicestershire, UK), and the edges were sealed with clear nail polish. Slides were protected from light and stored at 4ºC.

2.2.5.4　　　Labelling of nascent DNA by EdU incorporation

To visualise nascent DNA, cells were treated with 10 μM EdU for 15 min. For multiple immunofluorescence labelling, permeabilisation, blocking, and primary antibody incubations steps were performed as described. After washing to remove unbound antibody, Click reaction solution (10 μM 6-carboxyfluorescein TEG-azide or azide-fluor 545, 10 mM sodium-L-ascorbate, 2 mM $CuSO_4$) was pipetted onto the coverslips and incubated for 30 min in a dark humidified chamber. Cells were washed twice with PBS-TX (0.1%) and once with blocking solution, followed by incubation with secondary antibodies.

2.2.5.5 Microscopy

Images were captured using a DeltaVision Core system (Applied Precision) controlling an interline charge-coupled device camera (Coolsnap HQ2; Roper Technologies) mounted on an inverted microscope (IX-71; Olympus). Images were collected at 2x binning using a 60x or 100x oil objective. Z-series were collected using 0.2 μm intervals. Images were deconvolved and maximum intensity projected for presentation purposes using SoftWoRx (Applied Precision). All quantification procedures described were performed on single optical sections.

2.2.6 Flow cytometry

2.2.6.1 Ethanol fixation

Cells were collected by trypsinisation, washed with cold PBS and counted (Section 2.2.1.2). 5×10^5 cells were resuspended in 300 μl PBS, and 700 μl ethanol was added drop-wise while vortexing to fix (final concentration 70% ethanol). Samples were stored at -20ºC until processed for flow cytometry analysis.

2.2.6.2 DNA content analysis by propodium iodide staining

500 μl PBS was added to ethanol fixed cells, and vortexed briefly to mix. Samples were centrifuged (2000 xg, 5 min, 4ºC) and supernatant was discarded. Cells were resuspended in 500 μl propidium iodide (PI)/RNase A solution (BD Biosciences) and incubated in the dark for 30 min at room temperature. Samples were processed on a FACSCanto A instrument (BD Biosciences). 10,000 events were recorded for each sample. Results were exported and analysed on FlowJo X software.

2.2.7 Chromatin Immunoprecipitation (ChIP)

2.2.7.1 Cell plating

$8x10^6$ Flp-In T-REx 293 cells were plated in 15 cm tissue culture dishes and allowed to recover for 24 h. Doxycycline (1 μg/ml) was added to induce DBF4 expression, and cells were harvested 24 h after induction.

2.2.7.2 Dual cross-linking for chromatin immunoprecipitation

Cells growing on plates were washed once with cold PBS, and detached by trypsinisation (3 min, room temperature). Cells were pelleted by centrifugation (2000 xg, 5 min, 4ºC), and washed once with 20 ml cold PBS. At this point, cell numbers were determined (Section 2.2.1.2). Cells were pelleted by centrifugation, and resuspended in 20 ml room temperature PBS with 1.5 mM EGS (ethylene glycol bis(succinimidyl succinate). A 25 mM stock solution of EGS in DMSO was prepared fresh on day of use. Cells were placed on a tube roller for 25 min at room temperature. 610 μl of 37% PFA was added (final concentration of 1%), the tube was inverted gently several times to mix, and placed on the tube roller for a further 10 min. Fixation was quenched by the addition of glycine (final concentration 50 mM) and incubation for 10 min at room temperature. Cells were pelleted by centrifugation and the supernatant was disposed of.

2.2.7.3 Chromatin fragmentation by micrococcal nuclease (MNase) digestion

Cell pellet was resuspended in ChIP buffer A (1 ml/15 cm plate used) and incubated on ice for 15 min. Cells were pelleted (3000 xg, 3 min, 4°C) and incubated sequentially with the same volume of ChIP buffer B and ChIP buffer C on ice for 5 min each. This results in membrane lysis and allows separation of nuclei. Nuclei were then aliquot into 1.5 ml microfuge tubes ($5x10^6$/tube), centrifuged (3000 xg, 3 min, 4°C), and resuspended in 250 μl MNase digestion buffer. 5U MNase (Life Technologies; diluted to 1U/μl in MNase digestion buffer) was added to each tube, and tubes were placed in a 37°C water bath for 20 min, inverted to mix every 5 min.

MNase was inactivated by the addition of 20 mM EGTA and 5 min incubation on ice. Nuclei were pelleted by centrifugation (9000 x*g*, 5 min, 4°C) and resuspended in 200 µl ChIP IP buffer. Nuclei were lysed by sonication in a Bioruptor water bath (Diagenode) on High setting for 5 cycles (30 s on, 15 s off). Extract was centrifuged (16,000 x*g*, 10 min, 4°C) and 200 µl supernatant was transferred to a fresh tube. An aliquot of each extract was kept as the ChIP input sample.

2.2.7.4 Chromatin Immunoprecipitation (ChIP)

Extracts were diluted with 400 µl ChIP IP buffer (1:3 dilution), antibodies were added (amounts of each antibody used listed in Table 2.2), and incubated with end-over-end rotation at 4°C for 16 h. ChIP-grade Protein A/G Magnetic beads (Life Technologies, Cat: 26162; and Merck Millipore, Cat: 16-663) were added for 2 h to recover antibody complexes. Beads were separated on a magnetic tube rack and washed 5 times with 1 ml ChIP IP buffer, once with LiCl wash buffer, and once with TE buffer. Elution was performed with 150 µl ChIP elution buffer on a Thermomixer (Eppendorf) at 65°C for 45 min. Elutions and 2% Input samples were then incubated on a Thermomixer at 65°C for 18 h to reverse cross-links. DNA was recovered using a PCR purification kit (Qiagen, Cat: 28104) according to manufacturer's instructions, and eluted in a volume of 100 µl.

2.2.7.5 Quantitative PCR (qPCR)

All primers were synthesised by Sigma Aldrich. Primer sequences were selected to amplify a 201 b.p. centromeric sequence specific to chromosome 1 [198] (Cent1-F: GGCCTATGGCAGCAGAGGATATAACTGCC, Cent1-R: GTGAGTTT TCTCCCGTATCCAACGAAATCC), a 171 b.p. centromeric α-satellite sequence [199] (αSat-F: CATCACAAAGAAGTTTCTGAGAATGCTTC, αSat-R: TGCATTCAACTCACAGAGTTGAACCTTCC), and a 165 b.p. non-centromeric sequence corresponding to the GAPDH promoter (sequences provided by Life Technologies; GAPDH-F: TACTAGCGGTTTTACGGGCG, GAPDH-R: TCGAACAGGAGGAGCAGAGAGCGA).

Analysis was performed on a StepOnePlus Real-Time PCR System (Applied

65

Biosystems) with standard cycling conditions (initial denaturation: 95ºC, 2 min; denaturation: 95ºC, 15 sec; annealing/extension: 60ºC, 1 min). All reactions were prepared in triplicate, and three biological repeats were performed for each experiment. Amounts of each target sequence was determined with the comparative C_T method relative to the 2% Input sample using the formula: Percent input = 2% x $2^{[C_T(\text{Input}) - C_T(\text{Sample})]}$. Graphs and statistics were performed using GraphPad Prism (GraphPad Software). A 1x PCR reaction was as shown in Table 2.8.

Table 2.8 *qPCR reaction setup. Volumes are for one reaction of 10 μl.*

Reagent	Volume (μl)
2x SYBR Green Master Mix (Sigma, S4438)	5.0
100x ROX (passive reference dye)	0.1
Forward primer (10 μM)	0.3
Reverse primer (10 μM)	0.3
Input/Elution sample	2.0
Nuclease-free water	2.3
Total volume	10.0

Chapter 3: Characterisation of Flp-In T-Rex 293 cell lines for the inducible expression of CDC7 kinase subunits

3.1   Introduction

In order to elucidate novel roles of CDC7 kinase in the cell cycle, we set out to identify novel interacting proteins of each of the kinase subunits — CDC7, DBF4, and DBF4B — using an unbiased biochemical approach. We expect that immuno- and/or affinity purification coupled with mass spectrometric identification of interacting proteins might reveal previously unknown functions of CDC7 kinase. Given the lack of suitable reagents and the low levels of endogenous protein, we generated stable cell lines using the Flp-In T-REx 293 system (Invitrogen) to conditionally express epitope-tagged forms of the individual subunits to aid in their detection and purification. These cell lines are critical for much of the work presented in this thesis, and as such, a brief description of their generation and main features are included here.

3.2   Generation of stable cell lines for conditional expression of CDC7 kinase subunits

The Flp-In parental cell line (generated as described in the following paragraph) was obtained from Invitrogen. The subsequent establishment of Flp-In cell lines for the inducible expression of CDC7 kinase subunits (also described later) was performed by Gemma O'Brien and Michael Rainey.

HEK-293 cells were first transfected with a pFRT/lacZeo vector which contains a flippase recognition target (FRT) site fused immediately upstream of a Zeocin resistance gene (lacZ-Zeocin), under the control of the SV40 early promoter (pSV40). An ATG start codon is also present after the promoter (pSV40/ATG/FRT/lacZ-Zeocin). Transfected cells which were Zeocin-resistant

were then screened to identify those with a single FRT site integration. These were next transfected with the pcDNA6/TR vector which expresses the Tet repressor (TetR) controlled by a CMV promoter (pCMV), and a Blasticidin resistance gene. The Flp-In T-REx 293 host cell line is therefore established through the independent integration of these two vectors.

To facilitate Flp/FRT-mediated integration into the host cell line, a gene of interest (along with tandem FLAG and Twin-Strep epitope tags fused to the C-terminal) is cloned into a pcDNA5/FRT/TO expression vector, downstream of pCMV and two TetO2 operator sequences (which allow binding of TetR and repression of target gene expression). The plasmid also contains a FRT site fused to a Hygromycin resistance gene lacking an ATG start codon. Co-transfection of pcDNA5/FRT/TO and pOG44 (expressing the Flp recombinase) allows homologous recombination between the FLP sites, resulting in the genomic integration of the gene of interest. Successful integration results in resistance to Hygromycin and sensitivity to Zeocin, as the ATG is no longer proximal to lacZ-Zeocin. Clonal cell lines were then established from the resulting Hygromycin and Blasticidin-resistant cells. Expression of the integrated gene is only induced in the presence of tetracycline antibiotics (such as doxycycline) which bind to TetR, thus preventing its binding to TetO$_2$. This process is summarised in Figure 3.1.

At the outset of this project, clonal cell lines with conditional expression of wild type CDC7 (CDC7 WT), kinase-dead CDC7 (CDC7 KD), DBF4, DBF4B, and a vector only control (Empty vector; EV) had already been established according to the process described above. For brevity we refer to these cell lines as T-REx–EV, –CDC7 WT, –CDC7 KD, –DBF4, and –DBF4B throughout the text.

CDC7 KD is inactive due to a mutation of the conserved lysine to an alanine (K90A) within its phosphate-binding loop [147,200]. Since it is unable to complete its catalytic cycle, interactions with its substrates, which are usually transient, might be stabilised and in some cases this has been reported to increase the likelihood of their co-purification [201].
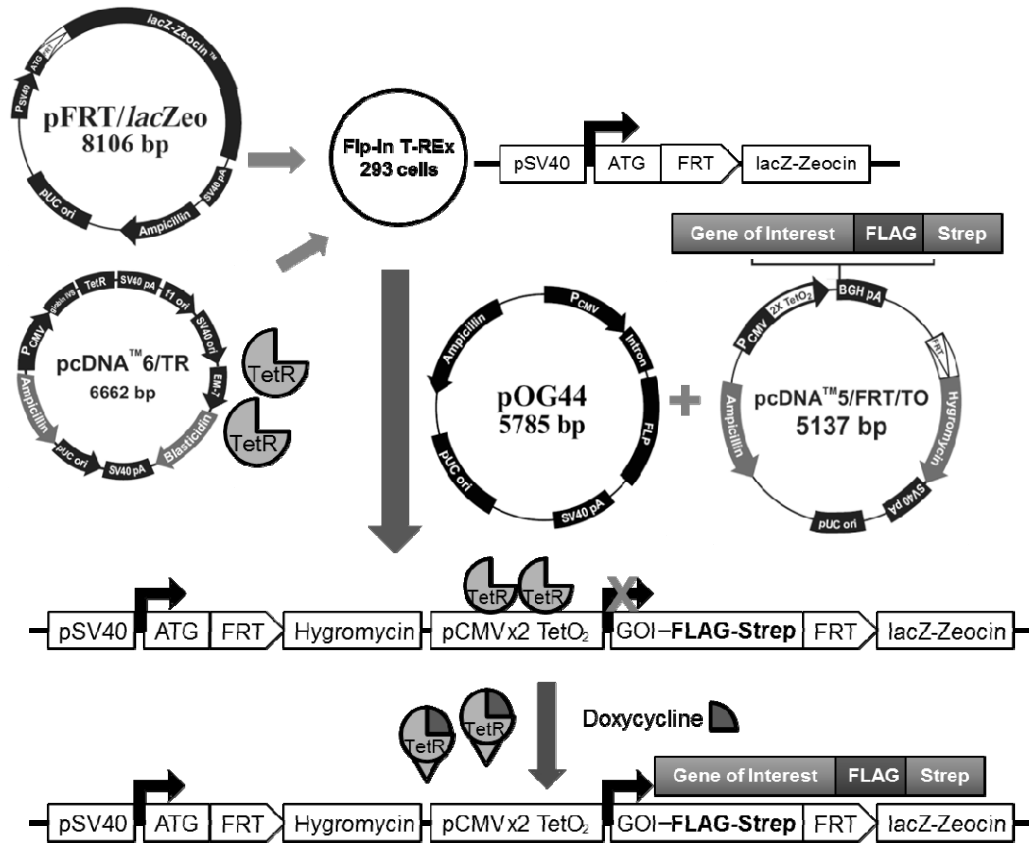
Figure 3.1 Establishment of Flp-In T-REx 293 cell lines as a system for the inducible expression of genes of interest. *pFRT/lacZeo and pcDNA6/TR were integrated into parental HEK 293 cells to establish the host Flp-In T-REx 293 cell line. Co-transfection of pOG44 (coding for FLP recombinase) and pcDNA5/FRT/TO (with the Gene of Interest, GOI) results in stable integration of the GOI. GOI expression is induced by the addition of doxycycline. For additional details see text. Figure contributed by Michael Rainey.*

3.3 Effects of doxycycline and dose-dependency of inducible gene expression

Doxycycline belongs to the tetracycline family of antibiotics, and while commonly used in inducible gene expression systems, it has been reported to impair proliferation in some cell lines through off-target effects on gene expression and metabolism [202]. To ensure that doxycycline alone does not impact on cell proliferation, we treated T-REx–EV cells with increasing concentrations of

doxycycline of up to 2 μg/ml. Neither the cell number nor the viability was affected following 72 h of treatment with any of the tested doses (Fig. 3.2 A).
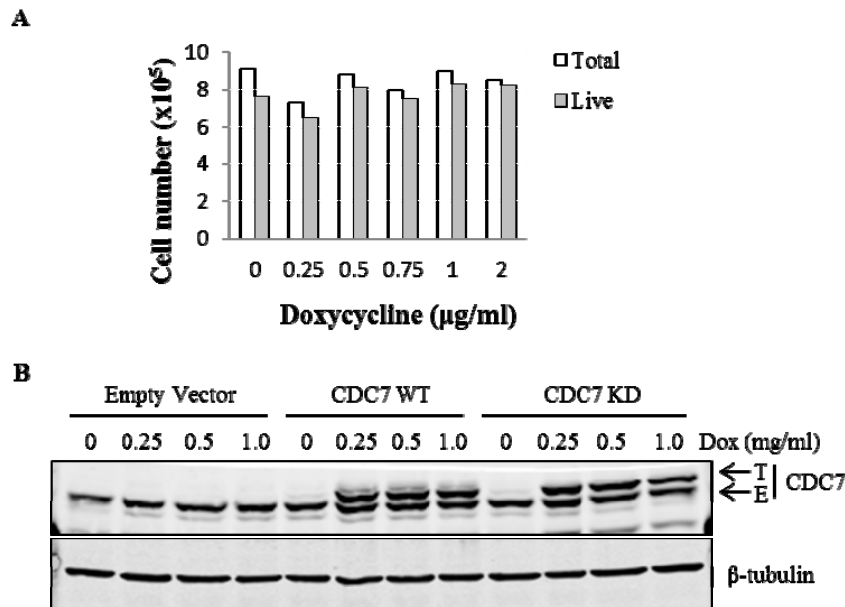
Figure 3.2 Doxycycline-induced expression of tagged CDC7 in Flp-In T-REx 293 cells. *(A) Empty Vector cells were treated with a range of doxycycline concentrations for 72 hours. Cell numbers and viability were determined by Trypan blue exclusion. (B) Cells were treated with the indicated doses of doxycyline for 24 hours. The expression of tagged CDC7 WT and KD was analysed by immunoblotting. Proteins tagged on the C-terminus with tandem FLAG-Twin Strep-tag (T) were detected as slower migrating forms relative to endogenous CDC7 (E).*

To determine if the expression of tagged protein using this cell system is dose-dependent, T-REx–CDC7 WT and –CDC7 KD cell lines were treated with doses of between 0.25 to 1 μg/ml doxycyline for 24 h, and the levels of CDC7 in the cell extracts were examined by immunoblotting with a CDC7 antibody. Due to the presence of the epitope tags, the higher molecular weight of inducibly-expressed CDC7 causes it to run as a distinct band just above that of endogenous CDC7 (Fig 3.2 B). At the lowest dose tested (0.25 μg/ml), expression of tagged CDC7 was comparable to the level of endogenous protein, and this was not increased at the higher doses. The half-life of doxycycline in cell culture medium is about 24-48 h

(T-REx manual, Invitrogen, https://goo.gl/fx8zsx, accessed on 24-09-15), so a dose of 1 μg/ml was used for all further experiments, as this should be sufficient to maintain the same level of gene expression for at least 72 h without the need for repeated addition of doxycycline.

3.4 Cellular effects of CDC7 kinase subunit overexpression

Since CDC7 kinase activity is tightly regulated in the cell cycle, we investigated if the increased expression of CDC7 subunits through the constitutive CMV promoter would affect cell proliferation, viability, or DNA content. Each of the T-REx cell lines was treated with doxycycline to induce the expression of individual tagged CDC7 kinase subunits, and samples were collected at 0, 24, 48, and 72 h post-induction. At each time point, cells were counted, cell viability was determined by Trypan blue exclusion, DNA content was analysed by flow cytometry, and protein extracts were prepared and subjected to immunoblotting.

Overexpression of either tagged CDC7 WT or CDC7 KD for up to 72 h did not impact on cell numbers, viability, or DNA content compared to control T-REx-EV cells (Fig. 3.3. A, B). To determine if tagged CDC7 was forming an active complex with DBF4 or DBF4B *in vivo*, we monitored the phosphorylation of MCM2 at S40/S41, a known CDC7-dependent site, as a marker for CDC7 kinase activity [155]. Immunoblotting with a specific MCM2 pS40/41 antibody showed that expression of either tagged CDC7 WT or KD did not alter total cellular kinase activity (Fig. 3.3 C). This suggests that the levels of its regulatory subunits are limiting in cells.
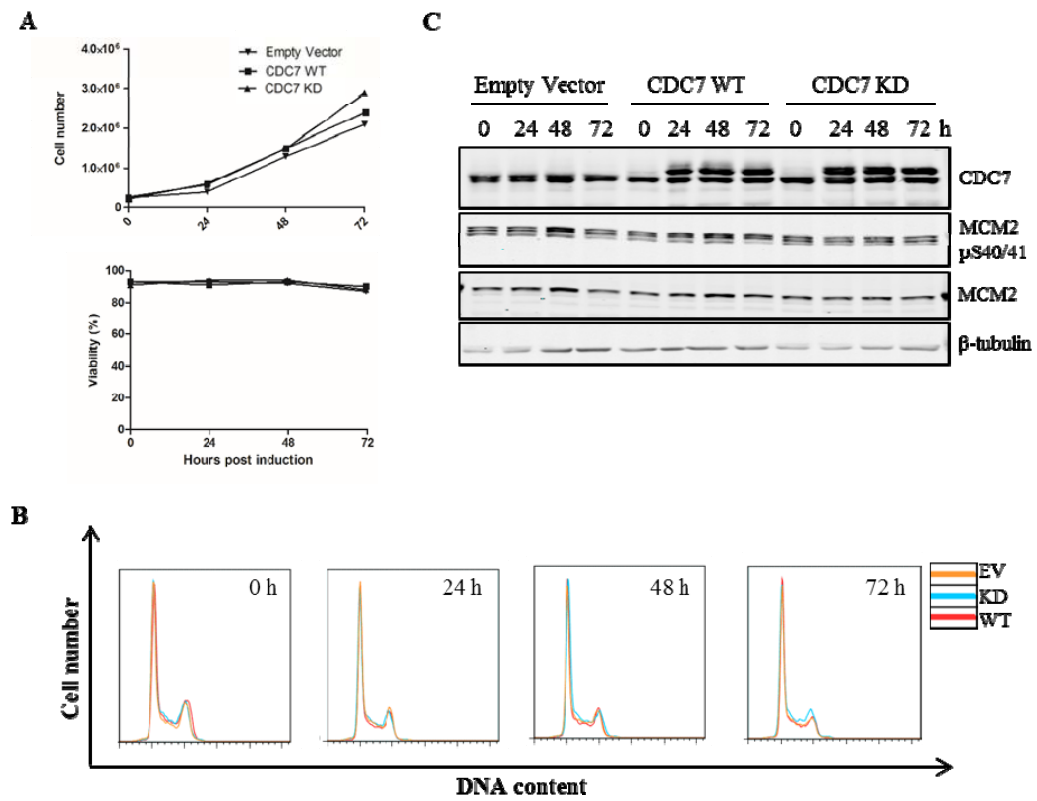
Figure 3.3 Inducible expression of CDC7 WT or KD does not affect cell proliferation. *T-REx-EV, CDC7 WT (wild type) and KD (kinase-dead) cells were treated with 1 μg/ml doxycycline and analysed at 24 h intervals for (**A**) cell number and viability and (**B**) DNA content by flow cytometry. (**C**) Protein extracts were also prepared and analysed by immunoblotting with the antibodies indicated. This experiment was performed once.*
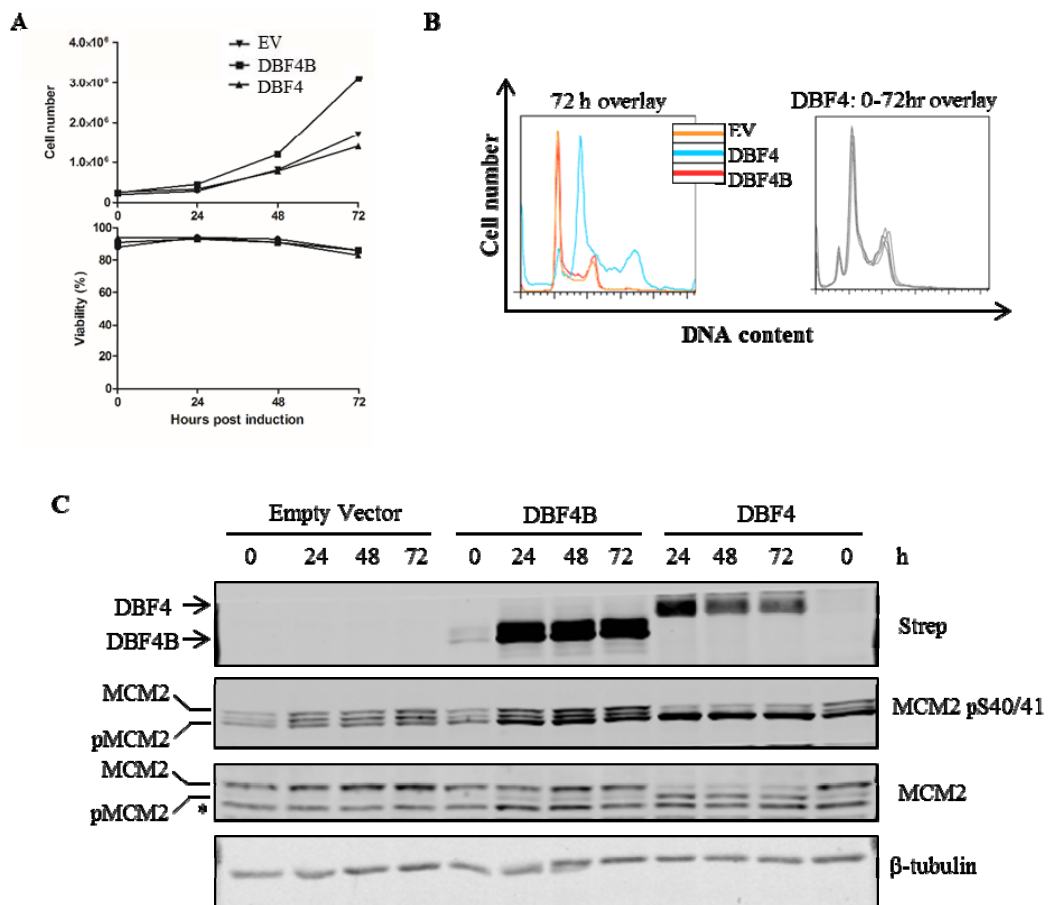
Figure 3.4 T-REx 293 cells continue to proliferate with induced expression of DBF4 and DBF4B. *T-REx-EV (Empty Vector), DBF4, and DBF4B cells were treated with 1 μg/ml doxycycline and analysed at 24 h intervals for (**A**) cell number and viability and (**B**) DNA content by flow cytometry. (**C**) Protein extracts were also prepared and analysed by immunoblotting with the antibodies indicated. MCM2 immunoreactive bands with lower apparent molecular weights correspond to more highly phosphorylated forms of MCM2. Phosphorylation of MCM2 at multiple sites (in addition to S40/41) contributes to the mobility shift observed. Asterisk indicates a cross-reactive band. This experiment was performed once.*

Expression of either tagged DBF4 or DBF4B also did not affect the proliferation or viability of T-REx cells (Fig. 3.4 A). The DNA content profile of DBF4B expressing cells was identical to Empty Vector cells (Fig. 3.4 B). It should be noted that although the profile of cells expressing tagged DBF4 is shifted to the

right indicating increased DNA content, new clonal T-REx-DBF4 cell lines that were subsequently generated in the lab did not exhibit this polyploid phenotype (not shown) - suggesting that this is likely to be an artifact that occurred during clonal expansion of this particular cell line. These new cell lines have also been characterised in a similar manner as described here, and one was selected for use in subsequent experiments described. Interestingly, tagged DBF4 and DBF4B expression did not have equivalent effects on MCM2 phosphorylation, even though DBF4 and DBF4B are expressed at comparable levels as detected by immunoblotting with the anti-Strep antibody. While both resulted in increased pS40/41, in DBF4 expressing cells, almost all the MCM2 is shifted to the faster migrating (and more highly phosphorylated) form, and this is detectable using both the phospho-specific and total MCM2 antibodies (Fig. 3.4 C). This mobility shift is observed to a much lesser extent in DBF4B expressing cells.

3.5   Localisation of CDC7, DBF4, and DBF4B by immunofluorescence

Consistent with their described roles, all three CDC7 kinase subunits have been reported to be nuclear proteins. In the case of CDC7 and DBF4, the residues required for their nuclear localisation and/or retention have already been identified [148,203-205]. Although the corresponding nuclear localisation sequences (NLS) in DBF4B have not yet been characterised, studies also indicate that it is nuclear localised [140,141]. Since the addition of epitope tags can sometimes affect the proper localisation and/or function of some proteins, we examined the subcellular localisation of CDC7 kinase subunits by indirect immunofluorescence with an antibody against the Strep-tag. As expected, the tagged CDC7 WT, KD, and DBF4 subunits were all detected in the nucleus of T-REx 293 cells. Surprisingly, DBF4B was found predominantly in the cytoplasm in a diffuse pattern (Fig. 3.5).
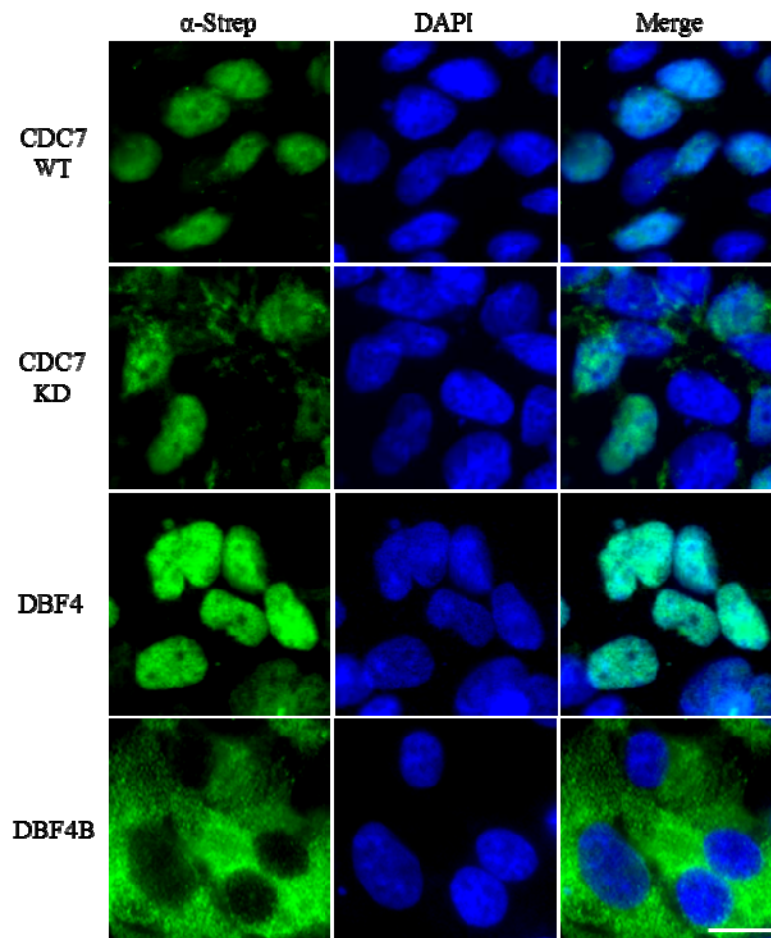
Figure 3.5 Localisation of CDC7 kinase subunits in Flp-In T-REx 293 cells. Expression of epitope–tagged proteins was induced by treatment with 1 µg/ml doxycycline for 24 h. Cells were fixed with 4% PFA and processed for immunofluorescence with anti-Strep-tag antibody. Results are representative of at least 2 independent experiments. Scale bar = 20 µm.

The strong cytoplasmic staining of DBF4B could be masking the detection of a smaller pool that might be present in the nucleus. To determine if DBF4B is being shuttled between the nucleus and cytoplasm, we used Leptomycin B (LMB), which inhibits CRM1/Exportin-1, the major nuclear export receptor in cells [206]. We proceeded to use U2OS cells for this experiment as they are more strongly adherent than T-REx 293, and are also flat, with a large cytoplasm to nucleus ratio [207]. Additionally, we also used a GFP-tagged DBF4B protein to avoid potential artifacts

of antibody-based detection. We transfected U2OS cells with a plasmid encoding DBF4B-GFP, and treated the cells with LMB. Detection was performed through direct observation of GFP fluorescence. In the majority of control-treated cells, DBF4B-GFP was confined to the cytoplasm (Fig. 3.6, top row), similar to the localisation of DBF4B-FLAG-Strep observed in T-REx cells (Fig. 3.5). Upon LMB treatment, DBF4B-GFP was detected within the nuclei of most cells (Fig. 3.6, bottom row). It is important to note, however, that nuclear DBF4-GFP was also observed in a small number of control-treated cells (Fig. 3.6, indicated by white arrows).
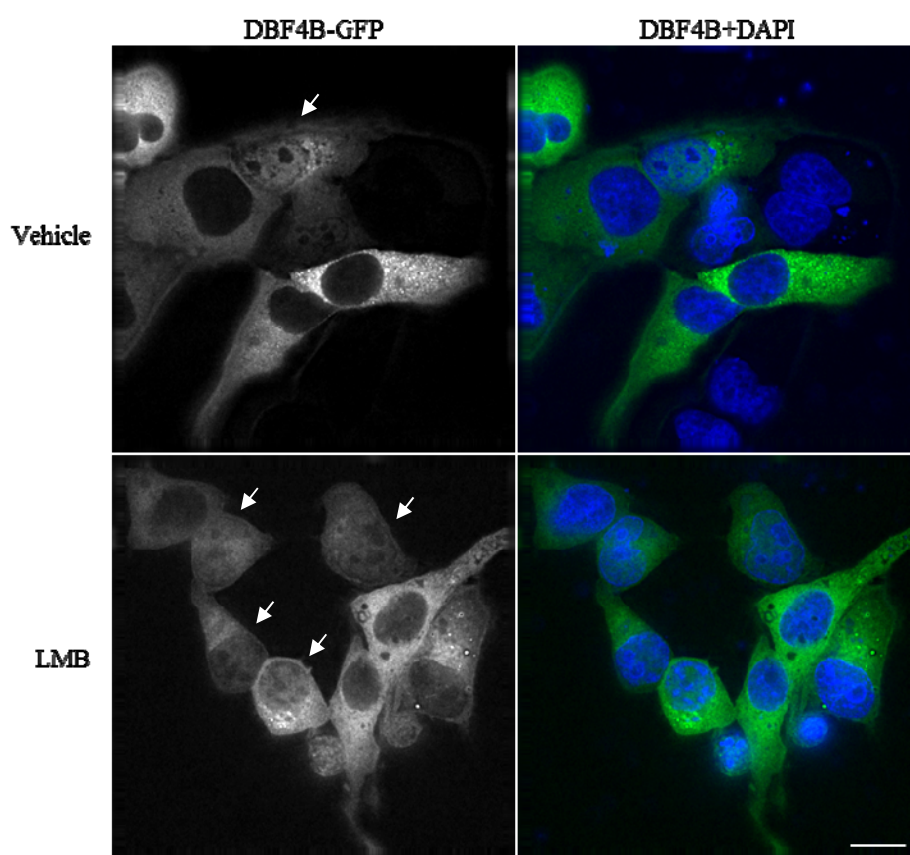
Figure 3.6. **DBF4B is exported from the nucleus in a CRM1-dependent manner.** *U2OS transiently transfected with DBF4B-GFP were treated with Leptomycin B (LMB; 40 nM) or vehicle control for 6 hours prior to fixation. Arrows indicate cells with nuclear localization of DBF4B-GFP. Experiment was performed twice with similar results. Scale bar = 20 μm.*

A

CDC7 (α-Strep) DAPI DBF4B-GFP DAPI

B

CDC7 (α-Strep) DBF4B-GFP DAPI Merge+DAPI
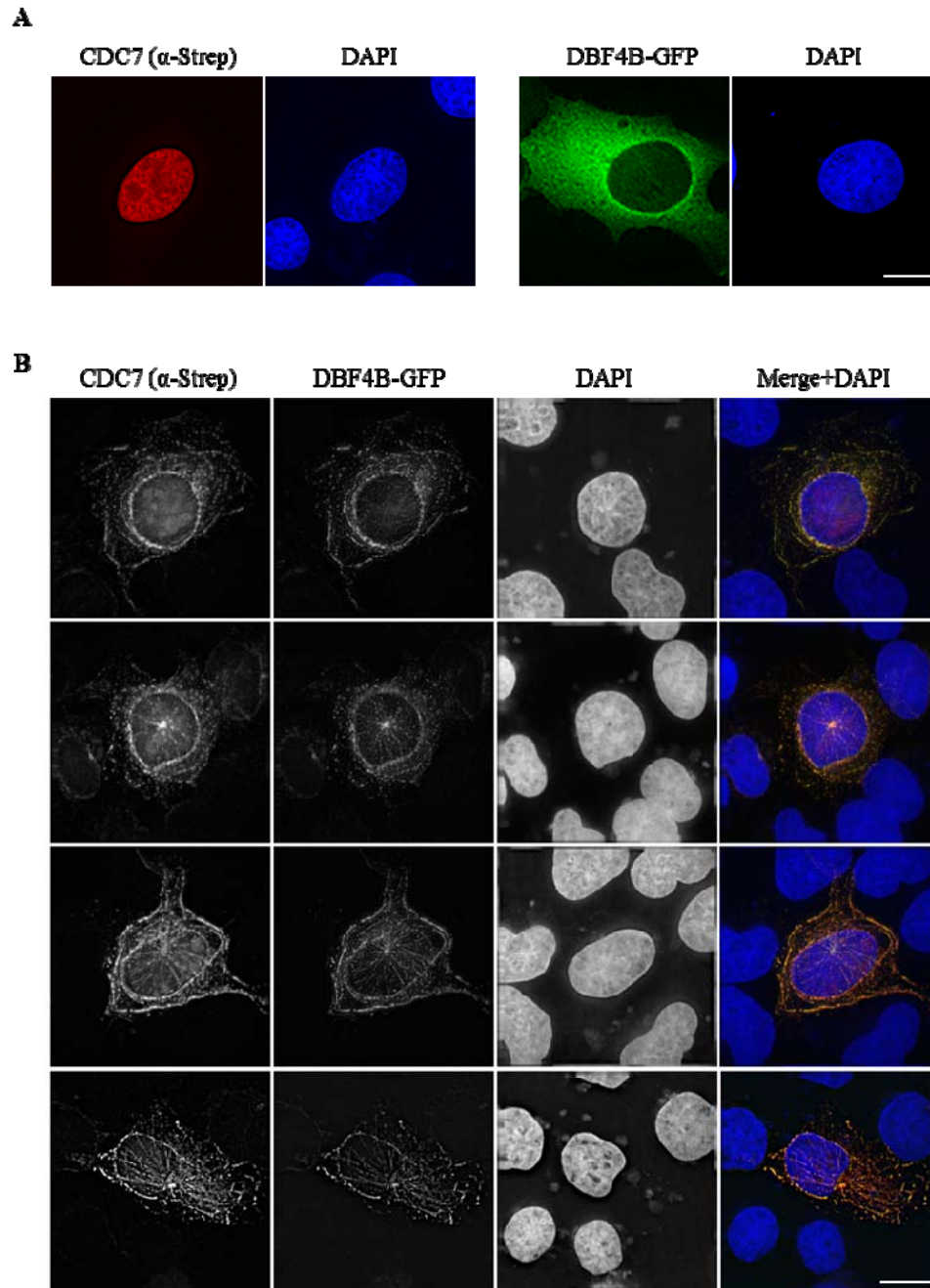
Figure 3.7. **Co-expression of CDC7 and DBF4B reveals novel cytoskeletal localisation.** *Tagged CDC7 and DBF4B were (**A**) overexpressed singly or (**B**) co-expressed in U2OS cells by transient transfection. Cells in (**B**) were pre-extracted with PTEM buffer prior to fixation with 4% PFA. 4 representative cells are shown in (B). In merged images, CDC7 is shown in red, DBF4B in green, and DAPI in blue. Results are representative of two independent experiments. Scale bar = 20 μm.*

77

Although having apparently distinct localisations when expressed separately (Fig. 3.7 A), we have shown that induced expression of tagged DBF4B alone can stimulate the phosphorylation of MCM2, a nuclear protein, in cells (Fig. 3.4 C). Taken together, this raises the possibility that DBF4B might interact with, and alter, the localisation of CDC7. In U2OS cells, transient co-expression of CDC7-FLAG-Strep and DBF4B-GFP resulted in a strong reduction of the nuclear signal for CDC7, and both proteins were instead detected at cytoskeletal-like structures in interphase cells, the appearance of which was enhanced by extraction of soluble proteins with PTEM buffer before fixation (Fig. 3.7 B). These structures resembled microtubules or intermediate filaments, so in order to determine which, we performed a co-transfection of CDC7-FLAG-Strep and untagged DBF4B into U2OS cells which were stably expressing EGFP-α-tubulin. Simultaneous detection was performed with the antibodies for the Strep-tag and DBF4B. We observed the co-localisation of CDC7 and DBF4B with α-tubulin. (Fig. 3.8).
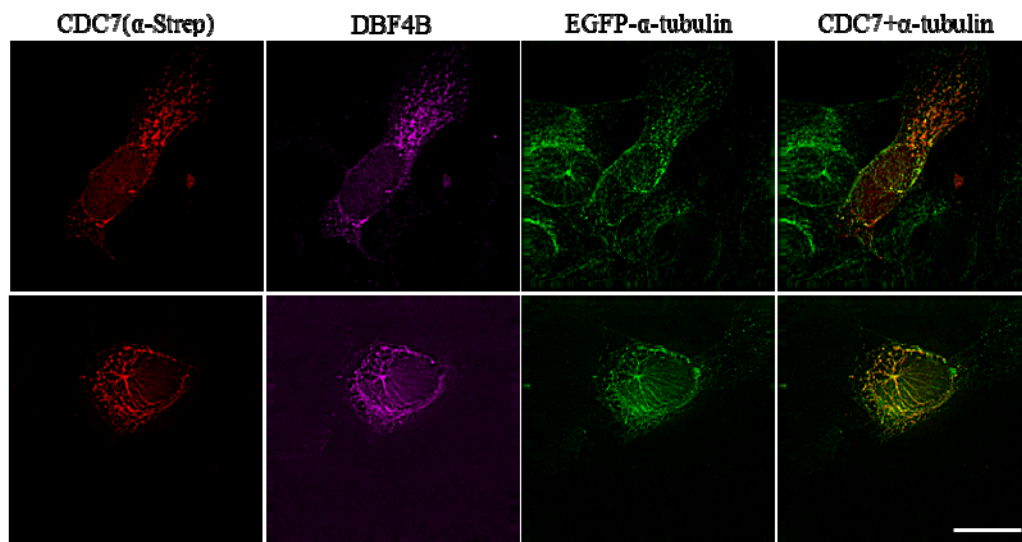
Figure 3.8 CDC7-DBF4B is associated with microtubules in interphase cells. *U2OS cells stably expressing EGFP-α-tubulin were co-transfected to express untagged DBF4B and CDC7-FLAG-Strep. CDC7 and DBF4B were detected using antibodies against the Strep-tag and untagged DBF4B, respectively. Experiment was performed once. Scale bar = 20 μm.*
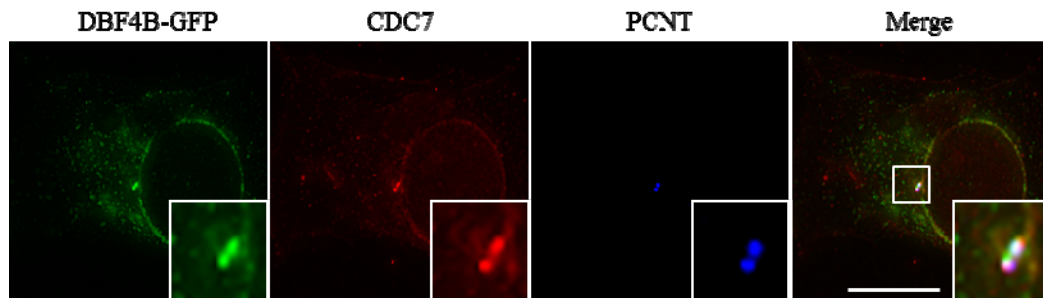
Figure 3.9 CDC7-DBF4B is detected at the centrosome. U2OS expressing DBF4B-GFP were simultaneously extracted and fixed with PTEMF buffer. Endogenous CDC7 and PCNT were detected using specific antibodies. Experiment was performed twice with similar results. Scale bar = 20 μm.

Overexpressed DBF4B were also frequently observed at 1-2 bright foci adjacent to the nucleus of interphase cells (for example see Fig. 3.7 B). U2OS cells were transfected with DBF4B-GFP, and co-immunofluorescence was performed with antibodies against endogenous CDC7 and pericentrin (PCNT), a component of the pericentriolar material. We found that tagged DBF4B is localised to centrosomes and it was able to recruit endogenous CDC7 as well (Fig. 3.9).

3.6   Conclusion

In this chapter, I have described the characterisation of human T-REx cell lines for the inducible expression of epitope-tagged CDC7 kinase subunits. Our results suggest that FLAG-Strep-tagged DBF4 and DBF4B are functional proteins as they are able to interact with endogenous CDC7 and increase phosphorylation of the known CDC7 substrate MCM2. We have also presented evidence that CDC7-DBF4 and CDC7-DBF4B are localised to different subcellular compartments. While DBF4 is a nuclear protein, DBF4B is exported to the cytoplasm in a CRM1-dependent manner.

Chapter 4: Insulin Receptor Substrate 4 is a novel CDC7-DBF4B interacting protein

4.1   Introduction

In the previous chapter, we have demonstrated the utility of the Flp-In T-REx 293 cell lines that have been generated for the inducible expression of tagged CDC7 subunits. Towards the aim of identifying CDC7 kinase interacting proteins, we have evaluated several different purification approaches utilising the tandem FLAG and Twin-Strep epitope tags that have been fused to the C-terminal of the proteins. For mass spectrometry-based identification of potential interacting proteins, the purifications were assessed based on two key parameters: purity, i.e. the number of non-specific contaminant proteins; and yield, i.e. sufficient amounts of the target and interacting proteins for detection [208,209]. The requirements for these parameters differs depending on the specific proteomics approach taken, and the selection of the appropriate purification and protein identification method can be critical to the success of the experiment.

4.2   Optimisation of protein purification

In order to minimise the number of non-specific proteins in the final elutions, we initially performed a tandem FLAG/Strep purification. Cell extracts from T-REx-CDC7 WT or -CDC7 KD were first incubated with ANTI-FLAG M2 affinity gel, and bound proteins were competitively eluted using an excess of 3xFLAG peptide. Elutions from the FLAG immunoprecipitation (IP) were then subjected to a second affinity purification step with Streptavidin resin. Samples from each step of the purification were analysed by immunoblotting with an anti-CDC7 antibody. Unfortunately, a significant proportion of tagged CDC7 is lost in the unbound fraction (Fig. 4.1 A, lanes 3, 4) or remained bound to the resin after the elution steps, particularly in the FLAG IP procedure (lanes 7, 8), and only a small fraction is recovered relative to the input (compare lanes 1 and 13, 2 and 14).
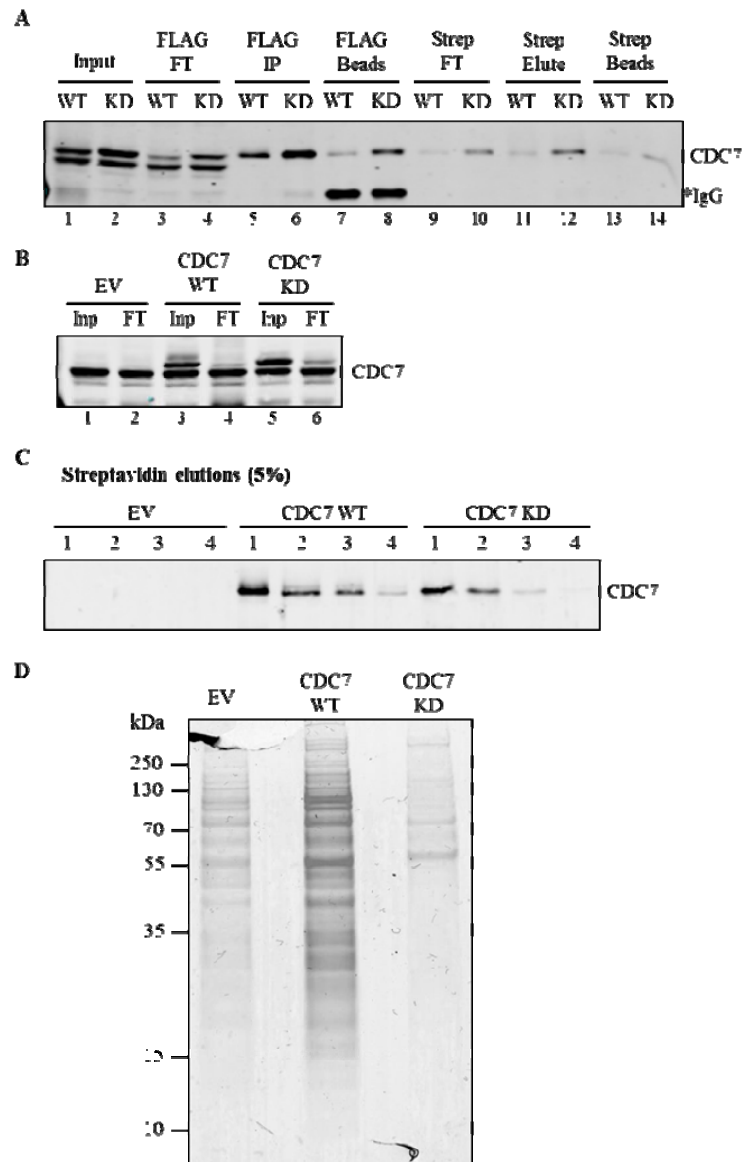
Figure 4.1 FLAG-tag and Streptavidin-based methods for CDC7 purification. *(A) Sequential purification of CDC7. Protein was competitively eluted from ANTI-FLAG M2 affinity gel with 3xFLAG peptide and bound onto Streptavidin resin. **(B-D)** Affinity purification using gravity flow Strep-Tactin Sepharose columns. Cell extracts from Empty Vector (EV), wild type CDC7 (WT), and kinase-dead CDC7 (KD) were passed through individual Strep-Tactin columns. Columns were washed, and proteins were eluted with 10 mM biotin. Equivalent fractions of **(B)** input (Inp) and flowthrough (FT) samples, and **(C)** elutions were analysed by immunoblotting for CDC7. Elutions were collected as 6x100µl fractions. **(D)** Elution fractions 1 and 2 were pooled, lyophilised, resuspended in Laemmli sample buffer, and 80% was run on 4-12% SDS-PAGE for Coomassie staining.*

Due to the low yield and incompatibility of batch purification methods for scale up to obtain sufficient amounts of protein for mass spectrometry analysis, we proceeded to test the suitability of Strep-Tactin Sepharose columns for this purpose. Cell extracts were allowed to pass through Strep-Tactin resin (200 µl bed volume) by gravity flow, followed by extensive wash steps and elution in six 100 µl fractions. Compared to the batch purification approach, near-complete depletion of tagged CDC7 from a larger amount of cell extract (>10 mg) was achieved (Fig. 4.1 B, compare lanes 3 and 4, 5 and 6). Competitive elution with excess biotin successfully eluted the bound protein (Fig. 4.1 C). The first 2 elution fractions containing most of the tagged CDC7 were pooled, lyophilised, and resuspended in Laemmli sample buffer. The resulting samples were separated by SDS-PAGE and Coomassie stained. While a larger number and more intensely stained bands were detected in the CDC7 WT sample compared to the control EV, suggestive of a successful co-purification experiment, there was still a significant level of background seen in the control which does not contain Strep-tagged protein (Fig. 4.1 D). Thus, we found that Strep-Tactin columns were suited to purifying proteins from larger amounts of extract, but a method to distinguish non-specifically bound proteins from specific interactors would be critical. To achieve this, a quantitative proteomics approach using SILAC was chosen.

4.3   Identification of CDC7 and DBF4B interacting proteins by Strep-Tactin purification and Stable Isotope Labelling of Amino Acids in Cell Culture (SILAC) proteomics

T-REx 293-EV, DBF4B, and CDC7 WT were grown in 'light' (R0K0), 'medium' (R6K4), and 'heavy' (R10K8) isotope labelled SILAC media respectively. Equal amounts of protein extract from each cell line (10 mg protein each) were pooled and purified with a single Strep-Tactin Sepharose column (Fig. 4.2 A). The first two elution fractions containing most of the tagged protein were lyophilised and reconstituted in sample buffer, and sent to Dundee Cell Proteomics where the subsequent analyses were performed. Proteins in the elution were separated by one-dimensional SDS-PAGE, subjected to band excision, and identified by mass

spectrometry. For each identified protein, the relative abundance of its 'light' (L), 'medium' (M) and 'heavy' (H) labelled forms were determined. Non-specifically bound 'contaminant' proteins are expected to originate equally from all three extracts (SILAC ratios of M/L or H/L ≤ 1.0), while proteins having SILAC ratios of greater than 1 are more likely to be specific interactors.

184 proteins were enriched with DBF4B (M/L > 1.0), including 48 proteins with a M/L ratio greater than 2 (Fig. 4.2 B). These proteins were manually assigned into groups according to their reported functions (Fig 4.2 C). The best represented group consisted of cytoskeletal proteins, with 9 of these belonging to the α- and β-tubulin families, which are the major components of microtubules. We also found 2 components of the centrosome, TUBGCP2 and IQCB1 [210,211]. Interestingly, the highest enrichment (after DBF4B and CDC7) was obtained for Insulin Receptor Substrate 4 (IRS4), a scaffold protein associated with receptor tyrosine kinase signalling (see Appendix A).

In contrast, only 19 proteins were enriched with CDC7 (H/L > 1.0). Apart from CDC7 itself and its regulatory subunit DBF4, all of these proteins were relatively poorly enriched (H/L < 2.0). The top hit (after DBF4) was Melanoma-associated antigen D1 (MAGED1; H/L = 1.86), which was also enriched five-fold over the control with DBF4B (see Appendix B). Unfortunately, due to the lack of suitable reagents, we have not been able to investigate this potential interaction further. Due to the low SILAC ratios of the other proteins on the list, we decided to focus on the list of DBF4B enriched proteins instead.
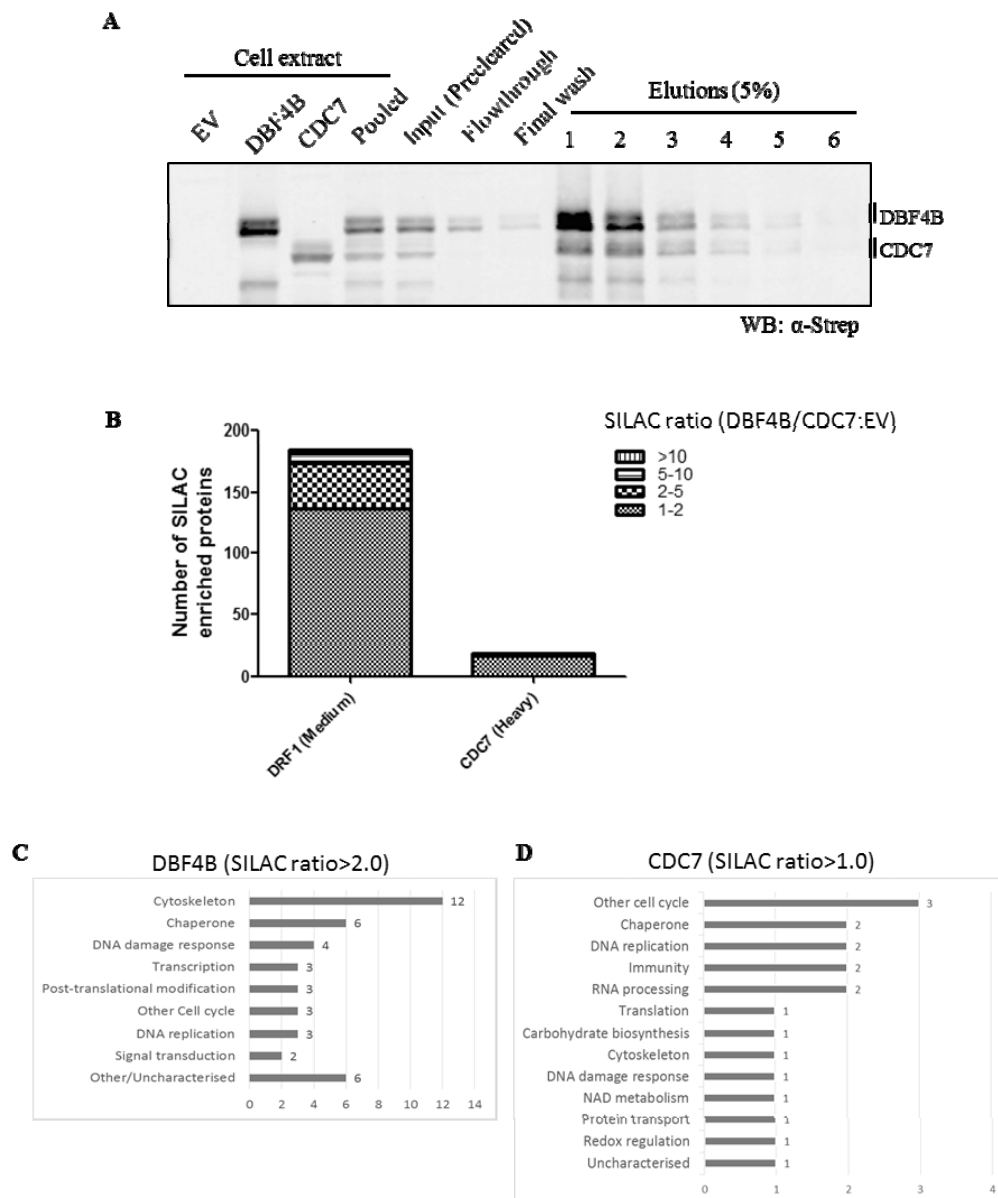
Figure 4.2 Identification of novel CDC7 and DBF4B-interacting proteins by Strep-Tactin – SILAC. *Extracts from T-REx-EV, DBF4B, and CDC7 WT cells grown in SILAC media were pooled in equal amounts and subjected to purification using a gravity flow Strep-Tactin Sepharose column. (**A**) Fractions at each step of the purification process were taken for Western blot analysis. Elution fractions 1 and 2 were lyophilised and resuspended in sample buffer. Proteins were separated by SDS-PAGE, band excised, and identified by quantitative mass spectrometry. The number of proteins with a SILAC ratio greater than 1 are represented in (**B**). Identified proteins were grouped according to their functions (**C, D**).*

4.4 CDC7, DBF4B, and IRS4 physically interact in cells

As discussed in the introduction (Section 1.2.3 and associated references), IRS family proteins are associated with membrane receptors, where, upon receptor activation, are phosphorylated on multiple tyrosine residues. IRSs do not have catalytic activity, but function as scaffold proteins with binding sites for many downstream signalling molecules.

To validate the interaction between DBF4B and IRS4, small-scale batch purifications with Strep-Tactin resin were carried out on cell extracts from T-REx-EV, CDC7 WT, -DBF4, and -DBF4B. Elutions were analysed by immunoblotting with the anti-Strep-tag and anti-IRS4 antibodies. IRS4 was co-purified with tagged DBF4B, but not with DBF4 or CDC7 alone (Fig 4.3 A), in agreement with the results of the DBF4B SILAC experiment (Section 4.3). We then performed the reciprocal IP from T-REx-EV, -DBF4, and –DBF4B cells using the IRS4 antibody. In T-REx-EV, we detected an interaction between CDC7 and IRS4 at endogenous levels (Fig. 4.3 B, lane 3). Tagged DBF4B was also co-immunoprecipitated with IRS4, along with a higher amount of endogenous CDC7, compared to the EV IP (Fig. 4.3 B, compare lanes 3 and 9). Interestingly, although tagged DBF4 expression appears to stabilise and increase endogenous CDC7 levels, no CDC7 or tagged DBF4 was co-immunoprecipitated (Fig. 4.3 B, lanes 4-6). Thus, we have demonstrated a biochemical interaction of IRS4 with CDC7-DBF4B but not CDC7-DBF4.

A

B
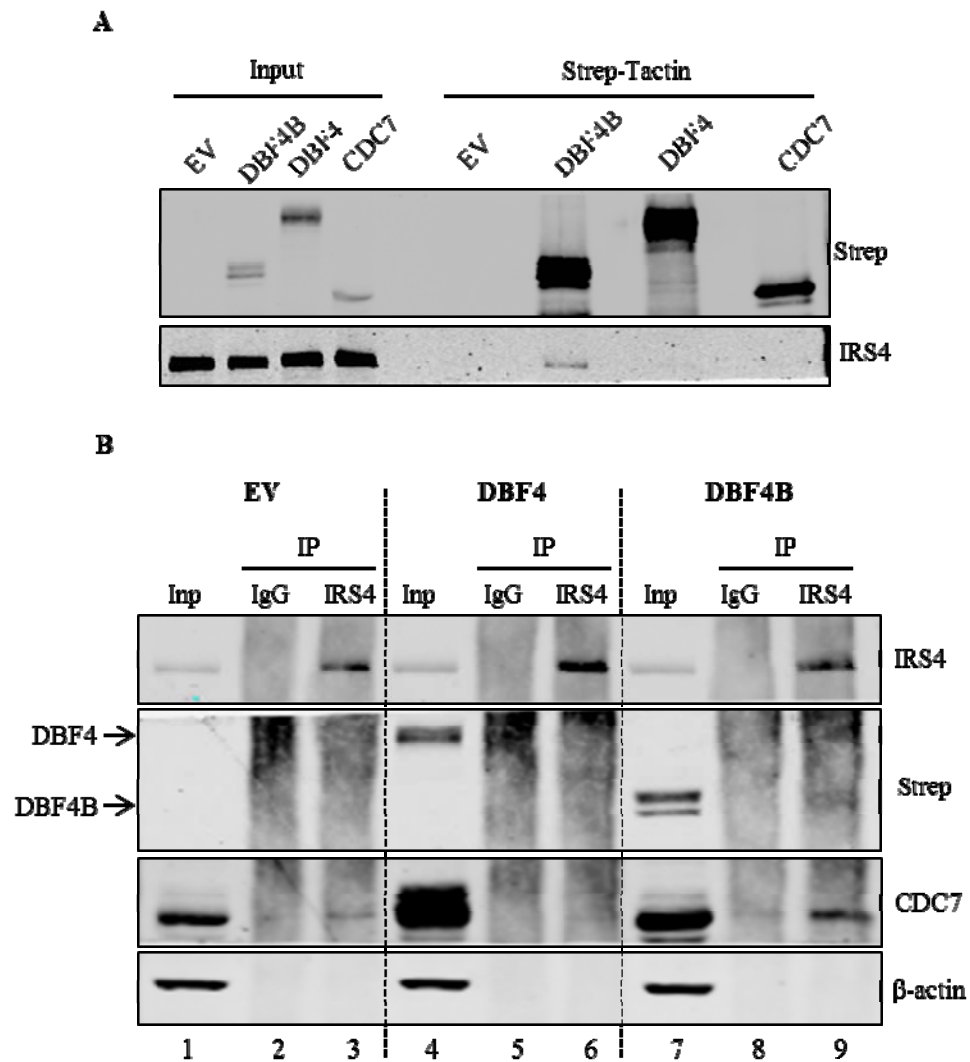
Figure 4.3 IRS4 interacts with CDC7-DBF4B in human cells. *(A) CDC7 kinase subunits were purified from T-REx 293 cells with Strep-Tactin magnetic beads and elutions were blotted for the presence of IRS4. (B) Endogenous IRS4 was immunoprecipitated with anti-IRS4 antibody and immunoblotted with anti-Strep and anti-CDC7 antibodies. Results are representative of at least 2 independent experiments.*

86

4.5 IRS4 is a predominantly membrane-associated and cytoplasmic protein

Consistent with its roles in receptor tyrosine kinase-mediated signalling, IRS4 is reported to be localised to the cytoplasm and associated with the plasma membrane [212]. A putative nuclear localisation sequence (NLS) has been identified [213], however it is still unclear if IRS4 becomes localised to the nucleus upon receptor stimulation [52,212]. We therefore examined the localisation of IRS4 in HEK293T cells under (a) normal culture conditions (10% FBS), (b) serum-starved (0% FBS) for 48 h, and (c) serum-starved and restimulated for 30 min. Cells were then fixed with paraformaldehyde and IF was performed with an IRS4 antibody. We confirmed that IRS4 is strongly membrane-associated and diffuse in the cytoplasm under conditions (a) and (b) (Fig. 4.4, top and middle rows). However, upon re-addition of FBS to serum-starved cells, a small fraction of IRS4 is detected in the nucleus (Fig. 4.4, bottom row).

In addition to their traditional roles in receptor signalling, several members of the IRS family have been shown to be translocated to the nucleus through multiple mechanisms, where they perform independent functions, impacting on DNA repair, gene expression, and cell proliferation (reviewed in [214]). Since both DBF4B and IRS4 show dynamic nucleo-cytoplasmic localisation, we then wanted to test the possibility that DBF4B might be involved in regulating the function of IRS4 through targeting it to a particular subcellular compartment. HEK293T cells were transfected with DBF4B-GFP, and the localisation of IRS4 was examined, but no differences were observed between transfected and untransfected cells (Fig. 4.5).
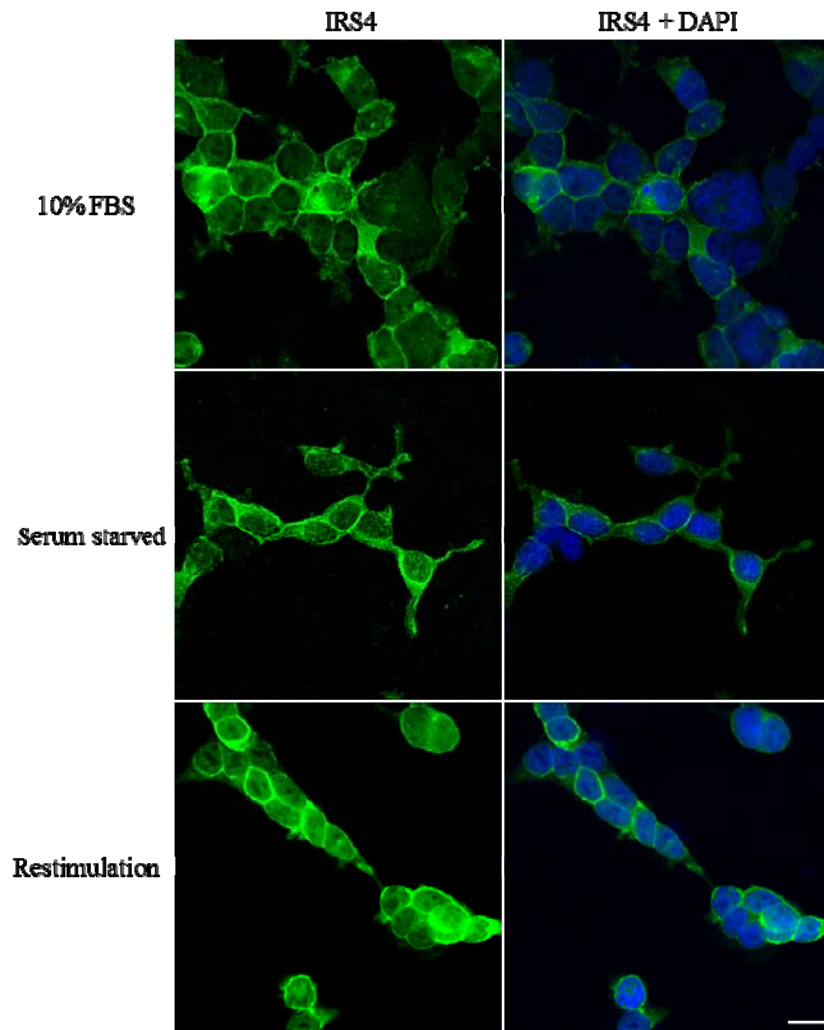
Figure 4.4 IRS4 is predominantly localised to the plasma membrane and cytoplasm. *HEK293 cells were plated in DMEM supplemented with 10% FBS, then either grown for a further 48 h in the same media (top row), media without serum (middle row), or media without serum followed by stimulation with 10% FBS for 30 min. Scale bar = 20 μm.*
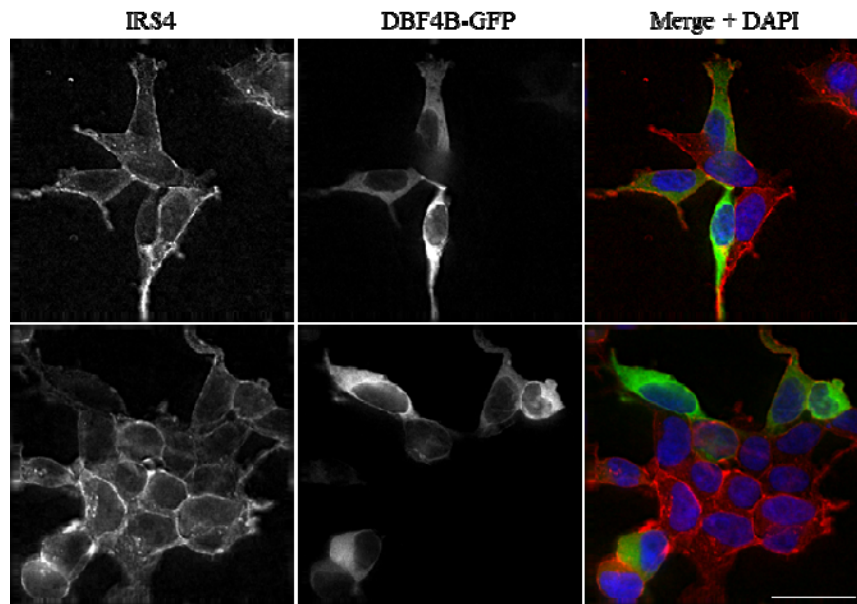
Figure 4.5 DBF4B overexpression does not affect IRS4 localisation. *HEK293 cells were transfected to express DBF4B-GFP and fixed with 4% PFA 24 h later. Cells were maintained in 10% serum-containing media. Two representative fields are shown. Scale bar = 20 μm.*

4.6 Effect of CDC7 kinase inhibition on PI3K/AKT signalling

Upon ligand binding, phosphorylation of IRSs allows the docking and activation of key signalling molecules, including phosphoinositide 3-kinase (PI3K) [37,40,215]. PI3K mediates the majority of the downstream effects (discussed in Section 1.2.2.1) and as a marker of PI3K pathway activation, we examined the PI3K-dependent phosphorylation of AKT S473, which is essential for full activation of AKT kinase activity [28,216].

To examine a possible role for CDC7 kinase in receptor signalling, human foreskin fibroblasts (HFF) immortalised by expression of telomerase reverse transcriptase (hTERT) were used. HFF were selected because, as untransformed cells, they undergo quiescence and cell cycle re-entry upon serum starvation and restimulation, respectively [217]. The PI3K/AKT pathway cannot be studied in transformed cells, such as HEK293T and T-REx 293, as they maintain a basal level

of signalling in the absence of FBS, do not undergo cell cycle arrest, and have an elevated rate of cell death (our results, not shown). Additionally, HFF are strongly adherent and tolerant of wash steps and media changes required for our experiments.

4.6.1 The CDC7 kinase inhibitor XL413 attenuates serum-stimulated AKT phosphorylation

We first wanted to determine if CDC7 affects the activation of the PI3K/AKT pathway downstream of receptor activation. HFFs were grown in non-serum limiting conditions (10% FBS) to allow attachment to plastic. Cells were then washed several times with PBS and maintained in serum-free media for 48 h to deactivate receptor signalling. Cells were pre-treated with DMSO control or the CDC7 kinase inhibitor XL413 [194] for 1 h before FBS was re-added to a final concentration of 10%. At different times following serum re-stimulation, cells were scraped on ice and reactions were stopped through the addition of 20% trichloroacetic acid (TCA) which extracts and precipitates proteins in a rapid and reproducible manner [218]. Levels of AKT pS473 were analysed by immunoblotting with a phospho-specific antibody (Fig. 4.6 A). Band intensities were quantified and normalised to β-actin (Fig. 4.6 B). Before serum addition, AKT pS473 levels were undetectable, indicating that PI3K/AKT signalling is completely inactive. Within 5 min of serum stimulation, AKT phosphorylation at S473 is detected, and reached a maximum at 30-60 min, followed by a decrease at 120 min. When cells were pre-treated with XL413, the initial increase of S473 phosphorylation measured at 5 min was comparable to control, however, levels did not increase further and plateau over the course of the experiment.

A

B
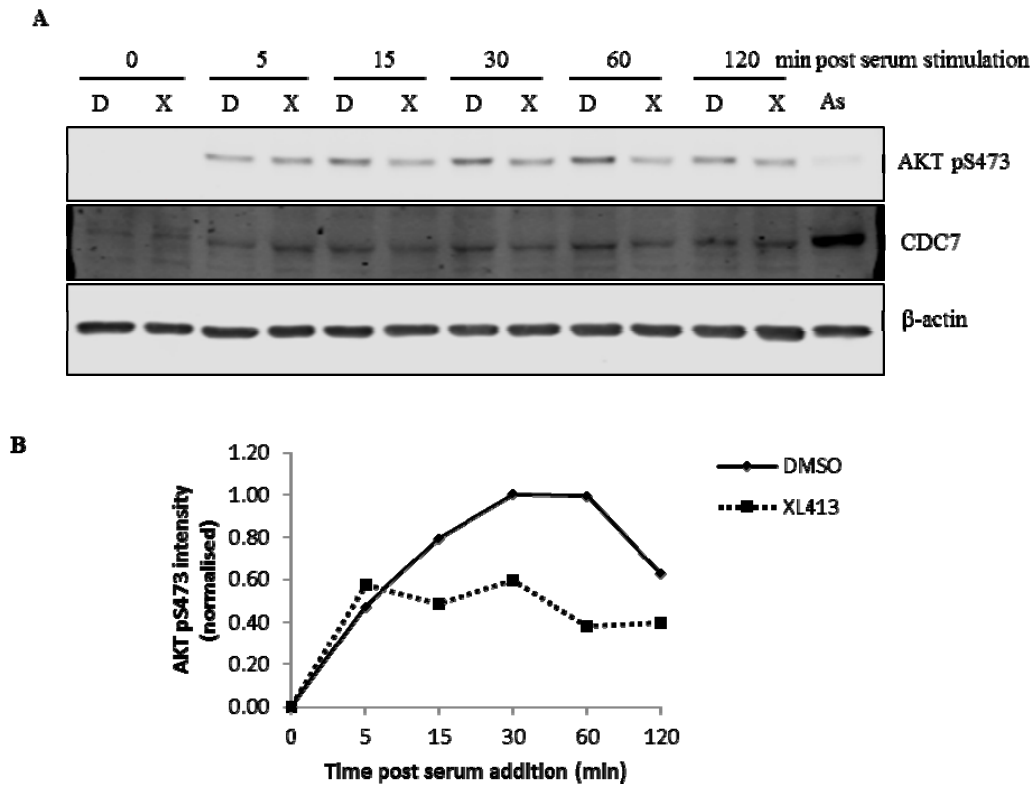
Figure 4.6 Treatment with the CDC7 kinase inhibitor XL413 attenuates phosphorylation of AKT at S473. hTERT immortalised human foreskin fibroblasts (HFF) were serum starved for 48 h, and treated with 10 μM XL413 (X; CDC7 kinase inhibitor) or DMSO (D) for 1 h prior to addition of 10% FBS. Cells were collected at the indicated time points following serum stimulation by the addition of 20% TCA. (A) Total cell extracts were analysed by immunoblotting. (B) The levels of AKT pS473 were quantified and normalised to β-actin using Image Studio software (Li-COR Biosciences). Experiment was performed once.

4.6.2 CDC7 depletion does not affect AKT phosphorylation

To determine if the effect on AKT pS473 seen with XL413 treatment is due to its specific inhibition of CDC7 kinase activity, we performed a similar assay in cells depleted of CDC7 using siRNA. Growth arrest due to serum starvation resulted in low CDC7 levels, as its expression is cell cycle regulated, but it was further decreased by transfection with siCDC7 (Fig. 4.7 A, compare lane 3 to 4 and 5). Due to the larger number of treatments to be tested, we did not collect samples later than

30 min since AKT pS473 levels reach a maximum by this point in control-treated cells, and the difference between control and XL413-treated cells is greatest at this time (Fig. 4.6 B). In agreement with our previous result, cells pre-treated with XL413 had attenuated AKT S473 phosphorylation at 15 and 30 min after serum stimulation. However, cells that were transfected with siCDC7 for 48 h did not exhibit reduced AKT S473 phosphorylation levels as compared to cells treated with a control non-targeting siRNA (siCTRL). Furthermore, combined treatment of XL413 and siCDC7 yielded comparable levels of AKT S473 phosphorylation as the treatment with XL413 alone, suggesting that the effect of XL413 is independent of CDC7 (Fig. 4.7 A, quantified in B-D).

A

B 5 min

C 15 min

D 30 min
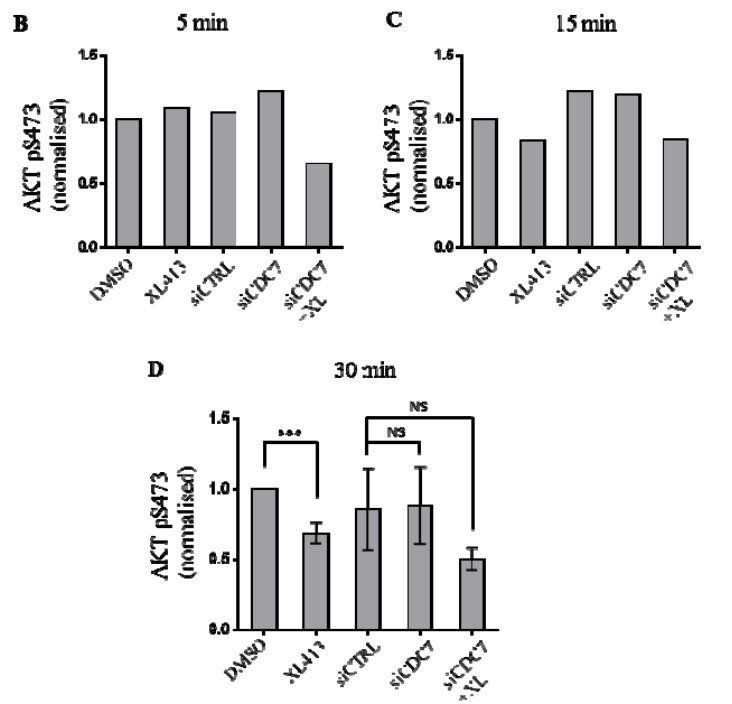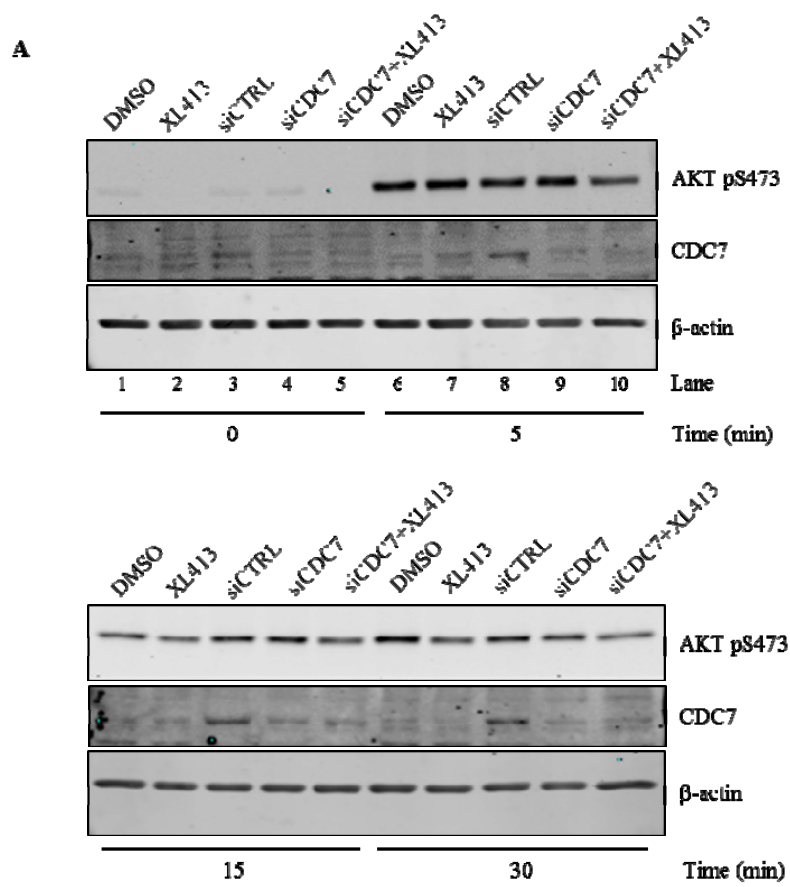
Figure 4.7 The CDC7 kinase inhibitor XL413, but not CDC7 depletion, attenuates phosphorylation of AKT at residue S473. Human foreskin fibroblasts (HFF) were treated with siCTRL or siCDC7 in serum-free media for 48 h. Indicated samples were pre-treated with 10 μM XL413 1 h prior to serum stimulation. Cells were collected at the indicated time points post serum stimulation. (A) Protein extracts were prepared by TCA precipitation and analysed by immunoblotting. The levels of AKT pS473 at (B) 5 min, (C) 15 min, and (D) 30 min were quantified and normalised to β-actin using Image Studio software (Li-COR Biosciences). Quantification shown in (B) and (C) are from one experiment, and (D) is a summary of 3 biological replicates. Bars represent the Mean ± S.D. *** P<0.005, Student's t-test.

4.7   IRS4 depletion impairs proliferation of HEK293T cells

We proceeded to test the alternate hypothesis that IRS4 plays a role in regulating CDC7 kinase activity. IRS4 was depleted from HEK293T cells with two different siRNAs, and extracts were examined by immunoblotting for IRS4, MCM2, and AKT pS473. Treatment with XL413 and LY294002 [219] were included as controls for inhibition of CDC7 kinase and PI3K, and they efficiently reduced the levels of MCM2 pS40/41 and AKT pS473, respectively (Fig. 4.8 A, lanes 2 and 3). Reductions in protein levels of IRS4, MCM2, and CDC7 by LY294002 treatment are likely due to cell death, as a significant loss of viability was recorded for this sample. Depletion of IRS4 was observed with both siRNAs, although to different extents. The depletion by siIRS4-B was less efficient than siIRS4-A; at 72 h, IRS4 levels in siIRS4-B-treated cells were almost 2-fold higher than siIRS4-A-treated cells (20% vs. 37% of control, respectively; Fig. 4.8 B). In accordance with IRS4 levels, AKT pS473 in siIRS4-A treated cells was reduced to about 40% of control levels throughout. In siIRS4-B treated cells, AKT pS473 levels were initially slightly decreased, but returned to near control levels at 72 h. In all siRNA-treated cells, MCM2 pS40/41 levels remained unchanged (lanes 4-12).

Cell numbers, viability, and DNA content were also monitored over a 72 h period. Compared to control siRNA, siIRS4-A, but not siIRS4-B, greatly impaired cell proliferation (Fig. 4.8 C). However, no major effects on viability by either

treatment were observed, as measured by Trypan blue exclusion (Fig. 4.8 D). Flow cytometry analysis showed that siIRS4-A caused an accumulation of cells with 4n DNA content with a corresponding decrease in the 2n population, indicating a defect in G2/M-phase progression. An intermediate phenotype was observed with siIRS4-B (Fig. 4.8 E, F). Since MCM2 pS40/41 levels and the proportion of cells in S-phase were not affected, IRS4 is unlikely to regulate CDC7 kinase activity or play a role in DNA replication in non-serum-limiting conditions.
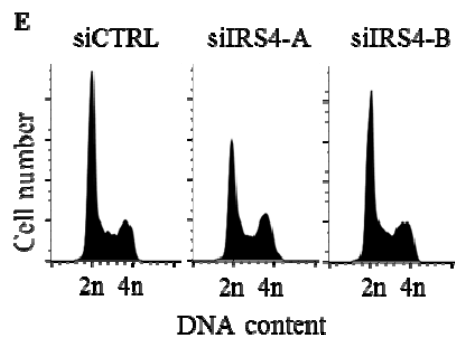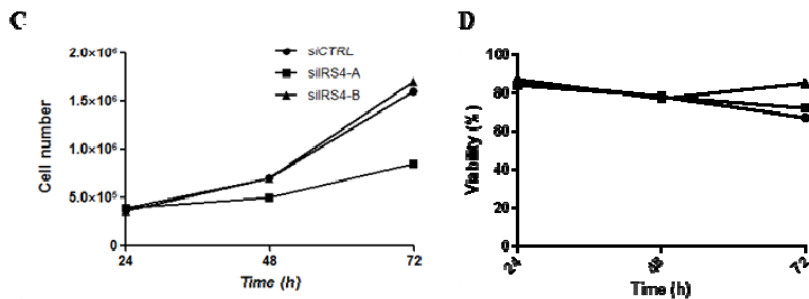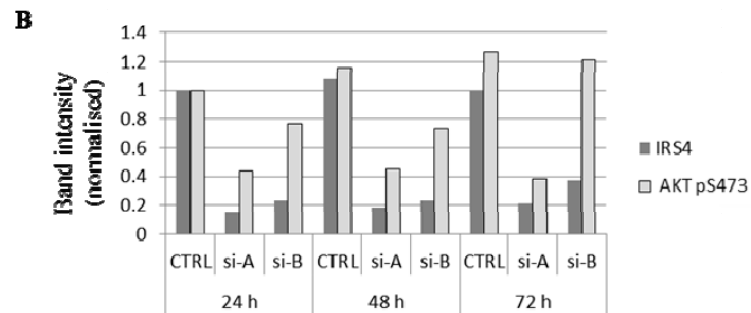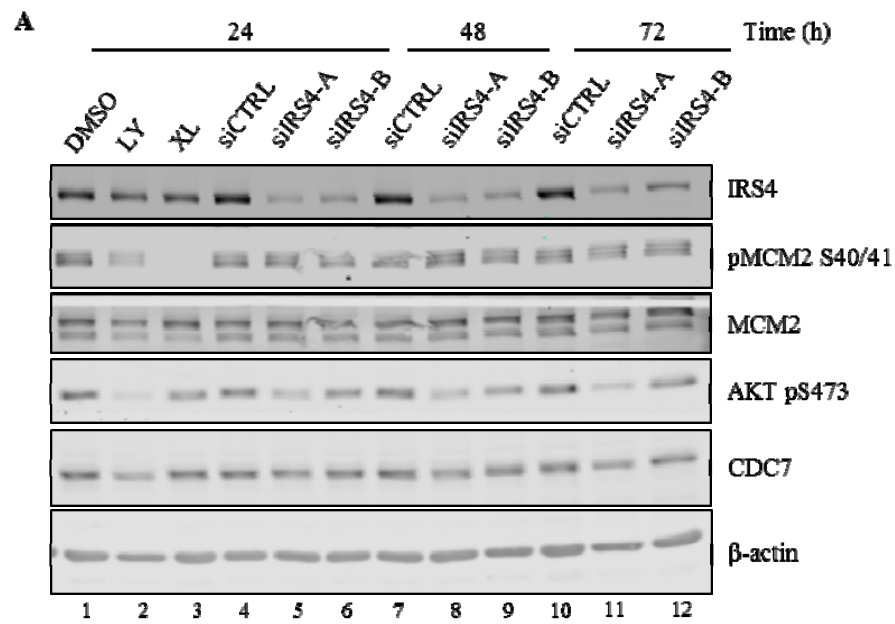
Figure 4.8 Effects of IRS4 depletion on cell proliferation. *HEK293T were treated with control siRNA (siCTRL), 2 siRNAs against IRS4 (siIRS4-A and –B), LY294002 (PI3K kinase inhibitor; LY), or the CDC7 kinase inhibitor XL413 (XL), and collected at 24 h intervals. At each time point, (**A**) protein extracts were prepared and analysed by immunoblotting with the indicated antibodies. (**B**) Quantification of IRS4 and AKT pS473 band intensities normalized to β-actin. (**C, D**) Cell number and viability were determined by Trypan blue exclusion, and (**E**) DNA content was analysed by flow cytometry. The result for the 72 h samples are shown here. (**F**) The proportion of cells in each cell cycle stage was determined by gating in FlowJo according to DNA content. Experiment was performed once.*

4.8   Conclusion

Using a Strep-Tactin-based purification for high protein yield, coupled with SILAC proteomics to exclude contaminant proteins, we have identified a number of potentially novel DBF4B-interacting proteins. We have demonstrated an *in vivo* interaction between endogenous CDC7 and IRS4, and tagged DBF4B but not DBF4. This could represent a novel mechanism directly linking receptor tyrosine kinase signalling to cellular proliferation. We have so far been unable to determine a role for CDC7 kinase in regulating PI3K–AKT signalling, or a role for IRS4 in regulating CDC7 kinase activity, albeit in limited cellular contexts. Future work will be focused on elucidating the functional significance of this interaction.

Chapter 5: CDC7-DBF4 determines the timing of TOP2A recruitment to centromeres in S-phase

5.1 Introduction

Nearly every cellular process involving DNA, including transcription, DNA replication, chromosome condensation and segregation, all result in changes in DNA topology, for instance through the formation of supercoils and entanglements, which are resolved by Type 1 and Type 2 topoisomerases ([109] and discussed in Section 1.5). Topoisomerase 2-alpha (TOP2A) catalyses the decatenation of double-stranded DNA molecules, and is essential for resolving topological structures formed during replication and mitosis [220]. In this chapter, we describe the identification of a novel interaction between TOP2A and CDC7-DBF4 kinase through immunoprecipitation-mass spectrometry. We have characterised this interaction through various biochemical assays, and demonstrate here a novel role for CDC7-DBF4 at centromeres.

5.2 Identification of DBF4 interacting proteins by FLAG Immunoprecipitation

The FLAG IP experiment presented in Figure 5.1 was performed by Gemma O'Brien, sample processing and mass spectrometry by Edel Mullen, and data analysis as summarised in Figure 5.1 C by Sandra Healy. These are included as contextual background for the work presented here.

A different approach was taken for the identification of DBF4 interacting proteins. To this end, optimisation of the FLAG IP protocol was being performed alongside the Strep-Tactin purification and SILAC proteomics methodology described previously. The optimised protocol included the following modifications: (1) significantly scaling up the amount of extract used to >50 mg protein/IP, (2) increasing antibody binding time to 16 h, (3) lowering the stringency of the binding

buffer from 300 mM to 150 mM NaCl, (4) improving elution efficiency with a greater excess of 3xFLAG peptide, and (5) utilising acetone precipitation to desalt and concentrate eluted proteins for mass spectrometry. The immunoprecipitation was followed by Western blotting of samples taken at each stage, and good enrichment of DBF4 was observed in the elution (Fig. 5.1 A). Separation of the immunoprecipitate by SDS-PAGE and Coomassie staining shows a significantly larger number of proteins in the DBF4 IP compared to the control Empty Vector (EV; Fig. 5.1 B). The remainder of the immunoprecipitate was subjected to in-solution tryptic digestion and peptide identification by mass spectrometry.

The list of 1800 protein entries identified in the DBF4 FLAG IP was reduced by first removing proteins also found in the EV IP, merging protein isoforms and duplicate UniProt entries, limiting analysis to proteins with at least 2 unique identified peptides, and further removal of unreviewed protein identifiers (sequences associated with computationally generated annotations and large-scale functional characterisation that have not been reviewed by UniProtKB curators) and duplicates, resulting in a list of 148 unique proteins. These were then queried against the Contaminant Repository for Affinity Purification (CRAPome, www.crapome.org), an online depository of common contaminants from affinity purification-mass spectrometry experiments [221]. For each protein query, a value is returned representing the frequency of which it has been identified in other experiments that have been uploaded to the database. The higher the frequency, the more likely it is to be non-specifically purified. Any proteins that were found with greater than 20% frequency (>70 of 343 experiments at the time of analysis; Database version 1.0) were excluded, thus forming the shortlist of 96 potential DBF4 interacting proteins (Appendix C). This process is summarised in Fig 5.1 C.

Of particular interest to us were the proteins involved in DNA replication, DNA damage response/repair, and mitosis (Table 5.1). Antibodies were obtained for a number of candidate proteins, and we attempted to validate these through immunoblotting. Using the same set of samples that were analysed by mass spectrometry, we confirmed the specific enrichment of many of these proteins in the DBF4 FLAG IP by immunoblotting (O'Brien, not shown). Through independent

smaller scale Strep-Tactin affinity purification experiments, we were able to identify interactions of DBF4 with Topoisomerase 2-alpha (TOP2A; further characterised here) and Replication Factor C subunit 1 (RFC1; not shown).

Table 5.1 Selected list of proteins co-immunoprecipitated with tagged DBF4 in a FLAG IP. A full list is included in Appendix C. CRAPome frequency is relative to a total number of 343 experiments (for details see text).

Function	Protein	CRAPome frequency (Ver. 1.0)	No. of unique peptides
DNA replication	CDC7	0	11
	DBF4	0	14
	RFC5	21	2
	RFC1	22	5
	RFC4	30	3
	USP7	25	2
	TOP2A	69	12
	SSRP1	44	3
	TOP1	57	13
	MCM3	69	2
DNA damage response/repair	MPG	5	2
	LIG3	12	2
	RAD23B	8	2
	MDC1	15	2
	APEX1	29	2
Mitosis	NUSAP1	13	2
	USP39	26	5
	NAT10	32	13
	NSUN2	35	8

5.3   CDC7-DBF4 and TOP2A form a complex in cells

The lambda protein phosphatase treatment presented in Figure 5.2 B was performed by Gemma O'Brien.

As additional confirmation of the interaction, we isolated nuclei from T-REx-DBF4 cells and prepared extracts using Benzonase nuclease treatment to solubilise chromatin-bound proteins. We then performed IP experiments using a

TOP2A antibody and found that tagged DBF4 and endogenous CDC7 were both co-purified (Fig. 5.2, lane 5). Furthermore, this interaction is lost upon treatment with the CDC7 kinase inhibitor XL413, suggesting that the interaction is dependent upon CDC7 kinase activity (lane 6). The large mobility shift of tagged DBF4 observed upon XL413 treatment (lanes 3 and 6) is likely due to loss of autophosphorylation, as lambda protein phosphatase treatment causes a similar effect (Fig. 5.2 B, O'Brien). Through *in vitro* kinase assays with recombinant CDC7-DBF4 performed by others in the lab, we have also identified several putative autophosphorylation sites on CDC7 and DBF4 (Wang, Fitzgerald, unpublished results).
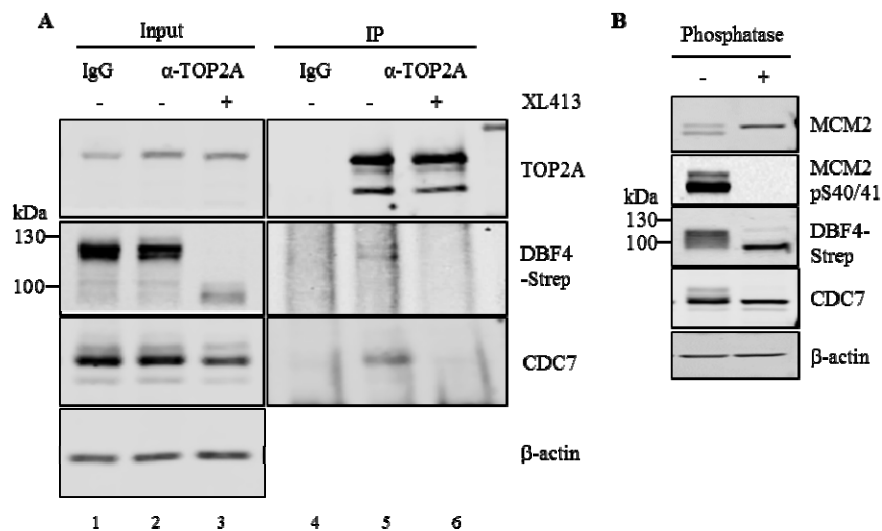
Figure 5.2 TOP2A and CDC7-DBF4 co-immunoprecipitate from human cells. (A) TOP2A was immunoprecipitated from Benzonase-treated nuclear extracts of T-REx-DBF4 cells, and immunoblotting was performed with the indicated antibodies. Cells were treated with DMSO or the CDC7 kinase inhibitor XL413 for 3 h prior to harvest. (B) T-REx-DBF4 cell extracts were mock-treated or lambda protein phosphatase-treated and analysed by immunoblotting. DBF4 undergoes a significant mobility shift upon dephosphorylation. Samples in (A) and (B) were analysed on 7.5% and 10% SDS-PAGE gels, respectively. Experiment in (B) was performed by Gemma O'Brien.

DBF4 contains three short conserved motifs, termed motifs N, M, and C (Section 1.6.1) [222]. Motif N contains a BRCT domain predicted to be involved in protein-protein interactions [200], while motifs M and C bind directly to the CDC7

subunit and activate its kinase activity [147]. Human DBF4 additionally contains a large tail region, representing almost half of the protein, which contains no recognisable motifs. To map the DBF4 domains required for interaction with TOP2A, we cloned several DBF4 sequences containing deletions of their N (residues 1-209), MC (210-350), or Tail (351-674) domains (represented in Fig. 5.3 A) into the pcDNA5/FRT/TO expression vector (see Section 3.2). Exact boundaries used here were as described by Hughes and colleagues [147]. The DBF4 deletion mutants were also fused to tandem FLAG-Twin-Strep tags on their C-termini. Stable cell lines for their conditional expression were then generated using the Flp-In T-REx system (by Huong Quachthithu, Michael Rainey, and Gemma O'Brien) as already described, and characterised in a similar manner as described in Chapter 3.4. Expression of tagged DBF4 fragments were confirmed by immunoblotting (Fig. 5.3 B).

IP of TOP2A from these cell lines were performed, and the co-purification of each of the DBF4 fragments was determined by immunoblotting with the Strep-tag antibody. Only the DBF4 MCT (210-674 a.a.) and NMC (1-350 a.a.) fragments were co-immunoprecipitated (Fig. 5.3 C, indicated by asterisks), suggesting that the MC domain is essential for this interaction. As this domain also interacts with CDC7, it is likely that the CDC7 subunit is also involved in the interaction with TOP2A.

5.4 TOP2A phosphorylation status is altered by CDC7 kinase inhibition

Next, we wanted to determine if TOP2A is phosphorylated by CDC7 kinase. For this purpose, we used a phosphorylation-dependent mobility shift assay. T-REx-EV cells were treated with two structurally distinct inhibitors of CDC7, XL413 and PHA767491, for 3 h. Under these conditions, MCM2 pS40/41 is strongly reduced (Fig. 5.4). On a standard 6% SDS-PAGE gel, no mobility shift was observed, and TOP2A was detected as a single band that was not altered by drug treatment. To facilitate separation of differentially phosphorylated TOP2A species, Phos-tag acrylamide was added to the SDS-PAGE gels. Phos-tag is a reagent which binds to phosphate groups and slows the migration of phosphorylated proteins relative to their unphosphorylated or lesser phosphorylated forms [223,224]. In the control DMSO-treated cells, the TOP2A band becomes less distinct in the presence of the Phos-tag reagent, with slight smearing observed beneath the main band. Upon treatment with either inhibitor, a second, faster migrating form was detected. This shift is more striking with XL413 (lanes 1 and 2), where the majority of TOP2A was detected in the lower band, while with PHA767491, both bands have about equal

intensity (lanes 1 and 3). Therefore it appears that the CDC7 inhibitors induce a phosphorylation-dependent mobility shift of TOP2A, the extent of which correlates with their potency (as determined by MCM2 phosphorylation status).
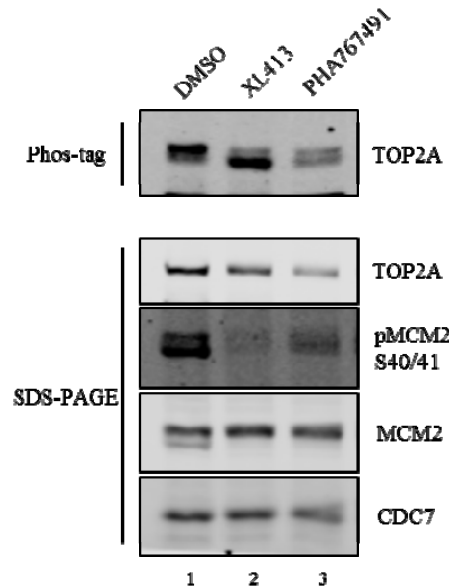
Figure 5.4 Treatment with CDC7 inhibitors induces TOP2A mobility shift on Phosphate-affinity SDS-PAGE. Total cell lysates from T-REx-EV cells treated with 10 μM of the indicated inhibitors for 3 h were separated by 6% SDS-PAGE or 5% SDS-PAGE supplemented with 5 μM Phos-tag acrylamide, and immunoblotting was performed with the indicated antibodies. By Phos-tag SDS-PAGE, faster migrating bands correspond to lesser phosphorylated species.

5.5   Cell cycle timing of the CDC7-DBF4 interaction with TOP2A

In order to determine when during the cell cycle the interaction of CDC7-DBF4 with TOP2A occurs, we performed TOP2A IPs from T-REx-DBF4 cells treated with mimosine or nocodazole. Mimosine, a plant amino acid, blocks S-phase entry through activation of ATM checkpoint signalling and inhibition of the chromatin binding of key replication proteins [225,226], while nocodazole, a microtubule depolymerising agent, prevents mitotic progression through activation of the spindle assembly checkpoint [227]. We found that more endogenous CDC7 and tagged DBF4 were co-immunoprecipitated from cells arrested with mimosine

106

compared to nocodazole (Fig. 5.5 A). The mobility shift of DBF4 observed in mimosine-treated cells is probably due to direct phosphorylation by ATM/ATR [103]. Flow cytometry analysis confirmed that treatment with mimosine and nocodazole had arrested cells with 2n and 4n DNA content respectively (Fig. 5.5 B, quantified in C).

A

	Input				IP: IgG	IP: TOP2A		
	IgG	As	Mim	Noc	IgG	As	Mim	Noc

TOP2A

DBF4-Strep

CDC7

β-actin

B As Mim Noc

Cell number

DNA content

C

%	As	Mim	Noc
G1	55.4	68.2	7.4
S	25.1	18.4	14.1
G2/M	18.4	11.7	78.5
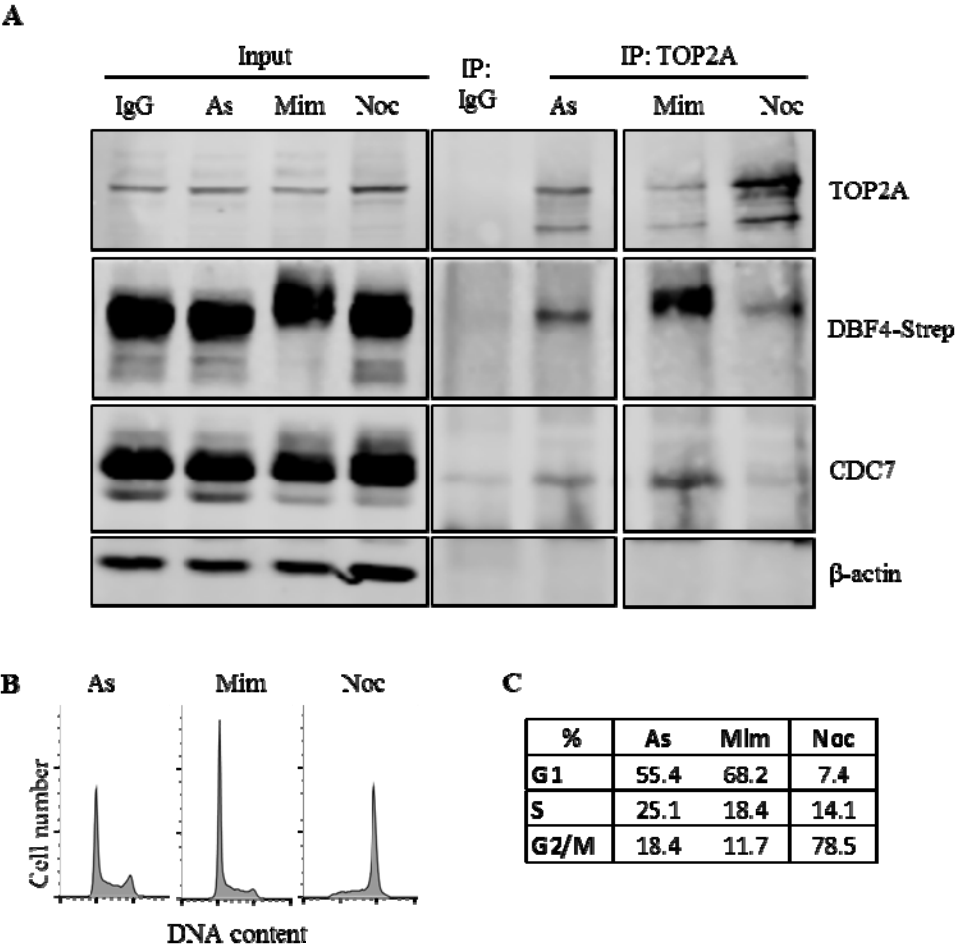
*Figure 5.5 CDC7-DBF4 interaction with TOP2A is increased in mimosine-trapped cells and reduced in nocodazole-trapped cells. Flp-In T-REx-DBF4 cells were treated with mimosine (Mim; 1 mM) or nocodazole (Noc; 1 μM) for 19 h. (**A**) TOP2A was immunoprecipitated from cell extracts and subjected to immunoblotting. (**B**) $5x10^5$ cells were fixed with 70% ethanol and PI stained for flow cytometry analysis of DNA content. (**C**) The proportion of cells in each cell cycle stage was determined by gating in FlowJo according to DNA content. Experiment was performed once.*

A

| Plate cells | + Doxycycline | Mimosine | Release | Collect samples at 0, 3, 6, 9, 12 h after release |

24h   9h   15h   12h

B

IgG (As) As 0 3 6 9 12

TOP2A

DBF4-Strep

CDC7

PCNA

C

IP: IgG   IP: TOP2A

As 0 3 6 9 12 h

TOP2A

DBF4-Strep

CDC7

IgG (Ponceau)

D

Cell number

As   0 h   3 h   6 h   9 h   12 h

DNA content
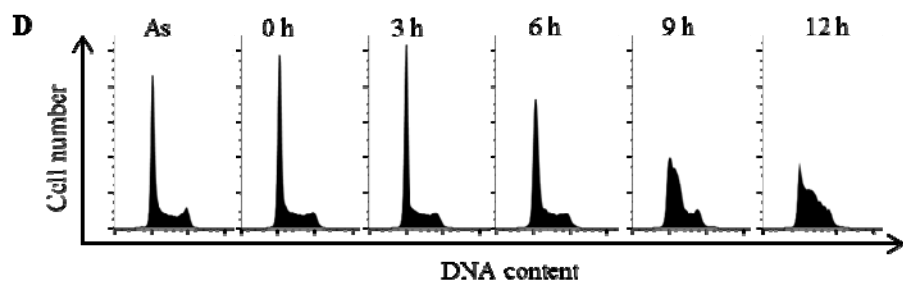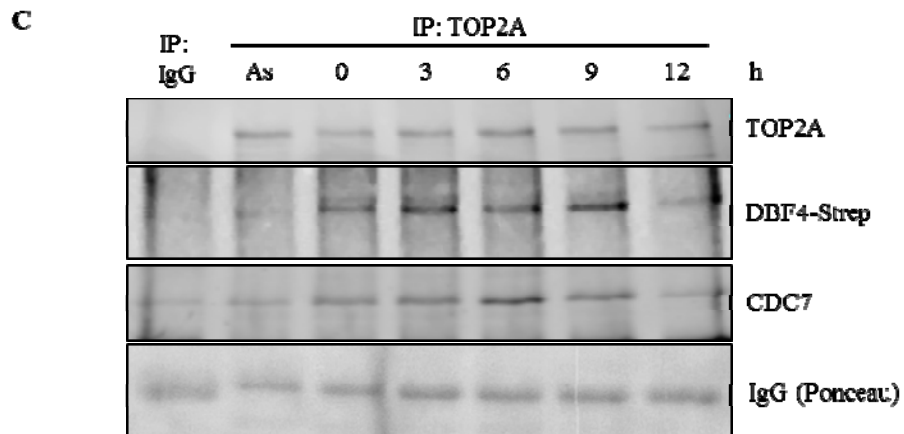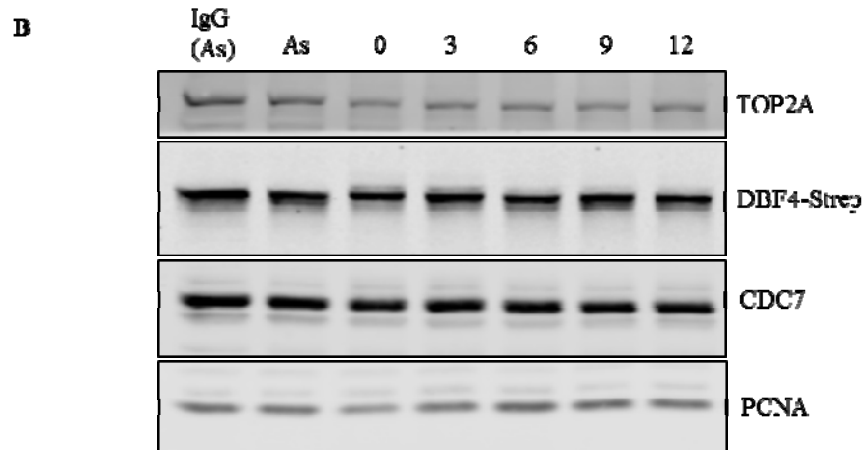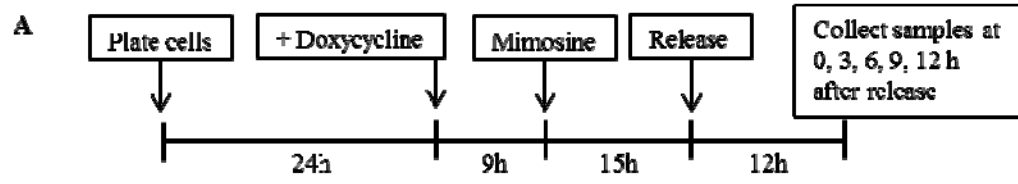
E

%	As	0 h	3 h	6h	9 h	12 h
G1	56.0	59.2	63.1	58.6	48.4	39.1
S	25.0	25.2	24.9	27.3	40.7	49.1
G2/M	16.9	13.9	9.8	12.2	8.5	9.7

108

Figure 5.6 CDC7/DBF4 interaction with occurs predominantly in G1-early S-phase. T-REx-DBF4 cells were synchronised by 1 mM mimosine treatment. (A) Schematic of the experimental design. Cells were collected at the indicated time points following release from mimosine. Nuclear extracts were prepared and subjected to (B) immunoblotting, and (C) TOP2A IP. (D) 5x10^5 cells were fixed with 70% ethanol and PI stained for flow cytometry analysis of DNA content. (E) The proportion of cells in each cell cycle stage was determined by gating in FlowJo according to DNA content. Experiment was performed once.

To examine this interaction during S-phase progression, T-REx-DBF4 cells were released from mimosine arrest and collected at 3 h intervals (outlined in Fig. 5.6 A). Total levels of TOP2A, tagged DBF4, and CDC7 monitored by immunoblotting did not fluctuate significantly in the experiment (Fig 5.6 B). After IP of TOP2A, we found that the interaction with CDC7 and tagged DBF4 was significantly higher in mimosine-trapped cells (0 h) compared to a control-treated asynchronous population, and was further increased at the initial timepoints after release, peaking between 3 - 9 h (late G1 – early S-phase) and decreased significantly at 12 h (mid to late S-phase; Fig. 5.6 C). DNA content analysis by flow cytometry was used to determine cell cycle profiles after release (Fig. 5.6 D, E).

5.6   Differential Retention of Topoisomerase assay

Next, we wanted to investigate the subcellular localisation of the CDC7-DBF4 and TOP2A interaction. TOP2A is abundant in the nucleus and readily detected by immunofluorescence (Fig. 5.7 A), however we wanted to determine if CDC7-DBF4 is associated with catalytically active TOP2A. We utilised the Differential Retention of Topoisomerase (DRT) assay as described by Agostinho and colleagues [228] to achieve this. Briefly, cells are treated with a TOP2A poison (e.g. etoposide) or inhibitor (e.g. ICRF-187/dexrazoxane), which prevents the release of catalytically committed TOP2A from DNA. Soluble proteins, including TOP2A molecules not involved in strand passage activity during the time of treatment, are then salt- and detergent-extracted with HPEM buffer (containing 350 mM NaCl and 0.5% Triton X-100) prior to fixation for immunofluorescence analysis. We first performed the DRT assay on DMSO control-treated or etoposide-treated cells, and

saw an increase in the HPEM unextractable fraction of TOP2A by immunofluorescence with etoposide treatment, as has been reported (Fig. 5.7 B) [228]. Etoposide, however, causes covalent TOP2A protein-DNA adducts which are processed to form double-strand breaks that could interfere with DNA replication [229]. We decided to use the catalytic inhibitor ICRF-187 in this assay instead, as it stabilises TOP2A in the closed clamp form which does not affect deoxyribonucleotide incorporation in the short time points used in our experiments (Fig. 5.7 D) [134]. However, we observed that extraction with buffer containing 350 mM NaCl, as used in the original method [228], disrupted normal nuclear structure (Fig. 5.7 B). To avoid this, we found that a reduction to 100 mM NaCl was necessary (Fig. 5.7 C).

A TOP2A DAPI

PFA

B

40x   100x

TOP2A   DAPI   TOP2A   DAPI

DMSO

Etop

C

DMSO   ICRF

300 mM   300 mM   100 mM   NaCl

TOP2A

DAPI

D TOP2A   EdU   DAPI

DMSO
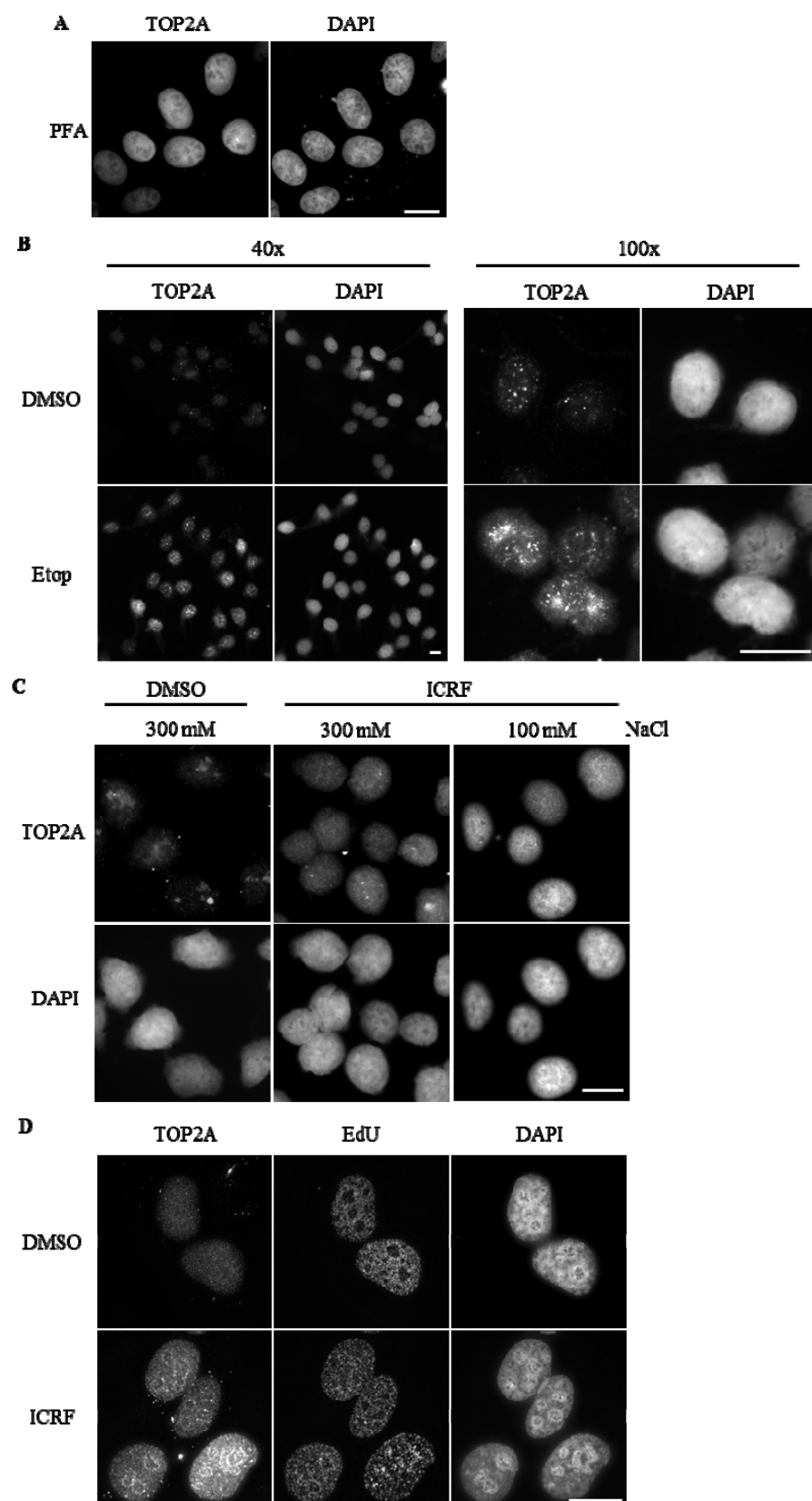
ICRF

Figure 5.7 Differential retention of topoisomerase (DRT) by etoposide and ICRF-187. (A)
U2OS cells were fixed with 4% PFA and the localisation of TOP2A was detected by
immunofluorescence microscopy with anti-TOP2A antibody. (B) U2OS were treated with
DMSO or 20 μM etoposide (Etop) for 30 min and pre-extracted with 350 mM NaCl HPEM
buffer. (C) U2OS treated with the topoisomerase 2 inhibitor ICRF-187 (50 μg/ml) for 15
min were pre-extracted with 300 mM or 100 mM NaCl HPEM buffer. (D) Detection of
nascent DNA synthesis in the presence of ICRF. EdU and ICRF were added 15 min before
pre-extraction with 100 mM NaCl HPEM buffer. Scale bar = 20 μm.

5.7 Localisation of TOP2A by immunofluorescence
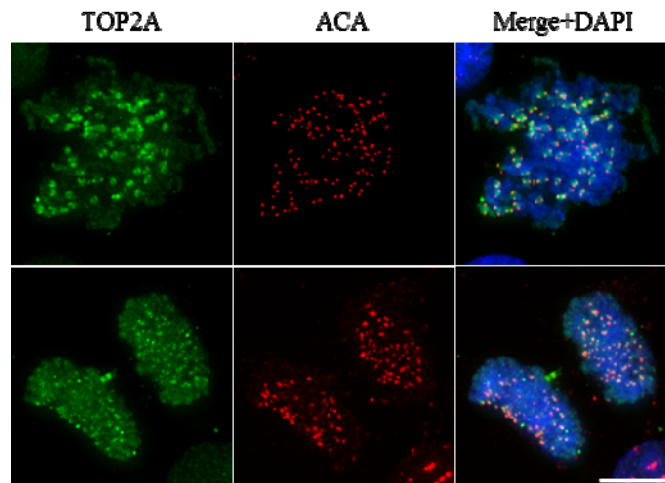
Figure 5.8 TOP2A is localised to chromosome arms and centromeres in mitosis. U2OS
cells were treated with 50 μg/ml ICRF-187 for 15 min prior to pre-extraction and fixation.
TOP2A is shown in green. Centromeres were labelled with an anti-centromere antibody
(Red; ACA). Mitotic cells were selected by their visibly condensed chromosomes. Scale bar
= 10 μm.

Using the DRT assay, we examined the localisation of TOP2A by IF in an asynchronously growing population of U2OS cells, and centromeres were detected using Anti-Centromere Antibodies (ACA) which recognise centromeric proteins. As previously reported, TOP2A was detected along the chromosome axes and concentrated at centromeres of mitotic chromosomes (Fig. 5.8 and [228,230]).

Interestingly, we also observed centromere localisation in a number of interphase cells, in which centromeric localisation of TOP2A has not previously been reported. In contrast to mitotic cells, however, not all centromeres co-localised with TOP2A, and the proportion of TOP2A positive centromeres differed between cells (Fig. 5.9 A). To further stratify the interphase cells, a brief treatment with the thymidine analogue EdU was introduced, and cells were determined to be in early, mid, or late S-phase according to the pattern of EdU incorporation observed [231]. The proportion of TOP2A positive centromeres per cell appeared to correlate with S-phase progression — low in early S-phase and increased in mid and late S-phase. To quantify this result, the total number of discernible centromeres in a single optical section of a cell were counted, and the percentage of centromeres that were also co-stained with TOP2A foci was determined. A significantly higher proportion of TOP2A-positive centromeres was found in late S-phase cells compared to early S-phase cells (Fig. 5.9 B).
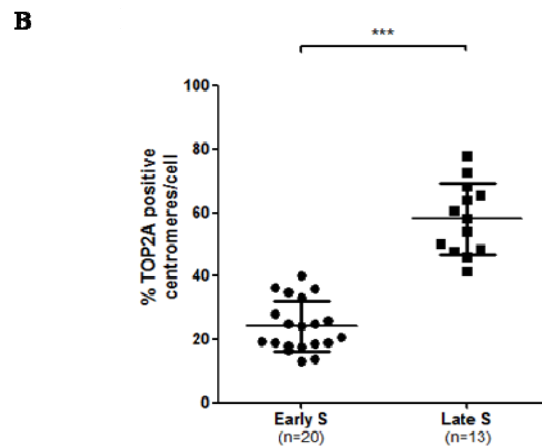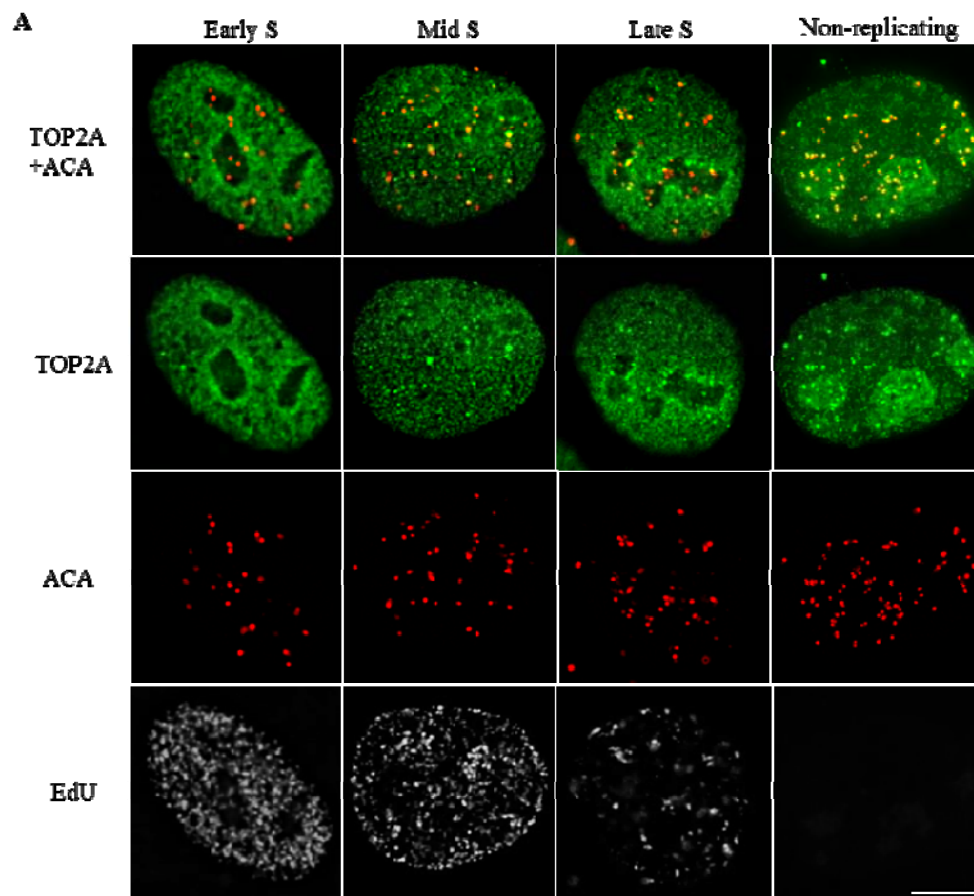
Figure 5.9 Recruitment of TOP2A to centromeres is a gradual process that occurs through S-phase. *U2OS cells were treated with 10 μM EdU and 50 μg/ml ICRF-187 for 15 min prior to pre-extraction, fixation, and immunofluorescence analysis. TOP2A is shown in green and centromeres (ACA) in red. (A) Representative images of early, mid, and late S-*

*phase cells, and a non-replicating interphase cell are shown (left to right). (**B**) Cells in early or late S-phase were randomly selected and the percentage of TOP2A positive centromeres in a single optical section was determined. Each point represents data from one cell. Bars represent the mean ± S.D. ***P<0.0001, Student's t-test. Experiment was performed once. Scale bar = 10 μm.*

5.8   Centromeric localisation of DBF4

5.8.1 Localisation of tagged DBF4 by immunofluorescence

Our initial immunofluorescence experiments had previously shown DBF4 to be pan-nuclear distributed (Fig. 3.5). For a more detailed analysis, we examined the localisation of DBF4 with the Strep-tag antibody under similar conditions to the DRT assay. Extraction of soluble proteins with HPEM buffer revealed the presence of tagged DBF4 in foci that did not co-localise with active replication, but were frequently observed immediately adjacent to replication foci in late S-phase cells (Fig. 5.10 A). Co-staining with ACA showed that these foci of tagged DBF4 corresponded to centromeres in all transfected interphase cells. Tagged DBF4 was present at centromeres at all stages of S-phase, and this was maintained when CDC7 was inhibited with XL413 (Fig. 5.10 B).

Using the deletion mutants described previously (Section 5.3), we investigated the requirements for DBF4 nuclear and centromeric recruitment. Expression plasmids for the DBF4 fragments were transfected into U2OS cells, and processed for IF both with and without a HPEM buffer pre-extraction step. DBF4 fragments carrying deletions of the MC region had impaired nuclear localisation, but a fraction remained in the nucleus (Fig. 5.11 A). When cells were subjected to pre-extraction, the MCT, NT, and T mutants were no longer detectable by IF. While both the N and NMC mutants were still present, only the NMC was localised to centromeres (Fig. 5.11 B). Therefore, the N-terminal domain is necessary for chromatin binding, but all three NMC domains are required for centromeric recruitment.
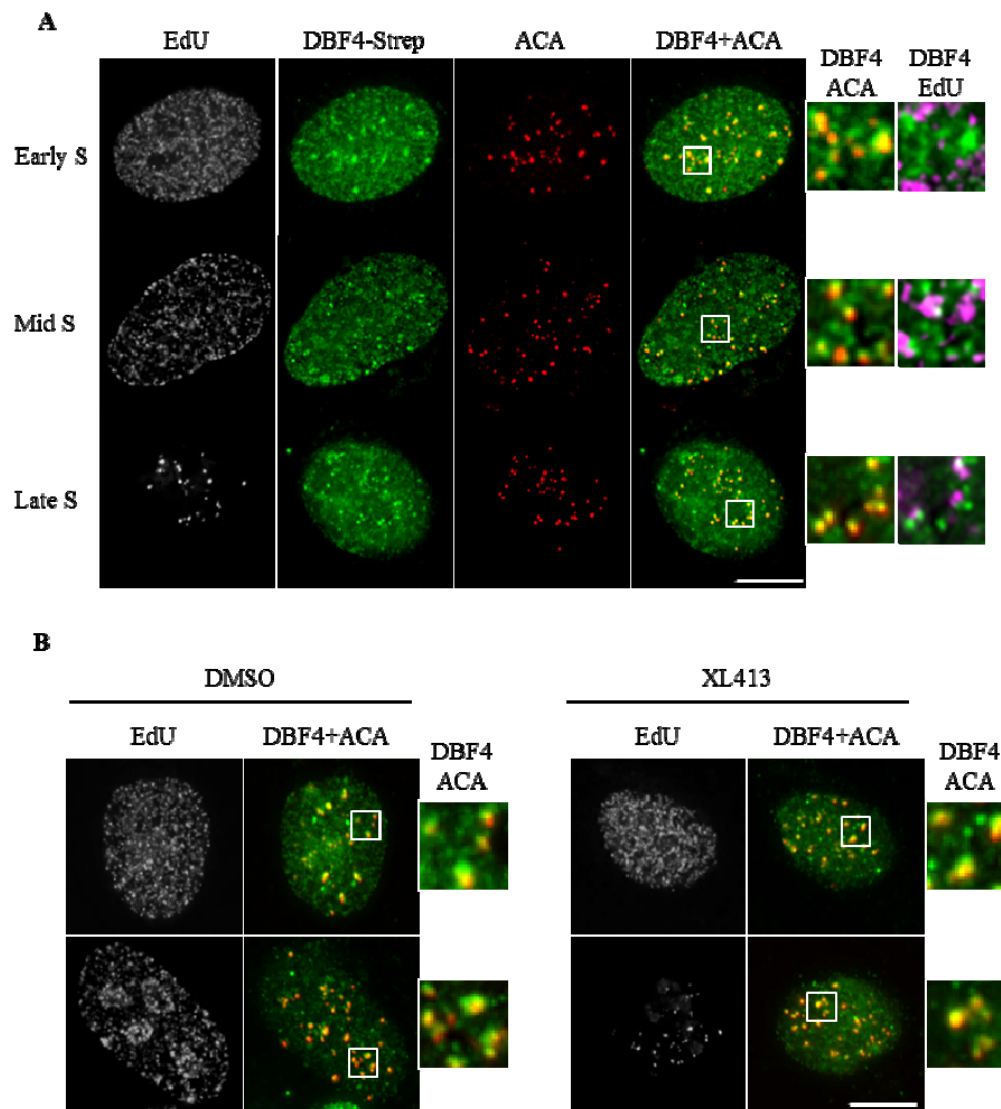
Figure 5.10 DBF4 localises to centromeres throughout S-phase independent of CDC7 kinase activity. *U2OS cells expressing DBF4-Strep were pre-extracted with 100 mM NaCl HPEM buffer and fixed with 4% PFA. Actively replicating regions were labelled by the addition of 10 μM EdU for 15 min immediately prior to extraction. (**A**) Representative images of cells in different stages of S-phase. (**B**) Cells were treated with DMSO or XL413 for 3 h before EdU addition. DBF4-Strep is shown in green, ACA in red, and EdU in grayscale/magenta. Scale bar = 10 μm.*
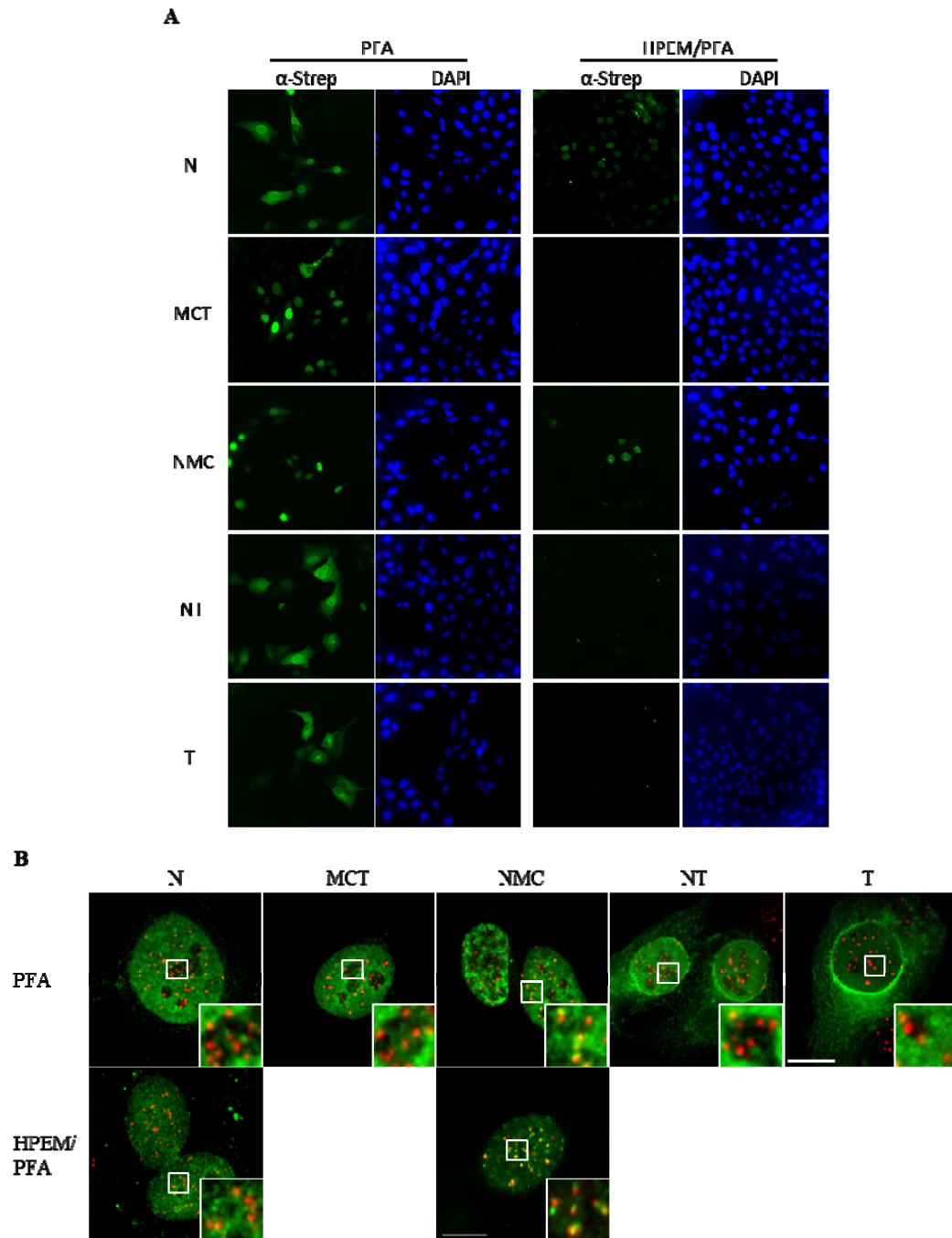
Figure 5.11 Both DBF4 N and MC domains are required for centromeric localisation.
U2OS cells were transfected with expression plasmids for Strep-tagged DBF4 mutants containing deletions in their N (1-209 a.a.), MC (210-350 a.a.) or Tail (T; 351-674 a.a.) domains. Cells were fixed directly with 4% PFA, or salt- and detergent-extracted (HPEM/PFA) prior to fixation and immunofluorescence analysis. The Strep-tag is shown in

green, centromeres (ACA) in red, and DAPI in blue. Images were collected with a (A) 40x or (B) 100x oil immersion objective. No positively stained cells were observed with the DBF4 MCT, NT, or T deletion mutants after pre-extraction. Scale bar = 10 μm.

5.8.2 Chromatin Immunoprecipitation of tagged DBF4

As an independent method to confirm DBF4 localisation at centromeres, we decided to use chromatin immunoprecipitation (ChIP). Primers were selected to amplify two centromeric targets — a chromosome 1-specific target sequence (Cent1) [198], and the (peri)centromeric α-satellite monomer (α-Sat) [199] — and a non-centromeric sequence corresponding to the GAPDH promoter close to the transcriptional start site. The amplification efficiencies of these primer pairs for quantitative PCR (qPCR) were determined using 10-fold serial dilutions of sheared genomic DNA from 100,000 T-REx 293 cells (equivalent to 2% of input for 1 ChIP reaction). Standard curves were constructed on a graph of threshold cycles (C_T) against the log Input (Fig. 5.12 A), and the amplification efficiencies were calculated from the slopes of the standard curves (Fig. 5.12 B, a slope of -3.3 equates to 100% efficiency). As all three primer pairs have efficiencies of greater than 80%, they were suitable for use in qPCR analysis. Primer specificities were also confirmed by the generation of a single amplicon by melt curve analysis and gel electrophoresis (Fig. 5.12 C). Cent1 specificity has been shown by *in situ* hybridisation to a single genomic locus [198], and it is also not tandemly duplicated as the PCR product appears as a single distinct band by electrophoresis (Fig. 5.12 C, middle lane). Since both Cent1 and GAPDH target sequences are located on Chromosome 1, and are present at one copy per chromosome, their enrichment values should be directly comparable. Slight smearing is observed in the α-Sat PCR product, possibly due to α-Satellites being arranged in tandem repeats [199].
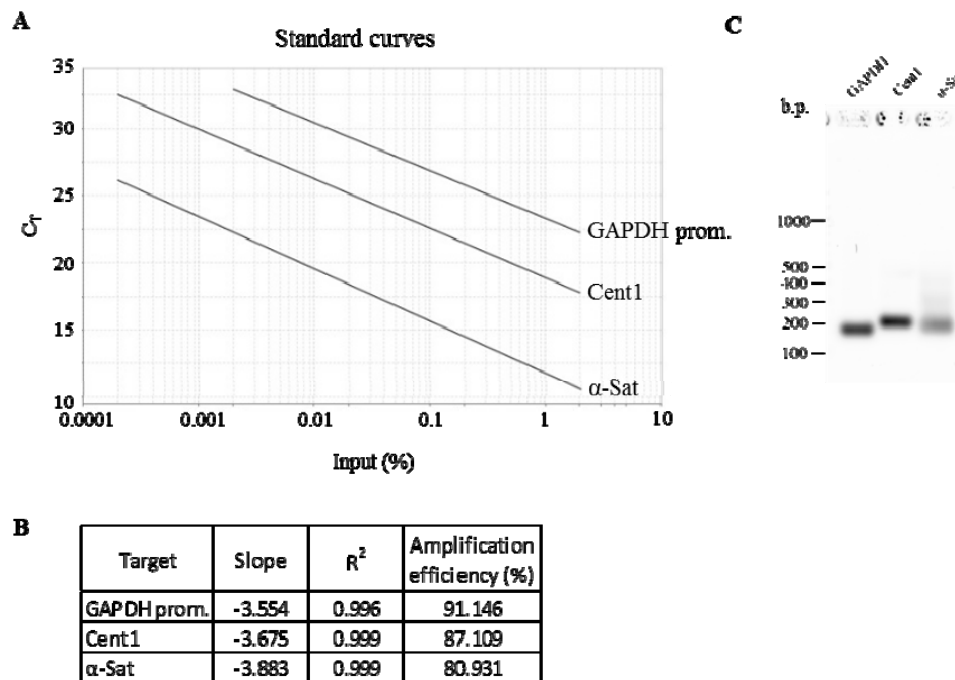
Figure 5.12 Evaluation of primer pair suitability for qPCR analysis. Up to 5 ten-fold serial dilutions of sheared, purified genomic DNA from 5 x 10⁶ cells (equivalent to 2% of ChIP input) were used as the template for qPCR analysis using primer pairs targeting the GAPDH promoter (GAPDH prom.), Chromosome 1 centromeric (Cent1), and α-satellite (α-Sat) loci. (A) Standard curves were constructed, and (B) amplification efficiencies were determined from the slopes using StepOne Plus Software. (C) For each primer pair, one sample from the qPCR reaction was analysed by gel electrophoresis to confirm amplification of a single product.

We next performed ChIP using a number of antibodies, including the anti-Strep-tag, anti-CDC7 (12A10), anti-DBF4 (6F4/6), and anti-RNA polymerase II (RPB1) antibodies. As the baseline control for background antibody binding, ChIP from T-REx-EV cells was performed alongside T-REx-DBF4 cells. Following qPCR analysis, the amount of each target locus recovered was calculated relative to the 2% input sample, and also expressed as a fold-enrichment relative to the corresponding EV ChIP. As the positive control for the ChIP protocol, occupancy of RPB1 at the GAPDH promoter was used (Fig. 5.13 A, top graph). ChIP with the Strep-tag antibody showed increased occupancy of tagged DBF4 at all 3 loci to varying extents, but the monoclonal antibodies for CDC7 and DBF4 showed negligible

119

increases over the background and do not appear to function in ChIP (Fig. 5.13 A). DBF4 ChIP with the Strep-tag antibody resulted in a 37-fold enrichment of the Cent1 locus, and more than 7-fold enrichments of both the α-Sat and GAPDH promoter loci (Fig. 5.13 B). Enrichment of the Cent1 locus was significantly higher than enrichment of the non-centromeric GAPDH locus, strongly supporting a specific accumulation of DBF4 at centromeres and not general chromatin binding. Due to its tandemly repeated nature in higher-order repeat (HOR) structures, the fold enrichment value of α-Sat was not directly comparable to the other single locus targets.
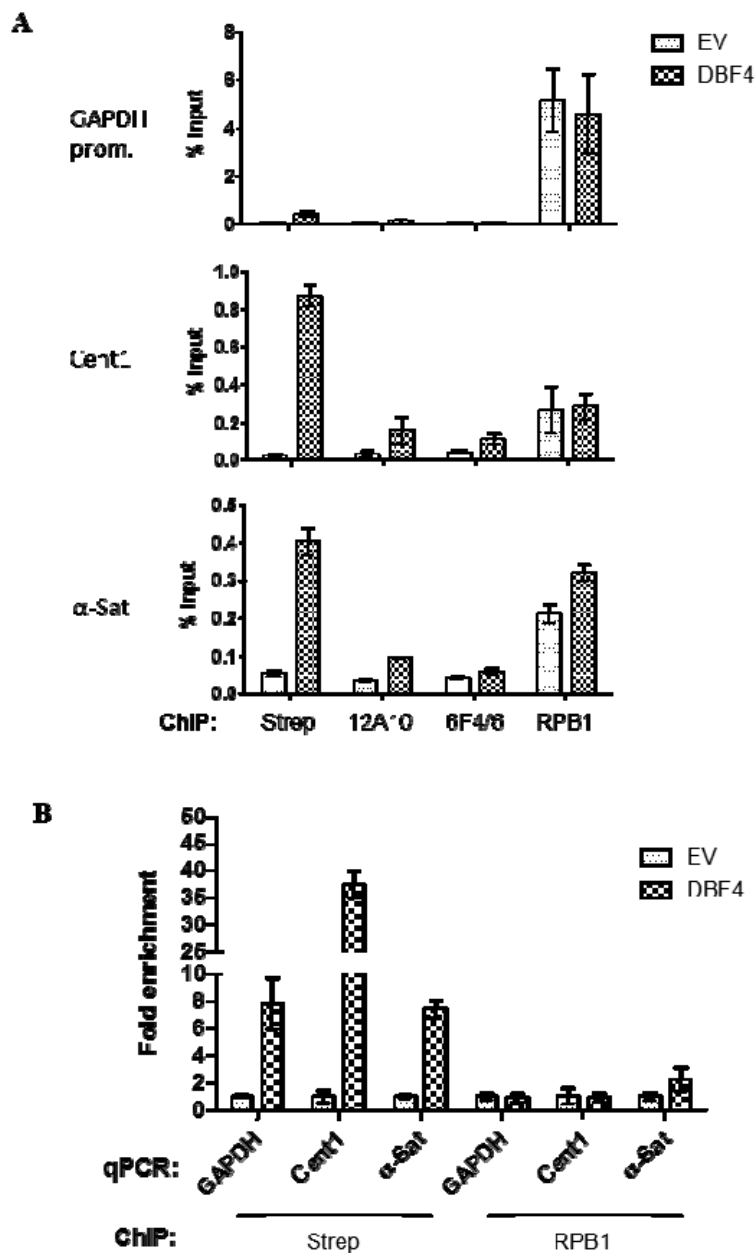
***Figure 5.13 Enrichment of centromeric DNA by chromatin immunoprecipitation (ChIP)
of DBF4-Strep.*** *ChIP was performed from T-REx-EV or –DBF4 cells with antibodies
against the Strep-tag (Strep), CDC7 (12A10), DBF4 (6F4/6), and RNA pol II (RPB1). The
amounts of the non-centromeric GAPDH promoter, Chromosome 1 centromeric (Cent1),
and α-satellite (α-Sat) loci recovered were determined by qPCR relative to (**A**) the input
samples, or (**B**) the corresponding EV sample. Bars represent the mean ± S.D of 3 technical
repeats. Results are representative of 3 biological replicates.*

121

5.9 Effect of CDC7 kinase inhibition or depletion on TOP2A centromeric recruitment

Since both CDC7-DBF4 and TOP2A are localised to centromeres in S-phase, we postulated that CDC7-DBF4 might regulate the recruitment of TOP2A to centromeres. We therefore examined the localisation of TOP2A in cells treated with CDC7 kinase inhibitors using the DRT assay. Indeed, in actively replicating cells, we noticed that an increased proportion of centromeres were positive for TOP2A when CDC7 kinase was inhibited. This was particularly striking in early S-phase, during which the number of TOP2A positive centromeres is typically low in unperturbed conditions (Fig. 5.9). Quantification in individual early S-phase cells confirmed a significant increase in TOP2A positive centromeres caused by CDC7 inhibition with either XL413 or PHA767491 (Fig. 5.14).

A similar result was obtained through siRNA-mediated depletion of CDC7 and/or DBF4. Endogenous levels of DBF4 are not detectable by immunoblotting, and the cellular effect of siRNA depletion was determined indirectly through a reduction in MCM2 phosphorylation instead (Fig. 5.15 A). Notably, combined depletion of CDC7 and DBF4 did not result in an additive effect on TOP2A centromeric recruitment despite a further reduction in MCM2 phosphorylation compared to DBF4 depletion alone, suggesting that this function is independent of DBF4B (Fig. 5.15 C).

Although each experiment was only carried out once, both the treatment with CDC7 kinase inhibitors, and the depletion of CDC7 and DBF4 by siRNAs independently produced similar results, leading us to the conclusion that loss of CDC7 kinase activity leads to increased recruitment of TOP2A to centromeres in early S-phase cells.

A

B
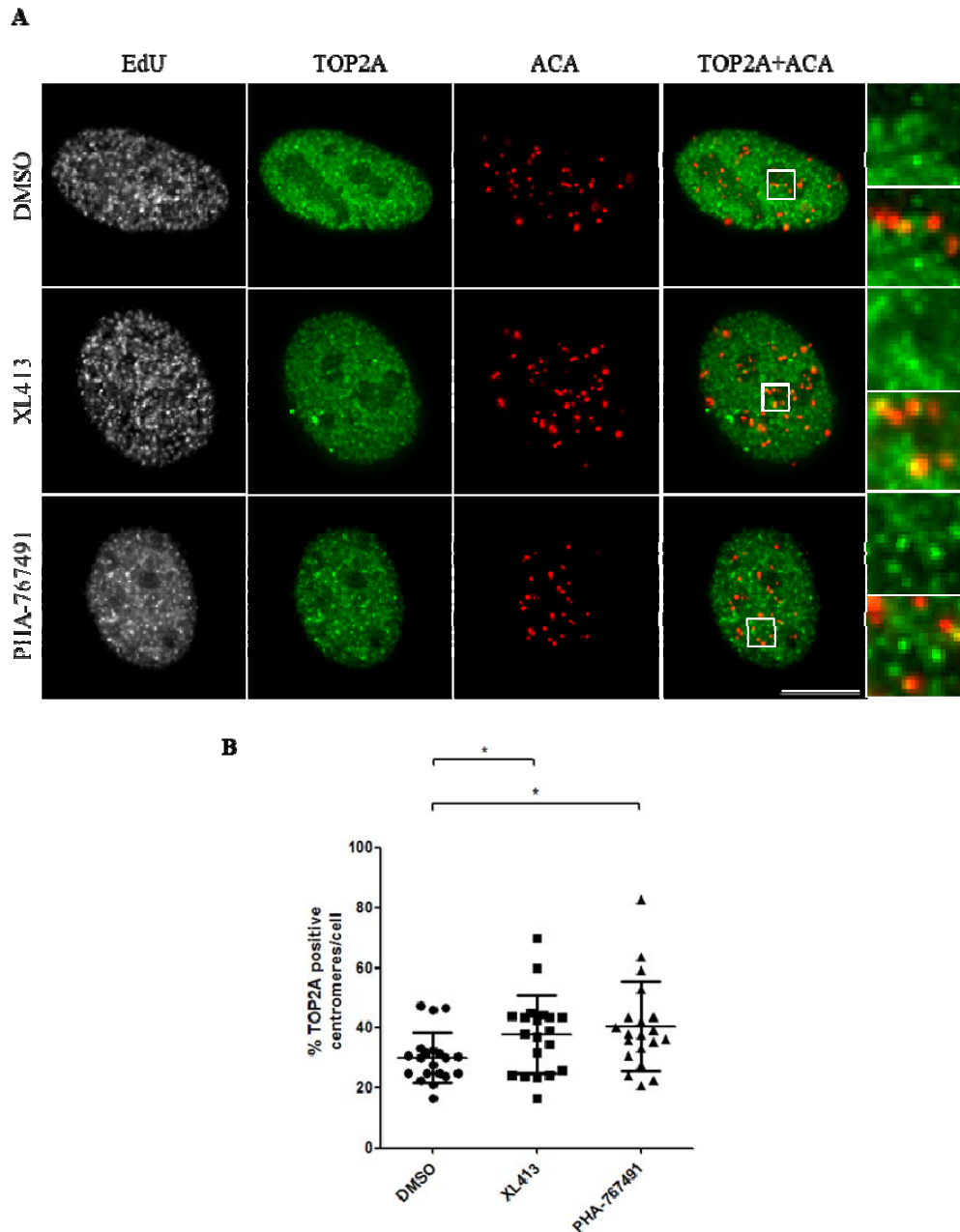
Figure 5.14 CDC7 kinase inhibition increases centromeric TOP2A recruitment. U2OS cells were treated with 10 μM XL413, PHA-767491, or DMSO control for 3 h. Cells were treated with 10 μM EdU and 50 μg/ml ICRF-187 for 15 min prior to pre-extraction, fixation and immunofluorescence analysis. (A) Representative images of early S-phase cells are shown. (B) The percentage of TOP2A positive centromeres in randomly selected early S-phase cells was quantified as described in Fig 5.9. 20 cells were scored per treatment (13-36 centromeres/cell). *P<0.05, Student's t-test. Scale bar = 10μm. Experiment was performed once.
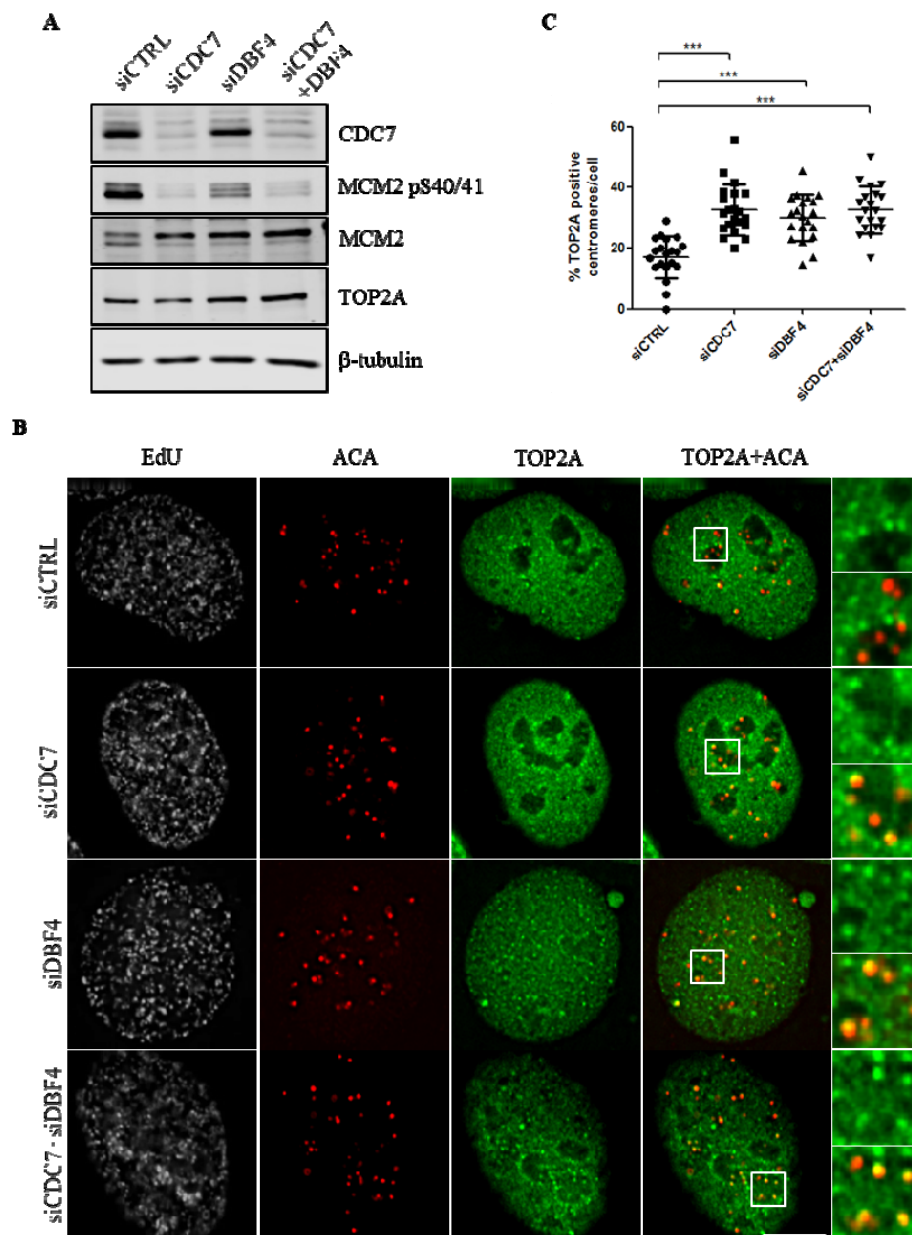
Figure 5.15 CDC7-DBF4 depletion increases the recruitment of TOP2A to centromeres.
U2OS cells were treated with siRNA against CDC7 and/or DBF4 for 48 h. Cells were
treated with 10 μM EdU and 50 μg/ml ICRF-187 for 15 prior to pre-extraction, fixation and
*immunofluorescence analysis. (**A**) Total cell lysates were analysed by immunoblotting. (**B**)*
*Representative images of early-mid S-phase cells are shown. (**C**) The percentage of TOP2A*
positive centromeres in randomly selected early S-phase cells was quantified as described in
Fig 5.9. 20 cells were scored per treatment. ***P<0.001, Student's t-test. Scale bar =
10μm. Experiment was performed once.

5.10 Conclusion

We have described the identification and characterisation of a novel interaction between CDC7-DBF4 and TOP2A. This interaction is likely to occur at centromeres during G1/early S-phase and is lost as cells complete S-phase. By deletion mapping, we have determined the DBF4 domains necessary for its centromeric localisation and interaction with TOP2A. Finally, we have demonstrated a novel role for CDC7-DBF4 kinase in regulating the timing of centromeric TOP2A recruitment in S-phase.

Chapter 6: Discussion

6.1   Effects of CDC7 kinase overexpression in human cell lines

Although the primary scope of this work was to identify novel interacting proteins of CDC7 kinase, the generation of these Flp-In T-REx 293 cell lines has also allowed us to examine the effects of CDC7 overexpression in human cells, a preliminary effort of which has been presented here. The importance of CDC7 kinase for S-phase entry and the strict regulation of its activity during the cell cycle would suggest that its constitutive expression might be detrimental to cells. This seems to be the case in *S. cerevisiae*, where cells co-overexpressing CDC7 and DBF4 failed to form viable colonies [232]. Guo and colleagues also reported that high levels of CDC7 or DBF4 in Chinese hamster ovary (CHO) cells causes a G1 arrest [233], but a separate study in human HeLa cells found no effect on cell cycle progression [148]. In our experimental system, the expression of the CDC7 subunit alone, resulting in a two-fold increase of protein levels, was not sufficient to affect the *in vivo* phosphorylation of MCM2 at a CDC7-dependent site. This is consistent with data from a proteomics study reporting copy number estimates, in which the CDC7 subunit was found to be on average 12-fold more abundant than DBF4 and DBF4B combined in HeLa cells [150]. Given this large excess, it is also unsurprising that the level of CDC7 KD expression achieved with our system failed to have a dominant-negative effect on MCM2 phosphorylation, DNA replication, or cell proliferation.

Despite significantly increased phosphorylation of the known substrate MCM2 resulting from DBF4 or DBF4B overexpression, we did not observe defects in cell proliferation or cell cycle progression. CDC7 kinase by itself is insufficient to trigger S-phase entry in human cells, likely due to limiting levels of CDK activity, which prevents unscheduled replication origin firing (reviewed in [69]). As a surrogate marker of *in vivo* CDC7 kinase activity, we have monitored the phosphorylation of MCM2 at a single site, pS40/41 [155]. However, the biological relevance of this phosphorylation site is undetermined, and it is the CDC7-mediated

phosphorylation of MCM4 that appears to be critical for its role in replication [153,160]. Under our experimental conditions, we cannot rule out the possibility that increased cellular CDC7 kinase activity results in phosphorylation of MCMs on residues that are non-essential for origin firing. However, in all the studies mentioned here (including this one), cells were only monitored in the short term (up to 4 days) [232]. Subtle or accumulative effects, requiring multiple rounds of cell division to cause an observable phenotype, would have been missed. This is supported by the fact that efforts within our group to generate stable cell lines with constitutive expression of DBF4 or DBF4B have been unsuccessful (our unpublished observations).

6.2 Distinct subcellular localisation and interactome of CDC7-DBF4 and CDC7-DBF4B

Whether or not CDC7-DBF4 and CDC7-DBF4B complexes are functionally distinct is an important question which has been largely unaddressed. Protein copy number estimates suggest that DBF4B is about 3-fold less abundant than DBF4 in HeLa cells [150]. We found that DBF4 expression results in more extensive phosphorylation of MCM2 compared to DBF4B. It is possible that they activate CDC7 kinase activity to different extents, that they are differentially regulated, or that they target CDC7 kinase to different substrates or different residues on the same protein. This may be achieved through their C-terminal regions which are poorly conserved [140].

Using immunofluorescence and biochemical fractionation approaches, two previous studies concluded that DBF4B was nuclear localised [140,141]. In contrast, we found that the C-terminally tagged DBF4B fusion proteins (FLAG-Strep and GFP) to be predominantly non-nuclear. We have shown that DBF4B is subject to nucleo-cytoplasmic shuttling, and that CDC7-DBF4B is recruited to microtubules and centrosomes. This novel localisation is in agreement with the Strep-Tactin purification – SILAC proteomics data, where multiple tubulin subunits, and centrosome-associated proteins were co-purified with DBF4B. The development of

sensitive and specific immunological reagents for the detection of endogenous DBF4B would avoid the necessity for overexpression and epitope tagging, which could be causing some degree of mis-localisation. In addition, the fluorescent labelling of endogenous DBF4B, for instance using CRISPR/Cas9, would allow us to investigate its protein localisation dynamics in living cells.

Consistent with the idea that the levels of its regulatory subunits are limiting, purification of the CDC7 subunit alone did not result in the identification of many interacting proteins — it is possible that the formation of an active complex may be a prerequisite for substrate binding. Notably, we did not detect any known substrates with either approach (see Table 1.2), suggesting that these are transient or low abundance interactions, or only occur under specific conditions, such as replication stress. Nevertheless, we have identified a number of promising novel candidates for future study, some of which have been validated through independent purification experiments. Despite the fact that induced expression of DBF4 and DBF4B in T-REx cells both increase the phosphorylation of the same substrate, MCM2, comparison of the DBF4 (FLAG IP) and DBF4B (Strep-Tactin) datasets revealed only two common proteins — CDC7, and MDN1, a nuclear chaperone. Taken together with their striking differences in subcellular localisation, we believe that DBF4 and DBF4B regulate CDC7 kinase activity by targeting it to different, but also overlapping sets of substrates.

6.3 IRS4 is important for receptor tyrosine kinase signalling and cell proliferation

We were able to demonstrate that IRS4 specifically interacts with CDC7-DBF4B but not with CDC7-DBF4. IRS4 is among the least well characterised of the IRS family members. It has been shown to be phosphorylated in response to stimulation with insulin, insulin-like growth factor I (IGF-1), growth hormone, and fibroblast growth factor (FGF) [212,234-237]. However, its physiological role remains elusive, and IRS4-null mice exhibit only mild defects in growth and insulin tolerance, in contrast to IRS1 and IRS2 which have major effects on growth and pancreatic β-cell proliferation respectively [45,46,49]. IRS1 and IRS2 are expressed in the majority of cell lines and tissues studied, while IRS4 expression is limited to a much smaller range [48]. IRS4 has been reported to mediate mitogenic signalling and the stimulation of DNA synthesis through the PI3K pathway in quiescent cells [234]. Elevated levels of IRS4 in cell lines, including HEK293T, have been described to be associated with upregulation of PI3K signalling, even in serum-limiting conditions [46,213]. However, to our knowledge, the effects of IRS4 depletion on cell cycle progression in non-serum-limiting conditions have not previously been examined.

We observed contrasting effects of IRS4 depletion with two different siRNAs. siIRS4-A, which resulted in the more efficient depletion, strongly inhibited proliferation, while the more modest, but significant depletion achieved with siIRS4-B did not appear to have any effect on cell proliferation. A simple interpretation of these results would point to off-target effects of siIRS4-A, but a BLAST search (http://blast.ncbi.nlm.nih.gov/Blast.cgi) did not reveal homology of the RNAs to other genes including other IRSs. Querying the siIRS4-A sequence in the siSPOTR prediction algorithm (siRNA Sequence Probability-of-Off-Targeting Reduction [238]) also indicated low off-targeting potential. Since the estimated number of IRS4 molecules in HEK293 cells is approximately 100-fold more than the number of insulin and IGF-1 receptors combined [212], saturation of the receptors could present an alternative explanation as to why milder IRS4 depletion (by siIRS4-B)

does not cause a phenotype unless levels are reduced past a certain threshold (such as by siIRS4-A).

6.4   IRS4 overexpression in cancer

While AKT S473 phosphorylation, and therefore activation, was impaired by IRS4 depletion in HEK293T cells, we did not observe any effects on S-phase progression. This could simply be due to the residual levels of IRS4 mediating sufficient levels of signalling for cell cycle entry. We did, however, observe a defect in G2-M progression. Interestingly, constitutive AKT activation has been shown to overcome a DNA-damage induced G2-M checkpoint, and it is proposed that this mechanism contributes to genetic instability in cancer cells [239]. In line with this, IRS4 is known to be overexpressed in hepatocellular carcinoma cell lines as well as in T-cell acute lymphoblastic leukemia (T-ALL) [39,240]. Additionally, point and deletion mutations in IRS4 have been detected in T-ALL and metastatic melanomas, although their influence on disease progression is unknown [241,242]. Taken together, we hypothesise that overexpression of IRS4 in cancer cells causes deregulation of and/or increased PI3K/AKT pathway activity, leading to increased mitogenic signalling, as well as mutagenesis through checkpoint bypass. This again, could result in an overdependence on CDC7 kinase for S-phase DNA damage response and tolerance pathways (Section 1.6.5).

6.5   IRS4 is a novel CDC7-DBF4B interacting protein

We have attempted to determine the biological significance of the CDC7-DBF4B interaction with IRS4. We investigated a potential role for CDC7 kinase in regulating growth factor signalling through the PI3K/AKT pathway. Treatment with the inhibitor XL413 resulted in attenuated AKT activation that unfortunately was not reproduced by CDC7 depletion. This can probably be attributed to XL413 off-target inhibition of PIM1 kinase ([147], supplementary information), which has known involvement in this pathway [243,244]. Neither did we find evidence of the reciprocal regulatory relationship – IRS4 depletion did not affect CDC7-dependent phosphorylation of MCM2.

There are several important caveats to our experiments. Firstly, we were not able to find a suitable cell type with high IRS4 expression which is also permissive to serum withdrawal and re-stimulation. IRS4 expression in HFFs is low compared to HEK293 cells (our results, not shown), and it is possible that IRS1/2 are more abundant and therefore would be the major effectors of tyrosine receptor signalling in these cells. In such a case, any IRS4-specific effects caused by CDC7 inhibition or depletion would be masked. It would be interesting to determine if CDC7-DBF4B interacts with other IRS proteins as well. Phosphorylation of serine residues on IRS1 has been reported to be involved in regulating its protein-protein interactions [245], and even inhibit insulin receptor tyrosine kinase activity [246]. A number of phosphoserine residues on IRS4 located within putative CDC7 consensus sites (adjacent to acidic residues D/E [155,247]) are recorded on the protein phosphorylation database PhosphoSitePlus (http://www.phosphosite.org). We made a preliminary attempt to investigate IRS4 phosphorylation status in the presence of CDC7 kinase inhibitors using Phos-tag SDS-PAGE gels, but the results were inconclusive due to the extensive phosphorylation of IRS4 causing it to run as a wide "smear" that may have masked changes at a small number of sites (not shown).

In order to determine the effects of IRS4 depletion, we examined CDC7 activity in a single experimental context: actively cycling cells. As discussed previously, CDC7 is also important for several aspects of the DNA damage response in S-phase. A role for IRS4 here would not be unprecedented, as IRS1 has been reported to regulate homologous recombination through RAD51 nuclear translocation [248,249]. Given the central nature and wide ranging effects of the PI3K/AKT axis in cell proliferation [250], CDC7-dependent and independent functions of IRS4 will need to be uncoupled. To achieve this, deletion mapping to identify the interacting domains (similar to the approach taken with DBF4-TOP2A in Chapter 5) could allow the generation of truncated forms of IRS4 or DBF4B that no longer interact, but are otherwise competent for their other functions. Using these in knockout-rescue experiments would be highly informative for determination of functions of this specific interaction.

6.6 Centromeric localisation of CDC7-DBF4

By immunofluorescence and chromatin immunoprecipitation, we have provided the first evidence that DBF4 is recruited to centromeres in human cells. During optimisation of the ChIP protocol for DBF4, we found that in addition to formaldehyde, the use of ethylene glycol bis(succinimidyl succinate) (EGS) was also necessary to immunoprecipitate DBF4-associated chromatin. EGS is a protein-protein cross-linking agent with a long spacer arm that, when used in combination with formaldehyde, stabilises proteins that are not directly bound to DNA [251]. This suggests that CDC7-DBF4 is instead recruited by other protein factor(s). We have demonstrated that the N-terminal 1-209 residues of DBF4 are essential and sufficient for chromatin binding. This region remains poorly characterised, but does contain a BRCT domain that is proposed to be involved in protein-protein interactions [200]. Interestingly, the equivalent domain of DBF4 in budding yeast, *S. cerevisiae,* has been shown to be required for interaction with several replication and checkpoint proteins, including ORC, RAD53 (homologue of CHK2), and RIF1, although it remains to be demonstrated if these interactions are also conserved in humans [205,252,253]. The mechanisms regulating its centromeric recruitment, however, are likely distinct, as the DBF4 MC domains (residues 210-350) and presumably the CDC7 subunit, are also essential for this.

A recent report showed that in budding yeast, CDC7-DBF4 is recruited to kinetochores where it promotes the replication of centromeric regions early in S-phase through the recruitment of the essential replication proteins SLD3 and SLD7 (Treslin/TICRR and MTBP in humans) to pericentromeric origins [254]. Unlike budding yeast, however, human centromeric DNA is replicated asynchronously between mid to late S-phase [255,256]. Furthermore, DBF4 was detected at all centromeres from early S-phase, inconsistent with centromeric replication timing. Therefore, this function in budding yeast does not appear to be conserved in human cells. That said, we cannot exclude the possibility of mis-regulation due to overexpression or epitope tagging of DBF4 that have been necessary for our experiments. In the same study, the authors also found that centromeric ScCDC7-

DBF4 independently recruits the SCC2-SCC4 cohesin loading complex for the establishment of robust pericentromeric sister chromatid cohesion [254]. *Xenopus* CDC7-DBF4B (the predominant CDC7 kinase complex in egg extracts) also physically interacts with SCC2-SCC4 and is required for its chromatin binding [169]. Consequently, it may be that the homologous complex in humans, NIPBL-MAU2, is regulated by CDC7 kinase in a similar manner.

6.7   TOP2A is not recruited to late replicating heterochromatin

Under our experimental conditions, TOP2A localisation to centromeres did not always coincide with the detection of ongoing replication at centromeric regions, and as such, our results do not support the recruitment of TOP2A to late replicating heterochromatin, as has been previously reported [228]. The reason for the observed differences could be technical; the authors reference 2 different monoclonal antibodies (Ki-S1, which was also used in our study; and 3D4, which specifically recognises pT1342 [257]), but they did not specify which was used for immunofluorescence labelling. Clone Ki-S1 recognises an epitope within the C-terminal 495 residues [258], a region containing a large number of phosphorylation sites (PhosphoSitePlus). It is possible that clones Ki-S1 and 3D4 recognise different subsets of phosphorylated TOP2A species. While pT1342 is detected throughout the cell cycle, its levels do not remain constant, and it is unclear if the entire pool of TOP2A is constitutively phosphorylated at this site [257]. An accurate determination of antibody specificity and a more thorough characterisation of the various phosphospecies could provide novel insight into how distinct pools of TOP2A are regulated with regard to their subcellular localisation and function.

6.8   A novel role for CDC7-DBF4 and TOP2A at centromeres

In addition to its essential roles in G2-M phase progression (discussed in Section 1.5.2 and 1.5.3), our work has revealed novel TOP2A localisation to centromeres in S-phase. TOP2A activity was detected at an increasing number of centromeres as cell progress through S-phase, and by kinase inhibition or depletion experiments, we have shown that this timing of TOP2A recruitment is regulated by

CDC7-DBF4 kinase activity. Based on our results, we propose that phosphorylation of TOP2A by CDC7-DBF4 in G1/early S-phase prevents its activity and/or localisation at centromeres. As cells approach late S/G2-phase, this mechanism is necessarily overcome, perhaps through the recruitment of other proteins to the centromere which inhibit or reverse CDC7-mediated phosphorylation of TOP2A (discussed later).

Chromosome cohesion is maintained by cohesin rings, which hold sister chromatids together (discussed in Section 1.1.4). Cohesin loading must be established during S-phase, as *S. cerevisiae* cohesin complexes expressed after S-phase become DNA-bound, but do not contribute to sister chromatid cohesion [259]. Based on work across several model organisms, one model proposes that cohesin is unstably loaded onto the unreplicated parental DNA strand, and that passage of the replisome through the cohesin ring results in the acetylation and stabilisation of cohesin around the resulting DNA duplexes ([260] and references therein). In *Xenopus* and *S. cerevisiae*, it was also demonstrated that the SCC2-SCC4 cohesin loading complex is dependent on CDC7 kinase [169,254]. From this it is clear that the establishment of cohesion is closely coupled to DNA replication. Thus, we hypothesise that CDC7 kinase activity contributes to centromeric cohesion in two ways – in addition to promoting cohesin loading through SCC2-SCC4 recruitment, it may also inhibit TOP2A activity to prevent premature separation of replicated centromeric DNA.

Upon mitotic entry, phosphorylation of cohesin by the mitotic kinase PLK1 facilitates its removal from chromosome arms [261]. To ensure that sister chromatids are properly aligned at the metaphase plate and do not become prematurely separated, centromeric cohesin is protected from PLK1 activity through the opposing action of the protein serine/threonine phosphatase PP2A [262,263]. PP2A has been shown to accumulate on centromeres in early mitosis, and is also reported to be active in interphase [263,264]. Therefore, PP2A may be a likely candidate counteracting CDC7-dependent phosphorylation of TOP2A.

Another possible role of CDC7 kinase at the centromere may be in the regulation of replication timing. Replication origins are fired in a defined temporal sequence, the timing of which is determined early in G1 phase. In mammals, the factors that distinguish an early firing origin from a late one are not easily defined, and go beyond simple classifications of eu- or hetero-chromatin state [265]. Increasing evidence indicates that the spatial positioning of origins within the three-dimensional structure of the nucleus is an important determinant of firing time – early origins are spread throughout the whole nucleus, and mid and late origins are localised to the nuclear and nucleolar boundaries or to heterochromatic foci [101,265-267]. The molecular mechanisms linking subnuclear positioning to replication timing are not yet well defined, with one notable exception. RIF1, originally identified as a telomere-associated protein, was recently discovered to be a key regulator of the replication-timing program. Depletion of RIF1 leads to the loss of the characteristic mid S-phase replication pattern, global changes in replication order and chromatin reorganisation [268,269]. RIF1 is thought to sequester mid-S replicating regions to the nuclear and nucleolar periphery where they are less accessible to initiation factors. Moreover, RIF1 has also been shown to recruit protein phosphatase 1 (PP1) to reverse CDC7-mediated phosphorylation of the MCM helicase, further preventing early firing of bound origins [252,270]. The accumulation of CDC7-DBF4 at centromeres alters the localised kinase:phosphatase ratio, and this suggests that centromeric CDC7-DBF4 regulates replication timing in this way as well.

Although TOP2A is not essential for DNA replication *per se*, as human and budding yeast cells lacking TOP2A complete genome duplication in the normal length of time [110,117], TOP2A may still regulate DNA replication. In the *Xenopus* system, TOP2A accumulates on chromatin in a replication-dependent manner, and has been found to promote the chromatin dissociation and degradation of ORC1/2 for the clearing of replicons in mitosis, as well as to regulate origin cluster firing time by restraining the loading of MCMs in G1 phase [118,119,271]. Whether or not there exists a functional interplay between CDC7-DBF4 and TOP2A in the temporal

135

or spatial regulation of DNA replication at centromeres, or indeed globally, is an exciting prospect for future study.

6.9 Concluding remarks

Overall, this work opens up novel avenues for the investigation of CDC7 kinase function through the identification and characterisation of its interacting proteins. While the main focus of this work has not been cancer biology, our study of these fundamental biological processes will hopefully allow us to understand the consequences of their mis-regulation and how these may contribute to cancer development or progression, and also provide insight into how they may be exploited for cancer therapy.

References

1. Wright NA, Poulsom R: **Omnis cellula e cellula revisited: cell biology as the foundation of pathology**. *J. Pathol.* 2012, **226**:145-147.

2. Malumbres M, Barbacid M: **Mammalian cyclin-dependent kinases**. *Trends Biochem. Sci.* 2005, **30**:630-641.

3. Sánchez I, Dynlacht BD: **New insights into cyclins, CDKs, and cell cycle control**. *Semin Cell Dev Biol* 2005, **16:**311-321.

4. Baserga R: **Oncogenes and the strategy of growth factors**. *Cell* 1994, **79**:927-930.

5. Pardee AB: **A Restriction Point for Control of Normal Animal Cell Proliferation**. *PNAS USA,* 1974, **71**:1286-1290.

6. Foster DA, Yellen P, Xu L, Saqcena M: **Regulation of G1 Cell Cycle Progression: Distinguishing the Restriction Point from a Nutrient-Sensing Cell Growth Checkpoint(s)**. *Genes Cancer* 2010, **1**:1124-1131.

7. Huberman JA, Riggs AD: **Autoradiography of chromosomal DNA fibers from Chinese hamster cells.** *PNAS USA,* 1966, **55**:599–606.

8. Sclafani RA, Holzen TM: **Cell Cycle Regulation of DNA Replication**. *Annu Rev Genet* 2007, **41**:237-280.

9. Woo RA, Poon RYC: **Cyclin-dependent kinases and S phase control in mammalian cells.** *Cell Cycle* 2003, **2**:316–324.

10. Taylor WR, Stark GR: **Regulation of the G2/M transition by p53.** *Oncogene* 2001, **20**:1803–1815.

11. Lindqvist A, Rodriguez-Bravo V, Medema RH: **The decision to enter mitosis: feedback and redundancy in the mitotic entry network**. *J Cell Biol* 2009, **185**:193-202.

12. Maiato H, DeLuca J, Salmon ED, Earnshaw WC: **The dynamic kinetochore-microtubule interface.** *J Cell Sci* 2004, **117**:5461–5477.

13. Musacchio A, Salmon ED: **The spindle-assembly checkpoint in space and time.** *Nat Rev Mol Cell Biol* 2007, **8**:379–393.

14. Peters JM: **The Anaphase-Promoting Complex: proteolysis in mitosis and beyond**. *Mol Cell* 2002, **9**:931-943.

15. Sherwood R, Takahashi TS, Jallepalli PV: **Sister acts: coordinating DNA replication and cohesion establishment.** *Genes Dev* 2010, **24**:2723–2731.

16. Glotzer M: **Animal cell cytokinesis.** *Annu Rev Cell Dev Biol* 2001, **17**:351–386.

17. O'Farrell PH: **Quiescence: early evolutionary origins and universality do not imply uniformity**. *Philos Trans R Soc Lond, B Biol Sci* 2011, **366**:3498-3507.

18. Campisi J, di Fagagna FD: **Cellular senescence: when bad things happen to good cells**. *Nat Rev Mol Cell Biol* 2007, **8**:729-740.

19. Campisi J: **Cellular senescence as a tumor-suppressor mechanism**. *Trends Cell Biol* 2001, **11**:S27-31.

20. Lemmon MA, Schlessinger J: **Cell Signaling by Receptor Tyrosine Kinases**. *Cell* 2010, **141**:1117-1134.

21. Blume-Jensen P, Hunter T: **Oncogenic kinase signalling.** *Nature* 2001, **411**:355–365.

22. Schlessinger J, Lemmon MA: **SH2 and PTB Domains in Tyrosine Kinase Signaling**. *Sci STKE* 2003, **2003**:RE12.

23. Vanhaesebroeck B, Leevers SJ, Panayotou G, Waterfield MD: **Phosphoinositide 3-kinases: a conserved family of signal transducers.** *Trends Biochem Sci* 1997, **22**:267–272.

24. Wymann MP, Pirola L: **Structure and function of phosphoinositide 3-kinases.** *Biochim Biophys Acta* 1998, **1436**:127–150.

25. Jackson AL, Pahl PM, Harrison K, Rosamond J, Sclafani RA: **Cell cycle regulation of the yeast Cdc7 protein kinase by association with the Dbf4 protein.** *Mol Cell Biol* 1993, **13**:2899–2908.

26. Harlan JE, Hajduk JE, Yoon HS, Fesik SW: **Pleckstrin homology domains bind to phosphatidylinositol-4,5-bisphosphate**. *Nature* 1994, **371**:168-170.

27. Alessi DR, Andjelkovic M, Caudwell B, Cron P, Morrice N, Cohen P, Hemmings BA: **Mechanism of activation of protein kinase B by insulin and IGF-1.** *EMBO J* 1996, **15**:6541–6551.

28. Sarbassov DD, Guertin DA, Ali SM, Sabatini DM: **Phosphorylation and regulation of Akt/PKB by the rictor-mTOR complex.** *Science* 2005, **307**:1098–1101.

29. Lawlor MA, Alessi DR: **PKB/Akt a key mediator of cell proliferation, survival and insulin responses?** *J Cell Sci* 2001, **114**:2903–2910.

30. Harmer SL, DeFranco AL: **Shc contains two Grb2 binding sites needed for efficient formation of complexes with SOS in B lymphocytes.** *Mol Cell Biol* 1997, **17**:4087–4095.

31. Boriack-Sjodin PA, Margarit SM, Bar-Sagi D, Kuriyan J: **The structural basis of the activation of Ras by Sos.** *Nature* 1998, **394**:337–343.

32. McCubrey JA, Steelman LS, Chappell WH, Abrams SL, Wong EWT, Chang F, Lehmann B, Terrian DM, Milella M, Tafuri A, et al.: **Roles of the Raf/MEK/ERK**

pathway in cell growth, malignant transformation and drug resistance. *Biochim Biophys Acta* 2006, **1773**:1263–1284.

33. Chang F, Steelman LS, Lee JT, Shelton JG, Navolanic PM, Blalock WL, Franklin RA, McCubrey JA: **Signal transduction mediated by the Ras/Raf/MEK/ERK pathway from cytokine receptors to transcription factors: potential targeting for therapeutic intervention**. *Leukemia* 2003, **17**:1263-1293.

34. Leonard WJ, Lin JX: **Cytokine receptor signaling pathways.** *J Allergy Clin Immunol* 2000, **105**:877–888.

35. Samatar AA, Poulikakos PI: **Targeting RAS-ERK signalling in cancer: promises and challenges.** *Nat Rev Drug Discov* 2014, **13**:928–942.

36. Fruman DA, Rommel C: **PI3K and cancer: lessons, challenges and opportunities**. *Nat Rev Drug Discov* 2014, **13**:140-156.

37. White MF: **The IRS-signalling system: a network of docking proteins that mediate insulin action**. *Mol Cell Biochem* 1998, **182:**3-11.

38. White MF, Maron R, Kahn CR: **Insulin rapidly stimulates tyrosine phosphorylation of a Mr-185,000 protein in intact cells**. *Nature* 1985, **318**:183-186.

39. Cuevas EP, Escribano O, Chiloeches A, Rubio SR, Román ID, Fernández-Moreno MD, Guijarro LG: **Role of insulin receptor substrate-4 in IGF-I-stimulated HEPG2 proliferation.** *J Hepatol* 2007, **46**:1089–1098.

40. Sun XJ, Crimmins DL, Myers MG, Miralpeix M, White MF: **Pleiotropic insulin signals are engaged by multisite phosphorylation of IRS-1.** *Mol Cell Biol* 1993, **13**:7418–7428.

41. Yamauchi T, Kaburagi Y, Ueki K, Tsuji Y, Stark GR, Kerr IM, Tsushima T, Akanuma Y, Komuro I, Tobe K, et al.: **Growth Hormone and Prolactin Stimulate Tyrosine Phosphorylation of Insulin Receptor Substrate-1, -2, and -3, Their Association with p85 Phosphatidylinositol 3-Kinase (PI3-kinase), and Concomitantly PI3-kinase Activation via JAK2 Kinase**. *J Biol Chem* 1998, **273**:15719-15726.

42. Knowlden JM, Jones HE, Barrow D, Gee JM, Nicholson RI, Hutcheson IR: **Insulin receptor substrate-1 involvement in epidermal growth factor receptor and insulin-like growth factor receptor signalling: implication for Gefitinib ("Iressa") response and resistance**. *Breast Cancer Res Treat* 2008, **111**:79–91.

43. Cai D, Dhe-Paganon S, Melendez PA, Lee J, Shoelson SE: **Two New Substrates in Insulin Signaling, IRS5/DOK4 and IRS6/DOK5**. *J Biol Chem* 2003, **278**:25323-25330.

44. White MF: **IRS proteins and the common path to diabetes**. *Am J Physiol Endocrinol Metab* 2002, **283**:E413-422.

45. Tamemoto H, Kadowaki T, Tobe K, Yagi T, Sakura H, Hayakawa T, Terauchi Y, Ueki K, Kaburagi Y, Satoh S, et al.: **Insulin resistance and growth retardation in mice lacking insulin receptor substrate-1**. *Nature* 1994, **372**:182-186.

46. Withers DJ, Gutierrez JS, Towery H, Burks DJ, Ren JM, Previs S, Zhang Y, Bernal D, Pons S, Shulman GI, et al.: **Disruption of IRS-2 causes type 2 diabetes in mice.** *Nature* 1998, **391**:900–904.

47. Brüning JC, Winnay J, Cheatham B, Kahn CR: **Differential signaling by insulin receptor substrate 1 (IRS-1) and IRS-2 in IRS-1-deficient cells.** *Mol Cell Biol* 1997, **17**:1513–1521.

48. Giovannone B, Scaldaferri ML, Federici M, Porzio O, Lauro D, Fusco A, Sbraccia P, Borboni P, Lauro R, Sesti G: **Insulin receptor substrate (IRS) transduction system: distinct and overlapping signaling potential.** *Diabetes Metab Res Rev* 2000, **16**:434–441.

49. Fantin V, Wang Q, Lienhard G: **Mice lacking insulin receptor substrate 4 exhibit mild defects in growth, reproduction, and glucose homeostasis**. *Am J Physiol Endocrinol Metab* 2000, **278:**E127-133.

50. Escribano O, Fernández-Moreno MD, Zueco JA, Menor C, Fueyo J, Ropero RM, Diaz-Laviada I, Román ID, Guijarro LG: **Insulin receptor substrate-4 signaling in quiescent rat hepatocytes and in regenerating rat liver**. *Hepatology* 2003, **37**:1461–1469.

51. Cantarini MC, de la Monte SM, Pang M, Tong M, D'Errico A, Trevisani F, Wands JR: **Aspartyl-asparagyl β hydroxylase over-expression in human hepatoma is linked to activation of insulin-like growth factor and notch signaling mechanisms**. *Hepatology* 2006, **44**:446-457.

52. Cuevas EP, Escribano O, Monserrat J, Martínez-Botas J, Sánchez MG, Chiloeches A, Hernández-Breijo B, Sánchez-Alonso V, Román ID, Fernández-Moreno MD, Guijarro LG: **RNAi-mediated silencing of insulin receptor substrate-4 enhances actinomycin D- and tumor necrosis factor-α-induced cell death in hepatocarcinoma cancer cell lines**. *J Cell Biochem* 2009, **108**:1292–1301.

53. Mardilovich K, Pankratz SL, Shaw LM: **Expression and function of the insulin receptor substrate proteins in cancer**. *Cell Commun Signal* 2009, **7**:14.

54. International Human Genome Sequencing Consortium: **Finishing the euchromatic sequence of the human genome.** *Nature* 2004, **431**:931–45.

55. Méchali M: **Eukaryotic DNA replication origins: many choices for appropriate answers**. *Nat Rev Mol Cell Biol* 2010, **11**:728-738.

56. Abbas T, Keaton MA, Dutta A: **Genomic Instability in Cancer**. *Cold Spring Harb Perspect Biol* 2013, **5**:a012914.

57. Fields S, Johnston M: **Cell biology: Whither Model Organism Research?** *Science* 2005, **307**:1885-1886.

58. Botstein D, Fink GR: **Yeast: An Experimental Organism for 21st Century Biology.** *Genetics* 2011, **189**:695-704.

59. Wyrick JJ, Aparicio JG, Chen T, Barnett JD, Jennings EG, Young RA, Bell SP, Aparicio OM: **Genome-wide distribution of ORC and MCM proteins in S. cerevisiae: high-resolution mapping of replication origins.** *Science* 2001, **294**:2357–2360.

60. Raghuraman MK, Winzeler EA, Collingwood D, Hunt S, Wodicka L, Conway A, Lockhart DJ, Davis RW, Brewer BJ, Fangman WL: **Replication Dynamics of the Yeast Genome**. *Science* 2001, **294**:115-121.

61. Li H, Stillman B: **The Origin Recognition Complex: A Biochemical and Structural View**. *Subcell Biochem* 2012, **62:**37-58.

62. Méndez J, Stillman B: **Chromatin association of human origin recognition complex, cdc6, and minichromosome maintenance proteins during the cell cycle: assembly of prereplication complexes in late mitosis.** *Mol Cel Biol* 2000, **20**:8602–8612.

63. Ballabeni A, Zamponi R, Caprara G, Melixetian M, Bossi S, Masiero L, Helin K: **Human CDT1 Associates with CDC7 and Recruits CDC45 to Chromatin during S Phase**. *J Biol Chem* 2008, **284**:3028–3036.

64. Fernández-Cid A, Riera A, Tognetti S, Samel S, Evrin C, Winkler C, Gardenal E, Uhle S, Speck C: **An ORC/Cdc6/MCM2-7 Complex Is Formed in a Multistep Reaction to Serve as a Platform for MCM Double-Hexamer Assembly**. *Mol Cell* 2013, **50**:577-588.

65. Remus D, Beuron F, Tolun G, Griffith JD, Morris EP, Diffley JFX: **Concerted loading of Mcm2-7 double hexamers around DNA during DNA replication origin licensing.** *Cell* 2009, **139**:719–730.

66. Symeonidou I-E, Kotsantis P, Roukos V, Rapsomaniki M-A, Grecco HE, Bastiaens P, Taraviras S, Lygerou Z: **Multi-step loading of human minichromosome maintenance proteins in live human cells.** *J Biol Chem* 2013, **288**:35852–35867.

67. Hua XH, Newport J: **Identification of a Preinitiation Step in DNA Replication That Is Independent of Origin Recognition Complex and cdc6, but Dependent on cdk2**. *The J Cell Biol* 1998, **140**:271-281.

68. Rowles A, Tada S, Blow JJ: **Changes in association of the Xenopus origin recognition complex with chromatin on licensing of replication origins**. *J Cell Sci* 1999, **112**:2011–2018.

69. Labib K: **How do Cdc7 and cyclin-dependent kinases trigger the initiation of chromosome replication in eukaryotic cells?** *Genes Dev* 2010, **24**:1208–1219.

70. Dutta A, Bell SP: **Initiation of DNA replication in eukaryotic cells**. *Annu Rev Cell Dev Biol* 1997, **13**:293-322.

71. Yeeles JT, Deegan TD, Janska A, Early A, Diffley JFX: **Regulated eukaryotic DNA replication origin firing with purified proteins.** *Nature* 2015, **519:**431-435.

72. Boos D, Sanchez-Pulido L, Rappas M, Pearl LH, Oliver AW, Ponting CP, Diffley JF: **Regulation of DNA Replication through Sld3-Dpb11 Interaction Is Conserved from Yeast to Humans**. *Curr Biol* 2011, **21**:1152-1157.

73. Boos D, Yekezare M, Diffley JF: **Identification of a heteromeric complex that promotes DNA replication origin firing in human cells**. *Science* 2013, **340**:981–984.

74. Aladjem MI: **Replication in context: dynamic regulation of DNA replication patterns in metazoans.** *Nat Rev Genet* 2007, **8**:588–600.

75. Wold MS: **Replication Proein A: A Heterotrimeric, Single-Stranded DNA-Binding Protein Required for Eukaryotic DNA Metabolism**. *Annu Rev Biochem* 1997, **66**:61-92.

76. Burgers PMJ: **Polymerase Dynamics at the Eukaryotic DNA Replication Fork**. *J Biol Chem* 2008, **284**:4041-4045.

77. Garg P, Burgers PMJ: **How the Cell Deals with DNA Nicks**. *Cell Cycle* 2005, **4**:221-224.

78. Majka J, Burgers P: **The PCNA–RFC families of DNA clamps and clamp loaders**. *Prog Nucleic Acids Res Mol Biol* 2004, **78**:227–260.

79. McElhinny SAN, Gordenin DA, Stith CM, Burgers PMJ, Kunkel TA: **Division of Labor at the Eukaryotic Replication Fork**. *Mol Cell* 2008, **30**:137-144.

80. Pursell ZF, Isoz I, Lundström E-B, Johansson E, Kunkel TA: **Yeast DNA polymerase epsilon participates in leading-strand DNA replication.** *Science* 2007, **317**:127–130.

81. Johnson RE, Klassen R, Prakash L, Prakash S: **A Major Role of DNA Polymerase δ in Replication of Both the Leading and Lagging DNA Strands.** *Mol Cell* 2015, **59**:163–175.

82. Seidman MM, Salzman NP: **Late replicative intermediates are accumulated during simian virus 40 DNA replication in vivo and in vitro.** *J Virol* 1979, **30**:600–609.

83. Chen MC, Birkenmeier E, Salzman NP: **Simian virus 40 DNA replication: characterization of gaps in the termination region.** *J Virol* 1976, **17**:614–621.

84. Dewar JM, Budzowska M, Walter JC: **The mechanism of DNA replication termination in vertebrates**. *Nature* 2015, **525**:345-350.

85. Lindahl T, Barnes DE: **Repair of Endogenous DNA Damage**. *Cold Spring Harb Symp Quant Biol* 2000, **65**:127-133.

86. De Bont R, van Larebeke N: **Endogenous DNA damage in humans: a review of quantitative data**. *Mutagenesis* 2004, **19**:169-185.

87. Shackelford RE, Kaufmann WK, Paules RS: **Cell cycle control, checkpoint mechanisms, and genotoxic stress.** *Environ Health Perspect* 1999, **107 Suppl 1**:5–24.

88. Abraham RT: **Cell cycle checkpoint signaling through the ATM and ATR kinases**. *Genes Dev* 2001, **15**:2177-2196.

89. Jackson SP, Bartek J: **The DNA-damage response in human biology and disease**. *Nature* 2009, **461**:1071-1078.

90. Durocher D, Jackson SP: **DNA-PK, ATM and ATR as sensors of DNA damage: variations on a theme?** *Curr Opin Cell Biol* 2001, **13**:225–231.

91. Zegerman P, Diffley JF: **DNA replication as a target of the DNA damage checkpoint.** *DNA Repair (Amst)* 2009, **8**:1077–1088.

92. Byun TS, Pacek M, Yee M, Walter JC, Cimprich KA: **Functional uncoupling of MCM helicase and DNA polymerase activities activates the ATR-dependent checkpoint**. *Genes Dev* 2005, **19**:1040-1052.

93. Shiotani B, Nguyen HD, Håkansson P, Maréchal A, Tse A, Tahara H, Zou L: **Two Distinct Modes of ATR Activation Orchestrated by Rad17 and Nbs1**. *Cell Rep* 2013, **3**:1651-1662.

94. Schleker T, Nagai S, Gasser SM: **Posttranslational modifications of repair factors and histones in the cellular response to stalled replication forks.** *DNA Repair (Amst)* 2009, **8**:1089–1100.

95. Zhao H, Piwnica-Worms H: **ATR-Mediated Checkpoint Pathways Regulate Phosphorylation and Activation of Human Chk1**. *Mol Cell Biol* 2001, **21**:4129-4139.

96. Lou H, Komata M, Katou Y, Guan Z, Reis CC, Budd M, Shirahige K, Campbell JL: **Mrc1 and DNA Polymerase ε Function Together in Linking DNA Replication and the S Phase Checkpoint**. *Mol Cell* 2008, **32**:106-117.

97. Lee J, Gold DA, Shevchenko A, Shevchenko A, Dunphy WG: **Roles of Replication Fork-interacting and Chk1-activating Domains from Claspin in a DNA Replication Checkpoint Response**. *Mol Biol Cell* 2005, **16**:5269-5282.

98. Smith J, Tho LM, Xu N, Gillespie DA: **The ATM–Chk2 and ATR–Chk1 Pathways in DNA Damage Signaling and Cancer**. *Adv Cancer Res* 2010, **108:**73-112.

99. Perry JA, Kornbluth S: **Cdc25 and Wee1: analogous opposites?** *Cell Div* 2007, **2**:12.

100. Liu Q, Guntuku S, Cui XS, Matsuoka S, Cortez D, Tamai K, Luo G, Carattini-Rivera S, DeMayo F, Bradley A, et al.: **Chk1 is an essential kinase that is regulated by Atr and required for the G(2)/M DNA damage checkpoint.** *Genes Dev* 2000, **14**:1448–1459.

101. Rhind N, Gilbert DM: **DNA Replication Timing**. *Cold Spring Harb Perspect Biol* 2013, **5**:a010132.

102. Blow JJ, Ge XQ, Jackson DA: **How dormant origins promote complete genome replication.** *Trends Biochem Sci* 2011, **36**:405–414.

103. Lee AY, Chiba T, Truong LN, Cheng AN, Do J., Cho MJ, Chen L, Wu X: **Dbf4 Is Direct Downstream Target of Ataxia Telangiectasia Mutated (ATM) and Ataxia Telangiectasia and Rad3-related (ATR) Protein to Regulate Intra-S-phase Checkpoint**. *J Biol Chem* 2012, **287**:2531–2543.

104. Couch FB, Bansbach CE, Driscoll R, Luzwick JW, Glick GG, Betous R, Carroll CM, Jung SY, Qin J, Cimprich KA, et al.: **ATR phosphorylates SMARCAL1 to prevent replication fork collapse**. *Genes Dev* 2013, **27**:1610-1623.

105. Labib K, Tercero JA, Diffley JF: **Uninterrupted MCM2-7 function required for DNA replication fork progression.** *Science* 2000, **288**:1643–1647.

106. Cortez D: **Preventing replication fork collapse to maintain genome integrity.** *DNA Repair (Amst)* 2015, **32**:149–157.

107. Bednar J, Horowitz RA, Grigoryev SA, Carruthers LM, Hansen JC, Koster AJ, Woodcock CL: **Nucleosomes, linker DNA, and linker histone form a unique structural motif that directs the higher-order folding and compaction of chromatin**. *PNAS USA* 1998, **95**:14173-14178.

108. Baxter J: **"Breaking up is hard to do": the formation and resolution of sister chromatid intertwines.** *J Mol Biol* 2014, **427**:590–607.

109. Wang JC: **Cellular roles of DNA topoisomerases: a molecular perspective.** *Nat Rev Mol Cell Biol* 2002, **3**:430–440.

110. Gonzalez R, Lim C, Cole K, Bianchini C, Schools G, Davis B, Wada I, Roninson I, Broude E: **Effects of conditional depletion of topoisomerase II on cell cycle progression in mammalian cells**. *Cell Cycle* 2011, **10**:3505–3514.

111. Lyu YL, Lin C-P, Azarova AM, Cai L, Wang JC, Liu LF: **Role of topoisomerase IIbeta in the expression of developmentally regulated genes.** *Mol Cell Biol* 2006, **26**:7929–7941.

112. Austin CA, Marsh KL: **Eukaryotic DNA topoisomerase II beta.** *Bioessays* 1998, **20**:215–226.

113. Meczes EL, Gilroy KL, West KL, Austin CA: **The impact of the human DNA topoisomerase II C-terminal domain on activity.** *PLoS ONE* 2008, **3**:e1754.

114. Ryu H, Yoshida MM, Sridharan V, Kumagai A, Dunphy WG, Dasso M, Azuma Y: **SUMOylation of the C-terminal domain of DNA topoisomerase IIα regulates the centromeric localization of Claspin.** *Cell Cycle* 2015, **14**:2777-2784.

115. Kimura K, Nozaki N, Enomoto T, Tanaka M, Kikuchi A: **Analysis of M phase-specific phosphorylation of DNA topoisomerase II.** *J Biol Chem* 1996, **271**:21439–21445.

116. Schvartzman JB, Martínez-Robles ML, Hernández P, Krimer DB: **The benefit of DNA supercoiling during replication.** *Biochem Soc Trans* 2013, **41**:646-651

117. Baxter J, Diffley JFX: **Topoisomerase II inactivation prevents the completion of DNA replication in budding yeast.** *Mol Cell* 2008, **30**:790–802.

118. Gaggioli V, Le Viet B, Germe T, Hyrien O: **DNA topoisomerase II controls replication origin cluster licensing and firing time in Xenopus egg extracts.** *Nucleic Acids Res* 2013, **41**:7313-7331.

119. Cuvier O, Stanojcic S, Lemaitre JM, Mechali M: **A topoisomerase II-dependent mechanism for resetting replicons at the S-M-phase transition.** *Genes Dev* 2008, **22**:860-865.

120. Carson DR, Christman MF: **Evidence that replication fork components catalyze establishment of cohesion between sister chromatids.** *PNAS USA* 2001, **98**:8270-8275.

121. Deming PB, Cistulli CA, Zhao H, Graves PR, Piwnica-Worms H, Paules RS, Downes CS, Kaufmann WK: **The human decatenation checkpoint.** *PNAS USA* 2001, **98**:12044–12049.

122. Luo K, Yuan J, Chen J, Lou Z: **Topoisomerase IIalpha controls the decatenation checkpoint.** *Nat Cell Biol* 2009, **11**:204–210.

123. Bower JJ, Karaca GF, Zhou Y, Simpson DA, Cordeiro-Stone M, Kaufmann WK: **Topoisomerase IIalpha maintains genomic stability through decatenation G(2) checkpoint signaling.** *Oncogene* 2010, **29**:4787–4799.

124. Deming PB, Flores KG, Downes CS, Paules RS, Kaufmann WK: **ATR Enforces the Topoisomerase II-dependent G2 Checkpoint through Inhibition of Plk1 Kinase.** *J Biol Chem* 2002, **277**:36832-36838.

125. Shintomi K, Takahashi TS, Hirano T: **Reconstitution of mitotic chromatids with a minimum set of purified factors.** *Nat Cell Biol* 2015, **17**:1014-1023.

126. Wang LH, Mayer B, Stemmann O, Nigg EA: **Centromere DNA decatenation depends on cohesin removal and is required for mammalian cell division.** *J Cell Sci* 2010, **123**:806–813.

127. Chan KL, North PS, Hickson ID: **BLM is required for faithful chromosome segregation and its localization defines a class of ultrafine anaphase bridges**. *EMBO J* 2007, **26**:3397-3409.

128. Broderick R, Nieminuszczy J, Blackford AN, Winczura A, Niedzwiedz W: **TOPBP1 recruits TOP2A to ultra-fine anaphase bridges to aid in their resolution**. *Nat Commun* 2015, **6**:6572.

129. Nitiss JL: **Targeting DNA topoisomerase II in cancer chemotherapy.** *Nat Rev Cancer* 2009, **9**:338–350.

130. Liu H, Ling Y, Gong Y, Sun Y, Hou L, Zhang B: **DNA damage induces N-acetyltransferase NAT10 gene expression through transcriptional activation.** *Mol Cell Biochem* 2007, **300**:249–258.

131. Evison BJ, Sleebs BE, Watson KG, Phillips DR, Cutts SM: **Mitoxantrone, More than Just Another Topoisomerase II Poison**. *Med Res Rev* 2015, doi: 10.1002/med.21364.

132. Meresse P, Dechaux E, Monneret C, Bertounesque E: **Etoposide: discovery and medicinal chemistry.** *Curr Med Chem* 2004, **11**:2443–2466.

133. Kerrigan D, Pommier Y, Kohn KW: **Protein-linked DNA strand breaks produced by etoposide and teniposide in mouse L1210 and human VA-13 and HT-29 cell lines: relationship to cytotoxicity.** *NCI Monogr* 1987, **4:**117-121.

134. Roca J, Ishida R, Berger JM, Andoh T, Wang JC: **Antitumor bisdioxopiperazines inhibit yeast DNA topoisomerase II by trapping the enzyme in the form of a closed protein clamp.** *PNAS USA* 1994, **91**:1781–1785.

135. Andoh T, Ishida R: **Catalytic inhibitors of DNA topoisomerase II.** *Biochim Biophys Acta* 1998, **1400**:155–171.

136. Skoufias DA, Lacroix FB, Andreassen PR, Wilson L, Margolis RL: **Inhibition of DNA Decatenation, but Not DNA Damage, Arrests Cells at Metaphase**. *Mol Cell* 2004, **15**:977-990.

137. Hasinoff BB, Hellmann K, Herman EH, Ferrans VJ: **Chemical, biological and clinical aspects of dexrazoxane and other bisdioxopiperazines.** *Curr Med Chem* 1998, **5**:1–28.

138. Hartwell L: **Three additional genes required for deoxyribonucleic acid synthesis in Saccharomyces cerevisiae**. *J Bacteriol* 1973, **115**:966–974.

139. Johnston LH, Thomas AP: **A further two mutants defective in initiation of the S phase in the yeast Saccharomyces cerevisiae.** *Mol Gen Genet* 1982, **186**:445–448.

140. Montagnoli A, Bosotti R, Villa F, Riall M, Rialland M, Brotherton D, Mercurio C, Berthelsen J, Santocanale C: **Drf1, a novel regulatory subunit for human Cdc7 kinase.** *EMBO J* 2002, **21**:3171–3181.

141. Yoshizawa-Sugata N, Ishii A, Taniyama C, Matsui E, Arai KI, Masai H: **A Second Human Dbf4/ASK-related Protein, Drf1/ASKL1, Is Required for Efficient Progression of S and M Phases.** *J Biol Chem* 2005, **280**:13062-13070.

142. Wu X, Lee H: **Human Dbf4/ASK promoter is activated through the Sp1 and MluI cell-cycle box (MCB) transcription elements.** *Oncogene* 2002, **21**:7786–7796.

143. Yamada M, Sato N, Taniyama C, Ohtani K, Arai K, Masai H: **A 63-base pair DNA segment containing an Sp1 site but not a canonical E2F site can confer growth-dependent and E2F-mediated transcriptional stimulation of the human ASK gene encoding the regulatory subunit for human Cdc7-related kinase.** *J Biol Chem* 2002, **277**:27668-27681.

144. Ferreira MG, Santocanale C, Drury LS, Diffley JF: **Dbf4p, an Essential S Phase-Promoting Factor, Is Targeted for Degradation by the Anaphase-Promoting Complex**. *Mol Cell Biol* 2000, **20**:242-248.

145. Weinreich M, Stillman B: **Cdc7p-Dbf4p kinase binds to chromatin during S phase and is regulated by both the APC and the RAD53 checkpoint pathway.** *EMBO J* 1999, **18**:5334–5346.

146. Kumagai H, Sato N, Yamada M, Mahony D, Seghezzi W, Lees E, Arai K, Masai H: **A novel growth- and cell cycle-regulated protein, ASK, activates human Cdc7-related kinase and is essential for G1/S transition in mammalian cells.** *Mol Cell Biol* 1999, **19**:5083–5095.

147. Hughes S, Elustondo F, Di Fonzo A, Leroux FG, Wong AC, Snijders AP, Matthews SJ, Cherepanov P: **Crystal structure of human CDC7 kinase in complex with its activator DBF4.** *Nat Struct Mol Biol* 2012, **19**:1101–1107.

148. Sato N, Sato M, Nakayama M, Saitoh R, Arai K, Masai H: **Cell cycle regulation of chromatin binding and nuclear localization of human Cdc7-ASK kinase complex**. *Genes Cells* 2003, **8**:451-463.

149. Yamashita N, Kim J-M, Koiwai O, Arai K, Masai H: **Functional analyses of mouse ASK, an activation subunit for Cdc7 kinase, using conditional ASK knockout ES cells.** *Genes Cells* 2005, **10**:551–563.

150. Kulak NA, Pichler G, Paron I, Nagaraj N, Mann M: **Minimal, encapsulated proteomic-sample processing applied to copy-number estimation in eukaryotic cells.** *Nat Methods* 2014,**11**:319-324.

151. Silva T, Bradley RH, Gao Y, Coue M: **Xenopus CDC7/DRF1 Complex Is Required for the Initiation of DNA Replication** *J Bioll Chem* 2006, **281**:11569–11576.

152. Jiang W, McDonald D, Hope T, Hunter T: **Mammalian Cdc7–Dbf4 protein kinase complex is essential for initiation of DNA replication**. *EMBO J* 1999, **18**:5703-5713.

153. Masai H, Taniyama C, Ogino K, Matsui E, Kakusho N, Matsumoto S, Kim JM, Ishii A, Tanaka T, Kobayashi T, et al.: **Phosphorylation of MCM4 by Cdc7 Kinase Facilitates Its Interaction with Cdc45 on the Chromatin** *J Biol Chem* 2006, **281**:39249–39261.

154. Sheu YJ, Stillman B: **Cdc7-Dbf4 Phosphorylates MCM Proteins via a Docking Site-Mediated Mechanism to Promote S Phase Progression**. *Mol Cell* 2006, **24**:101-113.

155. Montagnoli A, Valsasina B, Brotherton D, Troiani S, Rainoldi S, Tenca P, Molinari A, Santocanale C: **Identification of Mcm2 phosphorylation sites by S-phase-regulating kinases.** *J Biol Chem* 2006, **281**:10281–10290.

156. Lei M, Kawasaki Y, Young MR, Kihara M, Sugino A, Tye BK: **Mcm2 is a target of regulation by Cdc7-Dbf4 during the initiation of DNA synthesis**. *Genes Dev* 1997, **11**:3365-3374.

157. Chuang LC, Teixeira LK, Wohlschlegel JA, Henze M, Yates JR, Méndez J, Reed SI: **Phosphorylation of Mcm2 by Cdc7 promotes pre-replication complex assembly during cell-cycle re-entry.** *Mol Cell* 2009, **35**:206–216.

158. Hardy CF, Dryga O, Seematter S, Pahl PM, Sclafani RA: **mcm5/cdc46-bob1 bypasses the requirement for the S phase activator Cdc7p**. PNAS USA 1997, **94:**3151-3155.

159. Hoang ML, Leon RP, Pessoa-Brandao L, Hunt S, Raghuraman MK, Fangman WL, Brewer BJ, Sclafani RA: **Structural Changes in Mcm5 Protein Bypass Cdc7-Dbf4 Function and Reduce Replication Origin Efficiency in Saccharomyces cerevisiae**. *Mol Cell Biol* 2007, **27**:7594-7602.

160. Sheu YJ, Stillman B: **The Dbf4-Cdc7 kinase promotes S phase by alleviating an inhibitory activity in Mcm4.** *Nature* 2010, **463**:113–117.

161. Tenca P, Brotherton D, Montagnoli A, Rainoldi S, Albanese C, Santocanale C: **Cdc7 is an active kinase in human cancer cells undergoing replication stress.** *J Biol Chem* 2007, **282**:208–215.

162. Yamada M, Watanabe K, Mistrik M, Vesela E, Protivankova I, Mailand N, Lee M, Masai H, Lukas J, Bartek J: **ATR-Chk1-APC/CCdh1-dependent stabilization of Cdc7-ASK (Dbf4) kinase is required for DNA lesion bypass under replication stress.** *Genes Dev* 2013, **27**:2459–2472.

163. Rainey MD, Harhen B, Wang GN, Murphy PV, Santocanale C: **Cdc7-dependent and -independent phosphorylation of Claspin in the induction of the DNA replication checkpoint.** *Cell cycle* 2013, **12**:1560–1568.

164. Kim JM, Kakusho N, Yamada M, Kanoh Y, Takemoto N, Masai H: **Cdc7 kinase mediates Claspin phosphorylation in DNA replication checkpoint.** *Oncogene* 2008, **27**:3475–3482.

165. Suzuki T, Tsuzuku J, Hayashi A, Shiomi Y, Iwanari H, Mochizuki Y, Hamakubo T, Kodama T, Nishitani H, Masai H, et al.: **Inhibition of DNA damage-induced apoptosis through Cdc7-mediated stabilization of Tob.** *J Biol Chem* 2012, **287**:40256–40265.

166. Friedberg EC, Fischhaber PL, Kisker C: **Error-prone DNA polymerases: novel structures and the benefits of infidelity.** *Cell* 2001, **107**:9-12.

167. Day TA, Palle K, Barkley LR, Kakusho N, Zou Y, Tateishi S, Verreault A, Masai H, Vaziri C: **Phosphorylated Rad18 directs DNA Polymerase η to sites of stalled replication.** *J Cell Biol* 2010, **191**:953-966.

168. Ramer MD, Suman ES, Richter H, Stanger K, Spranger M, Bieberstein N, Duncker BP: **Dbf4 and Cdc7 proteins promote DNA replication through interactions with distinct Mcm2-7 protein subunits.** *J Biol Chem* 2013, **288**:14926–14935.

169. Takahashi TS, Basu A, Bermudez V, Hurwitz J, Walter JC: **Cdc7-Drf1 kinase links chromosome cohesion to the initiation of DNA replication in Xenopus egg extracts.** *Genes Dev* 2008, **22**:1894–1905.

170. Shi N, Chen SY: **Cell division cycle 7 mediates transforming growth factor-β-induced smooth muscle maturation through activation of myocardin gene transcription.** *J Biol Chem* 2013, **288**:34336–34342.

171. Shi N, Xie WB, Chen SY: **Cell Division Cycle 7 Is a Novel Regulator of Transforming Growth Factor-β-induced Smooth Muscle Cell Differentiation**. *J Biol Chem* 2012, **287**:6860–6867.

172. Gérard A, Koundrioukoff S, Ramillon V, Sergère JC, Mailand N, Quivy JP, Almouzni G: **The replication kinase Cdc7-Dbf4 promotes the interaction of the p150 subunit of chromatin assembly factor 1 with proliferating cell nuclear antigen**. *EMBO Rep* 2006, **7:**817-823.

173. Grishina I, Lattes B: **A Novel Cdk2 Interactor is Phosphorylated by Cdc7 and Associates with Components of the Replication Complexes** *Cell Cycle* 2005, **4**:1120-1126.

174. Montagnoli A, Valsasina B, Croci V, Menichincheri M, Rainoldi S, Marchesi V, Tibolla M, Tenca P, Brotherton D, Albanese C, et al.: **A Cdc7 kinase inhibitor restricts initiation of DNA replication and has antitumor activity.** *Nat Chem Biol* 2008, **4**:357–365.

175. Chen YC, Weinreich M: **Dbf4 Regulates the Cdc5 Polo-like Kinase through a Distinct Non-canonical Binding Interaction**. *J Biol Chem* 2010, **285**:41244-41254.

176. Miller CT, Gabrielse C, Chen YC, Weinreich M: **Cdc7p-Dbf4p Regulates Mitotic Exit by Inhibiting Polo Kinase.** *PLoS Genet* 2009, **5**:e1000498.

177. Murakami H, Keeney S: **Temporospatial Coordination of Meiotic DNA Replication and Recombination via DDK Recruitment to Replisomes.** *Cell* 2014, **158**:861–873.

178. Wan L, Niu H, Futcher B, Zhang C, Shokat KM, Boulton SJ, Hollingsworth NM: **Cdc28-Clb5 (CDK-S) and Cdc7-Dbf4 (DDK) collaborate to initiate meiotic recombination in yeast.** *Genes Dev* 2008, **22**:386–397.

179. Sasanuma H, Hirota K, Fukuda T, Kakusho N, Kugou K, Kawasaki Y, Shibata T, Masai H, Ohta K: **Cdc7-dependent phosphorylation of Mer2 facilitates initiation of yeast meiotic recombination.** *Genes Dev* 2008, **22**:398–410.

180. Lo HC, Kunz RC, Chen X, Marullo A, Gygi SP, Hollingsworth NM: **Cdc7-Dbf4 Is a Gene-Specific Regulator of Meiotic Transcription in Yeast** *Mol Cell Biol* 2011, **32**:541–557.

181. Corbi D, Sunder S, Weinreich M, Skokotas A, Johnson ES, Winter E: **Multisite phosphorylation of the Sum1 transcriptional repressor by S-phase kinases controls exit from meiotic prophase in yeast.** *Mol Cell Biol* 2014, **34**:2249–2263.

182. Matos J, Lipp JJ, Bogdanova A, Guillot S, Okaz E, Junqueira M, Shevchenko A, Zachariae W: **Dbf4-dependent CDC7 kinase links DNA replication to the segregation of homologous chromosomes in meiosis I.** *Cell* 2008, **135**:662–678.

183. Katis VL, Lipp JJ, Imre R, Bogdanova A, Okaz E, Habermann B, Mechtler K, Nasmyth K, Zachariae W: **Rec8 phosphorylation by casein kinase 1 and Cdc7-Dbf4 kinase regulates cohesin cleavage by separase during meiosis.** *Dev Cell* 2010, **18**:397–409.

184. Bonte D, Lindvall C, Liu H, Dykema K, Furge K, Weinreich M: **Cdc7-Dbf4 kinase overexpression in multiple cancers and tumor cell lines is correlated with p53 inactivation.** *Neoplasia* 2008, **10**:920–931.

185. Rivlin N, Brosh R, Oren M, Rotter V: **Mutations in the p53 Tumor Suppressor Gene: Important Milestones at the Various Steps of Tumorigenesis.** *Genes Cancer* 2011, **2**:466–474.

186. Hanahan D, Weinberg RA: **The hallmarks of cancer.** *Cell* 2000, **100**:57–70.

187. Hanahan D, Weinberg RA: **Hallmarks of cancer: the next generation.** *Cell* 2011, **144**:646–674.

188. Gorgoulis VG, Vassiliou LV, Karakaidos P, Zacharatos P, Kotsinas A, Liloglou T, Venere M, Ditullio RA, Kastrinakis NG, Levy B, et al.: **Activation of the DNA damage checkpoint and genomic instability in human precancerous lesions.** *Nature* 2005, **434**:907–913.

189. Montagnoli A, Tenca P, Sola F, Carpani D, Brotherton D, Albanese C, Santocanale C: **Cdc7 inhibition reveals a p53-dependent replication checkpoint that is defective in cancer cells.** *Cancer Res* 2004, **64**:7110–7116.

190. Rodriguez-Acebes S, Proctor I, Loddo M, Wollenschlaeger A, Rashid M, Falzon M, Sainsbury R, Stoeber K: **Targeting DNA Replication before it Starts**. *Am J Pathol* 2010, **177**:2034-2045.

191. Mulvey C, Tudzarova S, Crawford M, Williams GH, Stoeber K, Godovac-Zimmermann J: **Quantitative proteomics reveals a "poised quiescence" cellular state after triggering the DNA replication origin activation checkpoint.** *J Proteome Res* 2010, **9**:5445–5460.

192. Mulvey CM, Tudzarova S, Crawford M, Williams GH, Stoeber K, Godovac-Zimmermann J: **Subcellular proteomics reveals a role for nucleo-cytoplasmic trafficking at the DNA replication origin activation checkpoint.** *J Proteome Res* 2013, **12**:1436–1453.

193. Montagnoli A, Moll J, Colotta F: **Targeting cell division cycle 7 kinase: a new approach for cancer therapy.** *Clin Cancer Res* 2010, **16**:4503–4508.

194. Koltun ES, Tsuhako AL, Brown DS, Aay N, Arcalas A, Chan V, Du H, Engst S, Ferguson K, Franzini M, et al.: **Discovery of XL413, a potent and selective CDC7 inhibitor.** *Bioorg Med Chem Lett* 2012, **22**:3727–3731.

195. Swords R, Mahalingam D, O'Dwyer M, Santocanale C, Kelly K, Carew J, Giles F: **Cdc7 kinase – A new target for drug development**. *Eur J Cancer* 2010, **46**:33–40.

196. Natoni A, Murillo LS, Kliszczak AE, Catherwood MA, Montagnoli A, Samali A, O'Dwyer M, Santocanale C: **Mechanisms of action of a dual Cdc7/Cdk9 kinase inhibitor against quiescent and proliferating CLL cells.** *Mol Cancer Ther* 2011, **10**:1624–1634.

197. Drissi R, Wu J, Hu Y, Bockhold C, Dome JS:.**Telomere Shortening Alters the Kinetics of the DNA Damage Response after Ionizing Radiation in Human Cells**. *Cancer Prev Res (Phila)* 2011, **4**:1973-1981.

198. Dunham I, Lengauer C, Cremer T, Featherstone T: **Rapid generation of chromosome-specific alphoid DNA probes using the polymerase chain reaction.** *Hum Genet* 1992, **88**:457–462.

199. Willard HF, Waye JS: **Chromosome-specific subsets of human alpha satellite DNA: analysis of sequence divergence within and between chromosomal subsets and evidence for an ancestral pentameric repeat.** *J Mol Evol* 1987, **25**:207–214.

200. Jiang W, Hunter T: **Identification and characterization of a human protein kinase related to budding yeast Cdc7p**. *PNAS USA* 1997, **94:**14320-14325.

201. Dettori R, Sonzogni S, Meyer L, Lopez-Garcia LA, Morrice NA, Zeuzem S, Engel M, Piiper A, Neimanis S, Frodin M, et al.: **Regulation of the Interaction between Protein Kinase C-related Protein Kinase 2 (PRK2) and Its Upstream Kinase, 3-Phosphoinositide-dependent Protein Kinase 1 (PDK1)**. *J Biol Chem* 2009, **284**:30318-30327.

202. Ahler E, Sullivan WJ, Cass A, Braas D, York AG, Bensinger SJ, Graeber TG, Christofk HR: **Doxycycline alters metabolism and proliferation of human cell lines.** *PLoS ONE* 2013, **8**:e64561.

203. Kim BJ, Kim SY, Lee H: **Identification and characterization of human Cdc7 nuclear retention and export sequences in the context of chromatin binding.** *J Biol Chem* 2007, **282**:30029–30038.

204. Kim BJ, Lee H: **Importin-beta mediates Cdc7 nuclear import by binding to the kinase insert II domain, which can be antagonized by importin-alpha.** *J Biol Chem* 2006, **281**:12041–12049.

205. Duncker BP, Shimada K, Tsai-Pflugfelder M, Pasero P, Gasser SM: **An N-terminal domain of Dbf4p mediates interaction with both origin recognition complex (ORC) and Rad53p and can deregulate late origin firing.** *PNAS USA* 2002, **99**:16087–16092.

206. Wolff B, Sanglier JJ, Wang Y: **Leptomycin B is an inhibitor of nuclear export: inhibition of nucleo-cytoplasmic translocation of the human immunodeficiency virus type 1 (HIV-1) Rev protein and Rev-dependent mRNA.** *Chem Biol* 1997, **4**:139–147.

207. Martinez R, Burrage AM, Wiethoff CM, Wodrich H: **High temporal resolution imaging reveals endosomal membrane penetration and escape of adenoviruses in real time**. *Methods Mol Biol* 2013, **1064**:211–226.

208. Kaiser P1, Meierhofer D, Wang X, Huang L: **Tandem Affinity Purification Combined with Mass Spectrometry to Identify Components of Protein complexes**. *Methods Mol Biol* 2008, **439**:309-326.

209. ten Have S, Boulon S, Ahmad Y, Lamond AI: **Mass spectrometry-based immuno-precipitation proteomics - The user's guide**. *Proteomics* 2011, **11**:1153–1159.

210. Sang L, Miller JJ, Corbit KC, Giles RH, Brauer MJ, Otto EA, Baye LM, Wen X, Scales SJ, Kwong M, et al.: **Mapping the NPHP-JBTS-MKS protein network reveals ciliopathy disease genes and pathways.** *Cell* 2011, **145**:513–528.

211. Murphy SM, Urbani L, Stearns T: **The mammalian gamma-tubulin complex contains homologues of the yeast spindle pole body components spc97p and spc98p.** *J Cell Biol* 1998, **141**:663–674.

212. Fantin V, Sparling J, Slot J, Keller S: **Characterization of insulin receptor substrate 4 in human embryonic kidney 293 cells** *J Biol Chem* 1998, **273:**10726-10732.

213. Hoxhaj G, Dissanayake K, MacKintosh C: **Effect of IRS4 levels on PI 3-kinase signalling.** *PLoS ONE* 2013, **8**:e73327.

214. Reiss K, del Valle L, Lassak A, Trojanek J: **Nuclear IRS-1 and cancer.** *J Cell Physiol* 2012, **227**:2992–3000.

215. Sun XJ, Wang LM, Zhang Y, Yenush L, Glasheen E, Lane WS, Pierce JH, White MF: **Role of IRS-2 in insulin and cytokine signalling**. *Nature* 1995, **377**:173-177.

216. Hart JR, Vogt PK: **Phosphorylation of AKT: a Mutational Analysis.** *Oncotarget* 2011, **2**:467–476.

217. Liu K, Luo Y, Lin FT, Lin WC: **TopBP1 recruits Brg1/Brm to repress E2F1-induced apoptosis, a novel pRb-independent and E2F1-specific control for cell survival**. *Genes Dev* 2004, **18**:673-686.

218. Foiani M, Marini F, Gamba D, Lucchini G, Plevani P: **The B subunit of the DNA polymerase alpha-primase complex in Saccharomyces cerevisiae executes an essential function at the initial stage of DNA replication.** *Mol Cell Biol* 1994, **14**:923–933.

219. Vlahos CJ, Matter WF, Hui KY, Brown RF: **A specific inhibitor of phosphatidylinositol 3-kinase, 2-(4-morpholinyl)-8-phenyl-4H-1-benzopyran-4-one (LY294002).** *J Biol Chem* 1994, **269**:5241–5248.

220. Nitiss JL: **DNA topoisomerase II and its growing repertoire of biological functions.** *Nat Rev Cancer* 2009, **9**:327–337.

221. Mellacheruvu D, Wright Z, Couzens AL, Lambert JP, St-Denis NA, Li T, Miteva YV, Hauri S, Sardiu ME, Low TY, et al.: **The CRAPome: a contaminant repository for affinity purification–mass spectrometry data**. *Nat Methods* 2013, **10**:730-736.

222. Masai H, Arai K.: **Dbf4 Motifs: Conserved Motifs in Activation Subunits for Cdc7 Kinases Essential for S-Phase**. *Biochem Biophys Res Commun* 2000, **275**:228-232.

223. Kinoshita E, Kinoshita-Kikuta E, Ujihara H, Koike T: **Mobility shift detection of phosphorylation on large proteins using a Phos-tag SDS-PAGE gel strengthened with agarose.** *Proteomics* 2009, **9**:4098–4101.

224. Kinoshita E, Kinoshita-Kikuta E, Koike T: **Separation and detection of large phosphoproteins using Phos-tag SDS-PAGE**. *Nat Protoc* 2009, **4**:1513–1521.

225. Park SY, Im JS, Park SR, Kim SE, Wang HJ, Lee JK: **Mimosine arrests the cell cycle prior to the onset of DNA replication by preventing the binding of human Ctf4/And-1 to chromatin via Hif-1α activation in HeLa cells.** *Cell Cycle* 2012, **11**:761–766.

226. Kubota S, Fukumoto Y, Ishibashi K, Soeda S, Kubota S, Yuki R, Nakayama Y, Aoyama K, Yamaguchi N, Yamaguchi N: **Activation of the prereplication complex is

blocked by mimosine through reactive oxygen species-activated ataxia telangiectasia mutated (ATM) protein without DNA damage. *J Biol Chem* 2014, **289**:5730–5746.

227. Zieve GW, Turnbull D, Mullins JM, McIntosh JR: **Production of large numbers of mitotic mammalian cells by use of the reversible microtubule inhibitor nocodazole. Nocodazole accumulated mitotic cells.** *Exp Cell Res* 1980, **126**:397–405.

228. Agostinho M, Rino J, Braga J, Ferreira F, Steffensen S, Ferreira J: **Human topoisomerase IIalpha: targeting to subchromosomal sites of activity during interphase and mitosis.** *Mol Biol Cell* 2004, **15**:2388–2400.

229. Pommier Y, Huang SY, Gao R, Das BB, Murai J, Marchand C: **Tyrosyl-DNA-phosphodiesterases (TDP1 and TDP2).** *DNA Repair (Amst)* 2014, **19**:114–129.

230. Tavormina PA, Côme MG, Hudson JR, Mo YY, Beck WT, Gorbsky GJ: **Rapid exchange of mammalian topoisomerase II alpha at kinetochores and chromosome arms in mitosis.** *J Cell Biol* 2002, **158**:23–29.

231. Dimitrova DS, Berezney R: **The spatio-temporal organization of DNA replication sites is identical in primary, immortalized and transformed mammalian cells.** *J Cell Sci* 2002, **115**:4037–4051.

232. Nougarede R, Seta della F, Zarzov P, Schwob E: **Hierarchy of S-Phase-Promoting Factors: Yeast Dbf4-Cdc7 Kinase Requires Prior S-Phase Cyclin-Dependent Kinase Activation**. *Mol Cell Biol* 2000, **20**:3795–3806.

233. Guo B, Romero J, Kim BJ, Lee H: **High levels of Cdc7 and Dbf4 proteins can arrest cell-cycle progression** *Eur J Cell Biol* 2005, **84**:927–938.

234. Ursø B, Ilondo MM, Holst PA, Christoffersen CT, Ouwens M, Giorgetti S, van Obberghen E, Naor D, Tornqvist H, de Meyts P: **IRS-4 mediated mitogenic signalling by insulin and growth hormone in LB cells, a murine T-cell lymphoma devoid of IGF-I receptors.** *Cell Signal* 2003, **15**:385–394.

235. Qiu H, Zappacosta F, Su W, Annan R, Miller W: **Interaction between Brk kinase and insulin receptor substrate-4**. *Oncogene* 2005, **24:**5656-5664.

236. Uchida T, Myers M, White MF: **IRS-4 mediates protein kinase B signaling during insulin stimulation without promoting antiapoptosis**. *Mol Cell Biol* 2000, **20:**126-138.

237. Hinsby AM, Olsen JV, Mann M: **Tyrosine Phosphoproteomics of Fibroblast Growth Factor Signaling: a role for insulin receptor substrate-4**. *J Biol Chem* 2004, **279**:46438–46447.

238. Boudreau RL, Spengler RM, Hylock RH, Kusenda BJ, Davis HA, Eichmann DA, Davidson BL: **siSPOTR: a tool for designing highly specific and potent siRNAs for human and mouse**. *Nucleic Acids Res* 2012, **41**:e9.

239. Kandel ES, Skeen J, Majewski N, Di Cristofano A, Pandolfi PP, Feliciano CS, Gartel A, Hay N: **Activation of Akt/protein kinase B overcomes a G(2)/m cell cycle checkpoint induced by DNA damage.** *Mol Cell Biol* 2002, **22**:7831–7841.

240. Karrman K, Kjeldsen E, Lassen C, Isaksson M, Davidsson J, Andersson A, Hasle H, Fioretos T, Johansson B: **The t(X;7)(q22;q34) in paediatric T-cell acute lymphoblastic leukaemia results in overexpression of the insulin receptor substrate 4 gene through illegitimate recombination with the T-cell receptor beta locus**. *Br J Haematol* 2009, **144**:546–551.

241. Shull AY, Latham-Schwark A, Ramasamy P, Leskoske K, Oroian D, Birtwistle MR, Buckhaults PJ: **Novel Somatic Mutations to PI3K Pathway Genes in Metastatic Melanoma**. *PLoS ONE* 2012, **7**:e43369.

242. Karrman K, Isaksson M, Paulsson K, Johansson B: **The insulin receptor substrate 4 gene (IRS4) is mutated in paediatric T-cell acute lymphoblastic leukaemia**. *Br J Haematol* 2011, **155**:516–519.

243. Hu X, Li J, Vandervalk S, Wang Z, Magnuson NS, Xing PX: **Pim-1–specific mAb suppresses human and mouse tumor growth by decreasing Pim-1 levels, reducing Akt phosphorylation, and activating apoptosis**. *J Clin Invest* 2009, **119**:362-375.

244. Cen B, Mahajan S, Wang W, Kraft AS: **Elevation of Receptor Tyrosine Kinases by Small Molecule AKT Inhibitors in Prostate Cancer Is Mediated by Pim-1.** *Cancer Res* 2013, **73**:3402–3411.

245. Craparo A, Freund R, Gustafson TA: **14-3-3 (epsilon) Interacts with the Insulin-like Growth Factor I Receptor and Insulin Receptor Substrate I in a Phosphoserine-dependent Manner**. *J Biol Chem* 1997, **272**:11663–11669.

246. Hotamisligil GS, Peraldi P, Budavari A, Ellis R, White MF, Spiegelman BM: **IRS-1-mediated inhibition of insulin receptor tyrosine kinase activity in TNF-alpha- and obesity-induced insulin resistance.** *Science* 1996, **271**:665–668.

247. Cho WH, Lee YJ, Kong SI, Hurwitz J, Lee JK: **CDC7 kinase phosphorylates serine residues adjacent to acidic amino acids in the minichromosome maintenance 2 protein**. *PNAS* USA 2006, **103**:11521-11526.

248. Trojanek J, Ho T, del Valle L, Nowicki M, Wang JY, Lassak A, Peruzzi F, Khalili K, Skorski T, Reiss K: **Role of the Insulin-Like Growth Factor I/Insulin Receptor Substrate 1 Axis in Rad51 Trafficking and DNA Repair by Homologous Recombination**. *Mol Cell Biol* 2003, **23**:7510–7524.

249. Urbanska K, Pannizzo P, Lassak A, Gualco E, Surmacz E, Croul S, del Valle L, Khalili K, Reiss K: **Estrogen receptor β-mediated nuclear interaction between IRS-1 and Rad51 inhibits homologous recombination directed DNA repair in medulloblastoma.** *J Cell Physiol* 2009, **219**:392–401.

250. Xu N, Lao Y, Zhang Y, Gillespie: **Akt: a double-edged sword in cell proliferation and genome stability.** *J Oncol* 2012, **2012:**951724.

251. Zeng PY, Vakoc CR, Chen ZC, Blobel GA, Berger SL: **In vivo dual cross-linking for identification of indirect DNA-associated proteins by chromatin immunoprecipitation.** *BioTechniques* 2006, **41:** 694, 696, 698.

252. Hiraga SI, Alvino GM, Chang F, Lian HY, Sridhar A, Kubota T, Brewer BJ, Weinreich M, Raghuraman MK, Donaldson AD: **Rif1 controls DNA replication by directing Protein Phosphatase 1 to reverse Cdc7-mediated phosphorylation of the MCM complex.** *Genes Dev* 2014, **28**:372–383.

253. Matthews LA, Jones DR, Prasad AA, Duncker BP, Guarné A.: **Saccharomyces cerevisiae Dbf4 Has Unique Fold Necessary for Interaction with Rad53 Kinase.** *J Biol Chem* 2012, **287**:2378–2387.

254. Natsume T, Müller CA, Katou Y, Retkute R, Gierliński M, Araki H, Blow JJ, Shirahige K, Nieduszynski CA, Tanaka TU: **Kinetochores coordinate pericentromeric cohesion and early DNA replication by Cdc7-Dbf4 kinase recruitment.** *Mol Cell* 2013, **50**:661–674.

255. Erliandri I, Fu H, Nakano M, Kim JH, Miga KH, Liskovykh M, Earnshaw WC, Masumoto H, Kouprina N, Aladjem MI, Larionov V.: **Replication of alpha-satellite DNA arrays in endogenous human centromeric regions and in human artificial chromosome**. *Nucleic Acids Res* 2014, **42**:11502–11516.

256. Ten Hagen KG, Gilbert DM, Willard HF, Cohen SN: **Replication timing of DNA sequences associated with human centromeres and telomeres.** *Mol Cell Biol* 1990, **10**:6348–6355.

257. Ishida R, Iwai M, Marsh KL, Austin CA, Yano T, Shibata M, Nozaki N, Hara A: **Threonine 1342 in human topoisomerase IIalpha is phosphorylated throughout the cell cycle.** *J Biol Chem* 1996, **271**:30077–30082.

258. Boege F, Andersen A, Jensen S, Zeidler R, Kreipe H: **Proliferation-associated nuclear antigen Ki-S1 is identical with topoisomerase II alpha. Delineation of a carboxy-terminal epitope with peptide antibodies.** *Am J Pathol* 1995, **146**:1302–1308.

259. Uhlmann F, Nasmyth K: **Cohesion between sister chromatids must be established during DNA replication**. *Curr Biol* 1998, **8**:1095-1101.

260. Uhlmann F: **A matter of choice: the establishment of sister chromatid cohesion**. *EMBO Rep* 2009, **10**:1095-1102.

261. Hauf S, Roitinger E, Koch B, Dittrich CM, Mechtler K, Peters JM: **Dissociation of Cohesin from Chromosome Arms and Loss of Arm Cohesion during Early Mitosis Depends on Phosphorylation of SA2.** *PLoS Biology* 2005, **3**:e69.

262. Kitajima TS1 Sakuno T, Ishiguro K, Iemura S, Natsume T, Kawashima SA, Watanabe Y: **Shugoshin collaborates with protein phosphatase 2A to protect cohesin**. *Nature* 2006, **441**:46-52.

263. Tang Z, Shu H, Qi W, Mahmood NA, Mumby MC, Yu H: **PP2A is required for centromeric localization of Sgo1 and proper chromosome segregation**. *Dev Cell* 2006, **10:**575-585.

264. Vicart A, Lefebvre T, Imbert J, Fernandez A, Kahn-Perlès B: **Increased Chromatin Association of Sp1 in Interphase Cells by PP2A-mediated Dephosphorylations**. *J Mol Biol* 2006, **364**:897-908.

265. Renard-Guillet C, Kanoh Y, Shirahige K, Masai H: **Temporal and spatial regulation of eukaryotic DNA replication: from regulated initiation to genome-scale timing program.** *Semin Cell Dev Biol* 2014, **30**:110–120.

266. Moindrot B, Audit B, Klous P, Baker A, Thermes C, de Laat W, Bouvet P, Mongelard F, Arneodo A: **3D chromatin conformation correlates with replication timing and is conserved in resting cells**. *Nucleic Acids Res* 2012, **40**:9470-9481.

267. Dileep V, Ay F, Sima J, Vera DL, Noble WS, Gilbert DM: **Topologically associating domains and their long-range contacts are established during early G1 coincident with the establishment of the replication-timing program.** *Genome Res* 2015, **25**:1104–1113.

268. Cornacchia D, Dileep V, Quivy JP, Foti R, Tili F, Santarella-Mellwig R, Antony C, Almouzni G, Gilbert DM, Buonomo SB: **Mouse Rif1 is a key regulator of the replication-timing programme in mammalian cells**. *EMBO J* 2012, **31**:3678-3690.

269. Yamazaki S, Ishii A, Kanoh Y, Oda M, Nishito Y, Masai H: **Rif1 regulates the replication timing domains on the human genome**. *EMBO J* 2012, **31**:3667-3677.

270. Davé A, Cooley C, Garg M, Bianchi A: **Protein Phosphatase 1 Recruitment by Rif1 Regulates DNA Replication Origin Firing by Counteracting DDK Activity**. *Cell Rep* 2014, **7**:53-61.

271. Cuvier O, Hirano T: **A role of topoisomerase II in linking DNA replication to chromosome condensation**. *J Cell Biol* 2003, **160**:645-655.

Appendix A

List of proteins identified by SILAC with a DBF4B/EV ratio > 2.0. Experimental details in Chapter 4 (Section 4.3).

Mapped gene	Uniprot ID	DBF4B/EV	Notes	Function
DBF4B	Q8NFT6-1	**19.294**		DNA replication
CDC7	O00311	**12.957**		DNA replication
IRS4	O14654	**6.7568**		Signal transduction
TUBA1A	Q71U36	**6.2078**		Cytoskeleton
DNAJA1	P31689	**5.6272**		Chaperone
MAGED1	Q9Y5V3-2	**5.4798**		Cell cycle (other)
BAG6	B0UX85	**5.4225**	Complex with GET4	DDR
TUBA1C	Q9BQE3	**5.3173**		Cytoskeleton
TUBB?	B4DQN9	**5.312**		Cytoskeleton
CAD	P27708	**5.0198**		DNA replication
DNAJA2	O60884	**4.9524**		Chaperone
PEX3	P56589	**4.6424**		Peroxisome biogenesis
TUBB4B	P68371	**4.4834**		Cytoskeleton
N/A	B3KTT5	**4.1964**	Similar to HSP70	Chaperone
GET4	Q7L5D6-1	**4.1942**	Complex with BAG6	DDR
TUBB4A	P04350	**4.1161**		Cytoskeleton
HSPA8	P11142-1	**3.9451**		RNA metabolism
HSP1A/B	P08107	**3.5953**		Chaperone
CCAR2/DBC1	Q8N163-1	**3.5887**		Cell cycle (other)
KRT18	P05783	**3.5299**		Cytoskeleton
N/A	B4DP54	**3.456**	Similar to TUBB6	Cytoskeleton
VPS16	Q9H269-1	**3.4212**		Protein transport
TUBB6	Q9BUF5	**3.4048**		Cytoskeleton
POLR2B	P30876	**3.3186**		Transcription
MAP7D1	Q3KQU3-1	**3.2943**		Cytoskeleton
USP11	P51784	**3.1809**		DDR
TUBB3	Q13509	**3.1187**		Cytoskeleton
DNAJB6	O75190-1	**3.0333**		Chaperone
PI4KA	P42356-1	**3.024**		Signal transduction
AKAP8L	Q9ULX6	**2.9725**		Cell cycle (other)
TUBB2A	Q13885	**2.8562**		Cytoskeleton
IKBKAP	O95163	**2.7032**		Transcription
CNOT1	A5YKK6-1	**2.6439**		Transcription
TUBGCP2	B7ZKL8	**2.611**	γ Tub complex, centrosome	Cytoskeleton
UBAP2L	Q14157-2	**2.5531**		Stem cell function

SLFN11	Q7Z7L1	**2.5015**		DDR
IQCB1	Q15051-1	**2.2387**	Centrosome protein	Cilliogenesis
TCAF1	Q9Y4C2-1	**2.2364**		Migration
ISYNA1	Q9NPH2-1	**2.2331**		Myoinositol biosynthesis
NUP133	Q8WUM0	**2.2134**		mRNA export
N/A	A8K674	**2.1744**	Ubiquitin C	Protein modification
FARSA	Q9Y285	**2.169**		Translation
NEDD8	Q15843	**2.1675**		Protein modification
LAS1L	Q9Y4W2-1	**2.1607**		Ribosome biogenesis
PSMC2	P35998	**2.105**		Proteosome
N/A	N/A	**2.0938**	9 kDa protein	Uncharacterised
VBP1	P61758	**2.0142**		Chaperone
OGT	O15294-1	**2.0131**		Protein modification

Appendix B

List of proteins identified by SILAC with a CDC7/EV ratio > 1.0. Experimental details in Chapter 4 (Section 4.3).

Mapped gene	Uniprot	CDC7/EV	DBF4B/EV	Notes	Function
DBF4A	Q9UBU7-1	6.4952			DNA replication
CDC7	O00311	3.0309			DNA replication
MAGED1	Q9Y5V3-2	1.8632	5.4798		Other Cell cycle
ANXA5	P08758	1.3336			Uncharacterised
C1QBP	Q07021	1.3035			Immunity
EIF3E	P60228	1.2641			Translation
PC	P11498	1.2199			Carbohydrate biosynthesis
DDX5	P17844	1.2196	1.4038		Other Cell cycle
CBR1	P16152	1.1861			NAD metabolism
PRDX2	P32119	1.1801			Redox regulation
DNAJB6	O75190-1	1.1407			Chaperone
ILF3	Q12906-4	1.1281			Immunity
N/A	B4DP54	1.1033		TUBB6	Cytoskeleton
DNAJA1	P31689	1.0977			Chaperone
CAPRIN1	Q14444-1	1.0606			RNA processing
DDX3X	O00571	1.0384			RNA processing
USP9X	Q93008-2	1.0299	1.65		Other Cell cycle
FANCI	Q9NVI1-3	1.027	1.5137		DNA damage
ARF4	P18085	1.0017			Protein transport

Appendix C

List of proteins co-immunoprecipitated with DBF4-FLAG. For details of experiment and analysis see Chapter 5 (Section 5.2).

Mapped gene	No. of unique peptides	CRAPome frequency (Ver. 1.0)	Function
SRGAP2	2	2	Actin cytoskeleton
CDC5L	9	37	Cell cycle
GNL3	7	40	Cell cycle
MDN1	2	12	Chaperone
DNAJC9	3	19	Chaperone
CHD4	2	28	Chromatin structure
HP1BP3	4	32	Chromatin structure
HMGA1	2	33	Chromatin structure
MPG	2	5	DNA damage
RAD23B	2	8	DNA damage
LIG3	2	12	DNA damage
MDC1	2	15	DNA damage
APEX1	2	29	DNA damage
CDC7	11	0	DNA replication
DBF4A	14	0	DNA replication
RFC5	2	21	DNA replication
RFC1	5	22	DNA replication
USP7	2	25	DNA replication
RFC4	3	30	DNA replication
SSRP1	3	44	DNA replication
TOP1	13	57	DNA replication
MCM3	2	69	DNA replication
TOP2A	12	69	DNA replication
PGAM4	2	46	Glycolysis
PGAM1	2	56	Glycolysis
KIAA0020	4	14	Immunity
TRIM25	2	15	Immunity
FKBP3	4	21	Immunity
GLTSCR2	2	22	Immunity
MRPS27	2	14	Mitochondrial
SLC25A10	4	62	Mitochondrial
NUSAP1	2	13	Mitosis
USP39	5	26	Mitosis
NAT10	13	32	Mitosis
NSUN2	8	35	Mitosis

NMT1	4	14	Protein modification
MINA	2	0	Protein modification
AP2B1	2	34	Protein transport
GTPBP1	2	5	RNA met
EXOSC3	2	7	RNA met
RNMTL1	4	8	RNA met
SRBD1	2	8	RNA met
RBM42	3	11	RNA met
GTF3C4	3	12	RNA met
EXOSC7	2	13	RNA met
YTHDC2	3	13	RNA met
DDX52	2	15	RNA met
DHX29	5	15	RNA met
CTNNBL1	4	16	RNA met
DIMT1L	2	16	RNA met
DDX24	3	17	RNA met
FARSB	7	18	RNA met
RRP15	2	19	RNA met
SREK1	2	19	RNA met
DDX56	2	20	RNA met
BCAS2	2	21	RNA met
RBM15	2	22	RNA met
PDCD11	4	23	RNA met
THOC2	2	23	RNA met
DDX54	3	24	RNA met
TSR1	4	24	RNA met
DDX47	2	25	RNA met
EXOSC10	4	25	RNA met
ADAR	2	30	RNA met
BRIX1	5	30	RNA met
DDX18	4	31	RNA met
DDX23	2	32	RNA met
SRPK1	3	35	RNA met
DKC1	2	37	RNA met
SRRM1	3	41	RNA met
DHX30	7	42	RNA met
EXOSC6	3	43	RNA met
SRRT	2	46	RNA met
SNRNP70	4	61	RNA met
SF3A3	2	63	RNA met
ELAVL1	3	65	RNA met
SNRPA1	2	65	RNA met
CAPRIN1	4	68	RNA met
C22orf28	2	69	RNA met
PRPF19	6	70	RNA met

GLYR1	3	30	Signal transduction
POLR1B	3	10	Transcription
POLR1A	3	12	Transcription
MYEF2	3	13	Transcription
POLR1C	2	23	Transcription
XRN2	5	50	Transcription
EIF5	2	9	Translation
EIF2AK2	3	11	Translation
EIF5B	6	42	Translation
ABCF1	10	43	Translation
RPL32	4	52	Translation
NOP56	4	53	Translation
EIF3E	2	56	Translation
EIF3F	4	61	Translation
EIF3A	7	66	Translation
RPL28	7	69	Translation
C7orf50	2	18	Uncharacterised
SMU1	5	29	Uncharacterised